REPORT NO.
UCB/EERC-90/17
JUNE 1990

EARTHQUAKE ENGINEERING RESEARCH CENTER

BEHAVIOR OF PEAK VALUES AND SPECTRAL ORDINATES OF NEAR-SOURCE STRONG GROUND MOTION OVER THE SMART 1 ARRAY

by

MANSOUR NIAZI

PREFACE

by

BRUCE A. BOLT

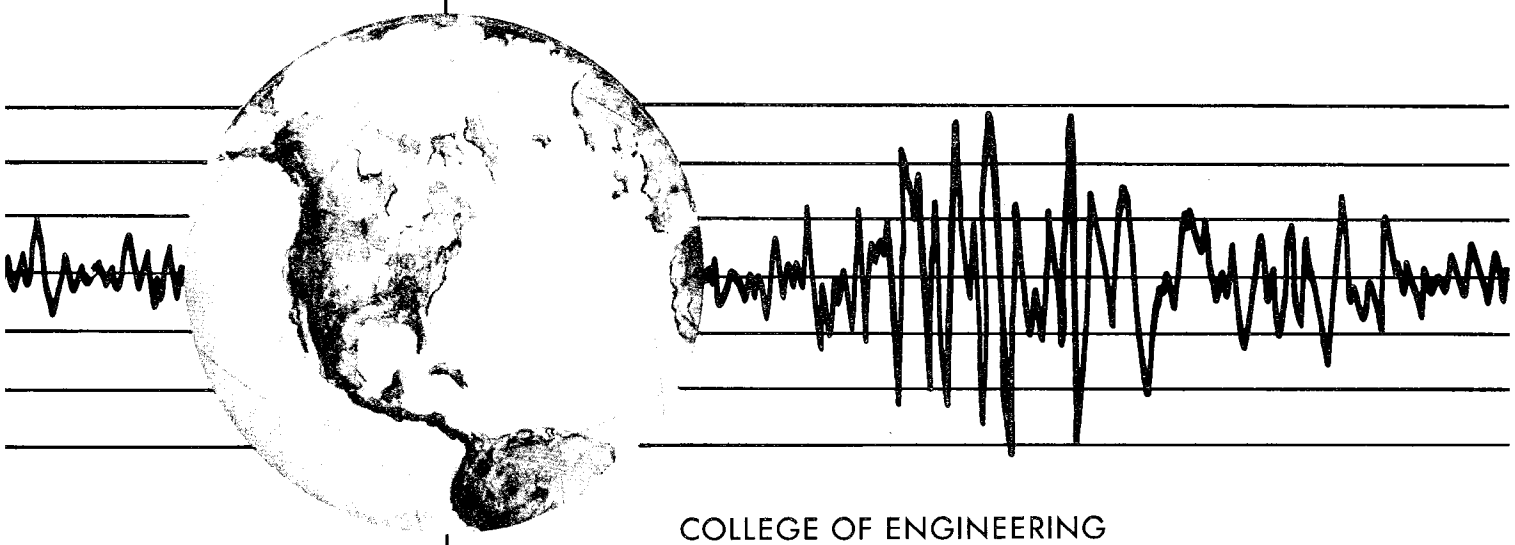

COLLEGE OF ENGINEERING

UNIVERSITY OF CALIFORNIA AT BERKELEY

For sale by the National Technical Information Service, U.S. Department of Commerce, Springfield, Virginia 22161.

DISCLAIMER

Any opinions, findings, and conclusions or recommendations expressed in this publication are those of the author and do not necessarily reflect the views of the National Science Foundation or the Earthquake Engineering Research Center, University of California at Berkeley.

50272-101

REPORT DOCUMENTATION PAGE	1. REPORT NO. NSF/ENG-90009	2.	PB93-114833

4. Title and Subtitle
Behavior of Peak Values and Spectral Ordinates of Near-Source Strong Ground Motion Over the SMART 1 Array

5. Report Date
June 1990

6.

7. Author(s)
Mansour Niazi

8. Performing Organization Rept. No.
UCB/EERC-90/17

9. Performing Organization Name and Address
Earthquake Engineering Research Center
University of California, Berkeley
1301 So. 46th Street
Richmond, Calif. 94804

10. Project/Task/Work Unit No.

11. Contract(C) or Grant(G) No.
(C)
(G)ISI-8619612

12. Sponsoring Organization Name and Address
National Science Foundation
1800 G Street, N.W.
Washington, D.C. 20550

13. Type of Report & Period Covered

14.

15. Supplementary Notes

16. Abstract (Limit: 200 words) The array recordings are used to investigate several important properties of the seismic ground motions themselves. The results reported here address the question of the variability of the peak vertical and horizontal accelerations, velocities and displacements. Statistical treatment of this variability is feasible when ground motions are recorded, as in SMART 1, at a group of stations within a limited distance. The three rings of the SMART 1 array have radii of 200 m, 1 km and 2 km. Since it became operational in September 1980, it has recorded accelerations up to 0.33g and 0.34g on the horizontal and vertical components, respectively. At present there are over 3,000 accelerograms from 53 local earthquakes available. From this set of observations, 12 earthquakes have been selected providing more than 700 accelerograms for analysis and statistical treatment. Nonlinear regression procedures are used to fit the peak values to an attenuation form which has as parameters, earthquake magnitude and source-to-site distance. Spectral information on ground motion is included; correlations are made between spectral ordinate values at 23 discrete frequencies in the range of engineering interest. Among the notable results is the finding that the ratio of the vertical to horizontal response spectral ordinates is less than the often used value of 2/3 for periods longer than about 0.2 second, and also for all frequencies at distances greater than 30 km from the source. By contrast, this value is unconservative for high-frequency ground motion in the very near field. The ground motion spectra for vertical and horizontal motions from the SMART 1 recordings are compared with the spectra defined in U.S. Nuclear Regulatory Guide 1.60. The comparison leads to some inferences concerning deviations under certain conditions with these recommended spectra. Of particular interest in this work, are the results for longer periods (greater than about 2 seconds).

17. Document Analysis a. Descriptors

b. Identifiers/Open-Ended Terms

c. COSATI Field/Group

18. Availability Statement:	19. Security Class (This Report)	21. No. of Pages
Release Unlimited	unclassified	126
	20. Security Class (This Page) unclassified	22. Price

BEHAVIOR OF PEAK VALUES AND SPECTRAL ORDINATES OF NEAR-SOURCE STRONG GROUND MOTION OVER THE SMART 1 ARRAY

by

Mansour Niazi

TENERA, L.P.
1995 University Avenue
Berkeley, CA 94704

PREFACE

by

Bruce A. Bolt

Prepared under NSF Grant ISI-8619612

Report No. UCB/EERC-90/17
Earthquake Engineering Research Center
College of Engineering
University of California at Berkeley

June 1990

/B

Preface

Four UCB/EERC Reports have been published previously, describing studies based on earthquake recordings made by the large-scale array of digital accelerometers in Taiwan, called SMART 1. The last such report was "Effects of Spatial Variation of Ground Motions on Large Multiply-Supported Structures," by Hong Hao (UCB/EERC-89/06). Rather than consider structural responses, the present report uses the array recordings to investigate several important properties of the seismic ground motions themselves. The reader is referred to a summary of related research entitled, "SMART 1 Accelerograph Array (1980-1987): A Review," by N. A. Abrahamson, B.A. Bolt, R.B. Darragh, J. Penzien, Y. B. Tsai, published in Earthquake Spectra, 3, 263-287, 1987.

The results reported here by M. Niazi address the question of the variability of the peak vertical and horizontal accelerations, velocities and displacements. Statistical treatment of this variability is feasible when ground motions are recorded, as in SMART 1, at a group of stations within a limited distance. The three rings of the SMART 1 array have radii of 200 m, 1 km and 2 km. Since it became operational in September 1980, it has recorded accelerations up to 0.33g and 0.34g on the horizontal and vertical components, respectively. At present there are over 3,000 accelerograms from 53 local earthquakes available. From this set of observations, Niazi has selected 12 earthquakes providing more than 700 accelerograms for analysis and statistical treatment. His method is to use nonlinear regression procedures to fit the peak values to an attenuation form which has as parameters, earthquake magnitude and source-to-site distance. Only one previous analysis of attenuation of peak ground accelerations and velocities using the SMART 1 array data has been published (Y. B. Tsai and B. A. Bolt, Bull. Inst. Ear. Sci., Academia Sinica, 3, 105-126,(1983). In addition, however, the present report includes spectral information on ground motion; correlations have been made between spectral ordinate values at 23 discrete frequencies in the range of engineering interest.

Among the notable results is the finding that the ratio of the vertical to horizontal response spectral ordinates is less than the often used value of 2/3 for periods longer than about 0.2 second, and also for all frequencies at distances greater than 30 km from the source. By contrast, this value is unconservative for high-frequency ground motion in the very near field. Dr. Niazi compares the ground motion spectra for vertical and horizontal motions from the SMART 1 recordings with the spectra defined in U.S.

Nuclear Regulatory Guide 1.60. The comparison leads to some inferences concerning deviations under certain conditions with these recommended spectra. Of particular interest in this work, are the results for longer periods (greater than about 2 seconds). The demand for design ground motions for large structures, such as large bridges, requires that scaling factors be known at periods greater than 1 second. In this range, representative ground motion spectra are not so well developed as those at the higher frequencies normally used in evaluations of smaller critical structures such as nuclear reactor containment vessels.

The basic research program based on the SMART 1 array in Taiwan has been supported by National Science Foundation (U.S.) grants (CES-8800457) and significant grants by the National Research Council (ROC) in Taiwan. Operation of the array, as well as record processing has been the responsibility of the Institute for Earth Sciences, National Research Council, Taipei, to whose seismologists much thanks is due.

B. A. Bolt

ACKNOWLEDGEMENTS

This study was supported by National Science Foundation grant ISI-8619612. The digital recordings from the SMART 1 array were provided by Professor Bruce Bolt of the University of California, Berkeley. Principal Investigator benefitted from discussions with Professor David Brillinger and Dr. Christian Mortgat. Dr. Yousef Bozorgnia contributed in every phase of the project. Mr. Mark Polit made important improvements in the written report.

TABLE OF CONTENTS

TABLE OF CONTENTS

(continued)

LIST OF TABLES

1.0 INTRODUCTION

The behavior of strong-ground motion in the near-source region of earthquakes is influenced by properties of the earthquake source, propagation path, and recording site. This study was motivated by the unexpectedly high vertical ground motion recorded in the near-source region of several recent earthquakes (including the 1976, Gazli, USSR; 1979 Coyote Lake and Imperial Valley, Ca.; and 1984 Morgan Hill, Ca.). In these events, vertical accelerations significantly exceeded the accepted 2/3 scaling relative to the horizontal component. Therefore, this study sought to examine the behavior of peak vertical ground motion under the favorable conditions provided by the SMART 1 array, where high quality digital data have been recorded for several large events by stations with nearly uniform sub-surface conditions. The present study expands beyond the original scope to encompass the entire response spectra, both vertical and horizontal.

A total of 12 events, more than 700 accelerograms, has been analyzed for investigating the behavior of vertical and horizontal peak and spectral ground motion. Peak horizontal and vertical ground acceleration (PGA), velocity (PGV), and displacement (PGD), as well as spectral ordinates at 23 discrete frequencies in the range of engineering interest have been subjected to nonlinear regression procedures in terms of magnitude and hypocentral distance. Also the soil amplification of ground motion was analyzed for two adjacent stations, one on rock and the other on soil, near the southern edge of the array.

Some of the noteworthy observations made during this study are cited below.

This study confirms the conservatism of the Regulatory Guide 1.60 horizontal spectra, except at high magnitudes between about 0.15 and 2.0 seconds. In this range, our near-field spectra significantly exceed that recommended by the regulatory guide. For the vertical component, our spectra exceed that of the regulatory guide in the high frequency range, in the very nearfield. However, the regulatory guide appears very conservative with respect to our results beyond about 0.25 second.

The 2/3 ratio of vertical to horizontal ground motion, commonly used in engineering applications, is unconservative in the very near field for high frequency ground motion. However, ratios of vertical to horizontal response spectral ordinates are less than 2/3 for

periods longer than about 0.20 second, and for all frequencies (and PGA) at distances greater than 30-50 km.

The 84th percentile horizontal estimate for V/A approaches the predictions of Hall et al. (1976). However, their ratio for the vertical component exceeds our 84th percentile estimate by nearly a factor of 2. Concerning the values of AD/V^2, the findings for the vertical component are slightly above and for the horizontal component substantially below the recommended value of 6. These observations implicitly lead to different shapes for the horizontal and vertical response spectra.

The observed dispersion of the data decreases as magnitude increases for all ground motion parameters. Therefore, the standard error of the regression can be modelled as magnitude dependent, reducing the uncertainty associated with predicted amplitudes of large magnitude events. Also when factors such as geology, structure type and azimuth do not vary, the major contributor to the uncertainty is the variation of ground-motion observations between earthquakes (inter-event uncertainty).

This study finds nearly total magnitude saturation for the vertical and horizontal high frequency spectral ordinates. A greater degree of saturation for the vertical component of PGA than for the horizontal was also observed.

For all peak parameters and over all frequencies, a recording station located on soil shows significant amplification of ground motion with respect to an adjacent station located on rock. However, this amplification varied significantly by component and, as expected, by frequency content of the parameter studied.

In comparison with other studies discussed in this report, the predictions show

- lower far-field attenuation for PGA and PGV
- lower near-source amplitudes of PGA
- higher magnitude saturation for vertical PGA
- lower magnitude saturation for horizontal PGA
- higher magnitude scaling for PGA.

The author recommends applying the methodology described in this report to an enhanced, worldwide data base in order to reduce some of the uncertainties associated

with this analysis and to extend the validity of these results to other regions. It is especially important to constrain the results concerning magnitude saturation, since this significantly affects predicted amplitudes for large magnitude events on the upper boundary of the data used here.

Additional data, for several recent earthquakes which occurred since 1987 are now available. A study of the extended data set in parallel with geological and seismological studies of source geometries should be extremely useful in further reduction of the uncertainties. Such studies would allow utilization of the shortest distance to the rupture surface as an independent variable of regression analysis.

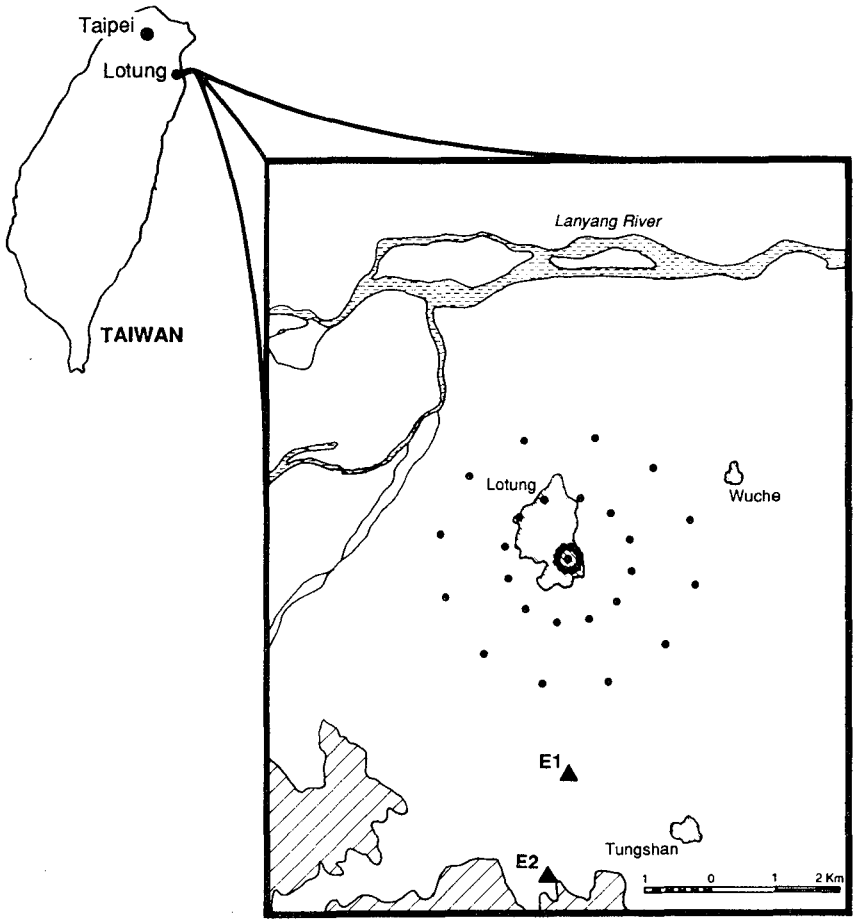

Figure 2.1 - Geographic location of SMART1 and the auxiliary array in northeast Taiwan.

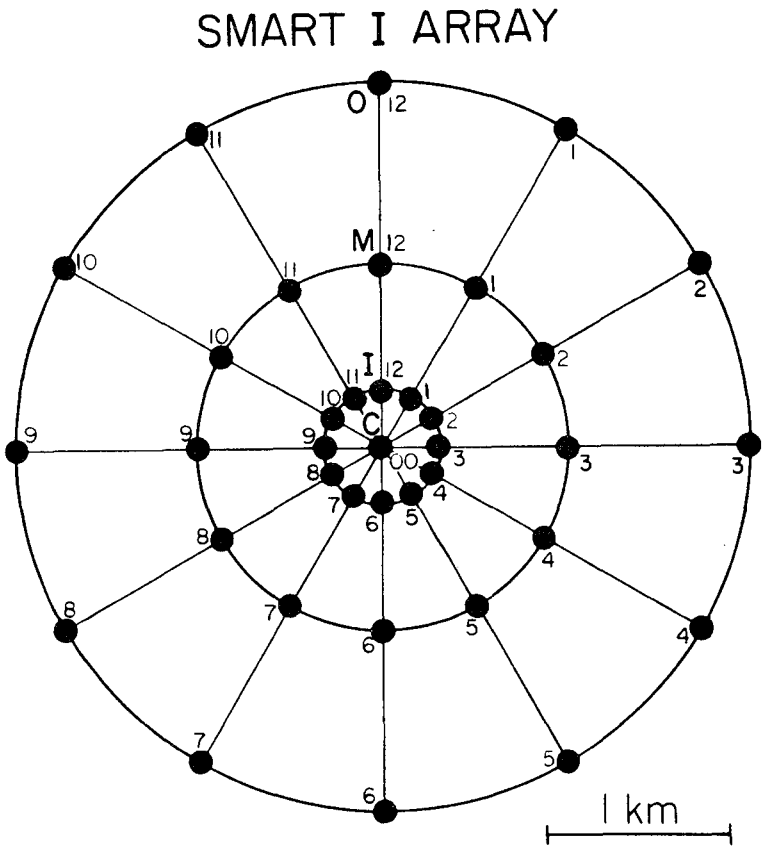

Figure 2.2 - Geometry of the elements of inner- middle- and outer-ring of SMART1 around the central station COO.

2.0 DATA BASE

2.1 SMART-1 ARRAY

This study examined accelerograms recorded in the near-source region of moderate-to-large earthquakes across the SMART-1 array in northeast Taiwan (Figure 2-1). The array consists of three rings with twelve equally spaced stations in each ring (see Figure 2-2). The array's outer radius is 2 km, while the middle ring and inner ring's radii are 1 km and 200 meters, respectively. In addition, there are two adjacent stations E_1 and E_2 to the south of the outer ring, one located on soil and the other on rock (Figure 2-1). These two stations are used in the analysis of soil amplification effects (Section 3.9).

The array is situated on the Lan-Yang Plain, near the city of Lotung, in northeastern Taiwan. On the basis of a 1973 seismic survey by the Chinese Petroleum Corporation, the array is located on top of approximately 450 meters of post-Miocene sedimentary sections. According to Wen and Yeh (1984), the P-wave velocity is in the range of 3.3 to 4.0 km/sec for the Miocene basement complex, 1.8-2.0 km/sec for the overlying Pleistocene, and 1.4-1.7 km/sec for the recent alluvium. The thickness of the topsoil ranges between 3 and 18 meters under the array, with a P-wave velocity of 0.43-0.70 km/sec. Detailed descriptions of the geology and instrumentation are provided by Bolt et al. (1982) and Abrahamson (1985).

Several factors influencing the amplitudes and characteristics of strong-ground motion have been largely eliminated by the choice of this data set:

- Subsurface geology over these stations is fairly homogeneous with about 400 meters of Pleistocene to recent sediments overlying basement rock which slopes gently to the north-northeast at about 6 degrees (Wen and Yeh, 1984).

- Variations due to structural interface and embedment have been minimized since these are all free field instruments mounted on four inch thick concrete base mats, approximately two by three feet across.

- For a specific earthquake, differences due to propagation path have been minimized by the proximity of the recording stations.

- In parts of the study, the effects of distance within individual earthquakes are further reduced by restricting the analysis to the inner ring of the array.

The quality of data is greatly enhanced by the employment of matched instruments and digital recordings. The instruments are SA-3000 triaxial accelerometers, having a natural frequency of approximately 80 Hertz (Abrahamson, 1985). The array's DR-100 digital event recorders have a resolution of 1 cm/sec^2 (1 count = 0.96 gal).

2.2 DATA SELECTION

By 1987, 48 earthquakes were recorded by two or more stations across the array. Twelve of these events are used in this study. Earthquakes were selected to cover a broad range of magnitude, distance and azimuth at the same time ensuring thorough coverage at the array. The selected events met the following criteria:

- At least 25 stations recorded the event.
- The focal depth was less than 30 kilometers (all but one was less than 15 kilometers).
- Hypocentral distance was less than 50 kilometers, except for two large events selected beyond 50 kilometers in order to constrain the slope of the attenuation relationship with respect to distance.
- A wide range of magnitude and azimuth was represented.

The resultant data set contains earthquakes with an azimuthal distribution between 60 and 230 degrees. Thus no earthquakes were recorded from the west or north.

The data base includes the twelve station inner ring and the central station, although recordings exist for most of the 37 stations in the array. For the attenuation analyses, stations from the outer rings along the line of azimuth of the individual events are included. This provides additional spread with distance for a given event.

The 12 earthquakes and the recordings selected represent a total of 721 time-histories (239 vertical and 482 horizontal) with a sampling interval of 0.01 second. The selected events are listed in Table 2-1, together with the number of recording stations utilized from each event. The distribution of these data by magnitude and distance is graphically displayed in Figure 2-3. Locations of recording stations are given in Table 2-2.

Assuming an average record length of 15 seconds, these accelerograms represent 1.1 million acceleration data points. After baseline and instrument correction, the accelerograms are integrated to obtain velocity and displacement time-histories, Fourier amplitude, and response spectra. Thus the processed data base represents approximately 4 million data points.

2.3 DEFINITION OF PARAMETERS

The parameters used to describe the data are defined below:

Peak Acceleration

The PGA value is taken from the corrected record. The 0.01 second digital interval provides an accurate representation of the peak arrival. The recording resolution of the system is approximately one gal (1 cm/sec^2).

PGV/PGD/Spectral Amplitudes

Peak Ground Velocity (PGV), Peak Ground Displacement (PGD), and Fourier amplitude and phase spectra are computed in the frequency domain employing the approach used by Sunder (1981), as described in Section 2.4. Response spectra are computed at 23 discrete frequencies, using numerical integration.

Table 2-1

List of Earthquake Sources Used in this Study

Event	Year	Date	N.Lat. deg	E.Long. deg	Depth km	M	Dist. to Cent. km	Source Type(*)	No. Obs. (Compnts.)
5	1981	Jan 29	24.43	121.90	11.1	6.3	30.20	Reverse	30
14	1981	Aug 30	24.46	121.75	0.2	5.0	23.15		51
15	1981	Oct 5	24.66	121.74	3.6	3.6	3.10		45
20	1982	Dec 17	24.38	122.87	27.3	6.4	119.73	Obliq.R	60
22	1983	May 10	24.46	121.51	1.2	6.4	35.39	Normal	57
29	1984	Apr 23	24.79	122.09	8.7	6.0	35.13		60
31	1985	Mar 9	24.76	122.23	4.1	5.9	48.24		60
33	1985	Jun 12	24.57	122.19	3.3	6.5	44.98	Obliq.N	66
36	1985	Sep 20	24.53	122.20	6.1	6.3	46.57	Normal	81
39	1986	Jan 16	24.76	121.96	10.2	6.5	22.19	Normal	66
43	1986	Jul 30	24.63	121.79	1.6	6.2	5.77	Normal	81
45	1986	Nov 14	23.99	121.83	13.9	7.8	77.09	Reverse	66

* Based on teleseismically determined fault plane solutions

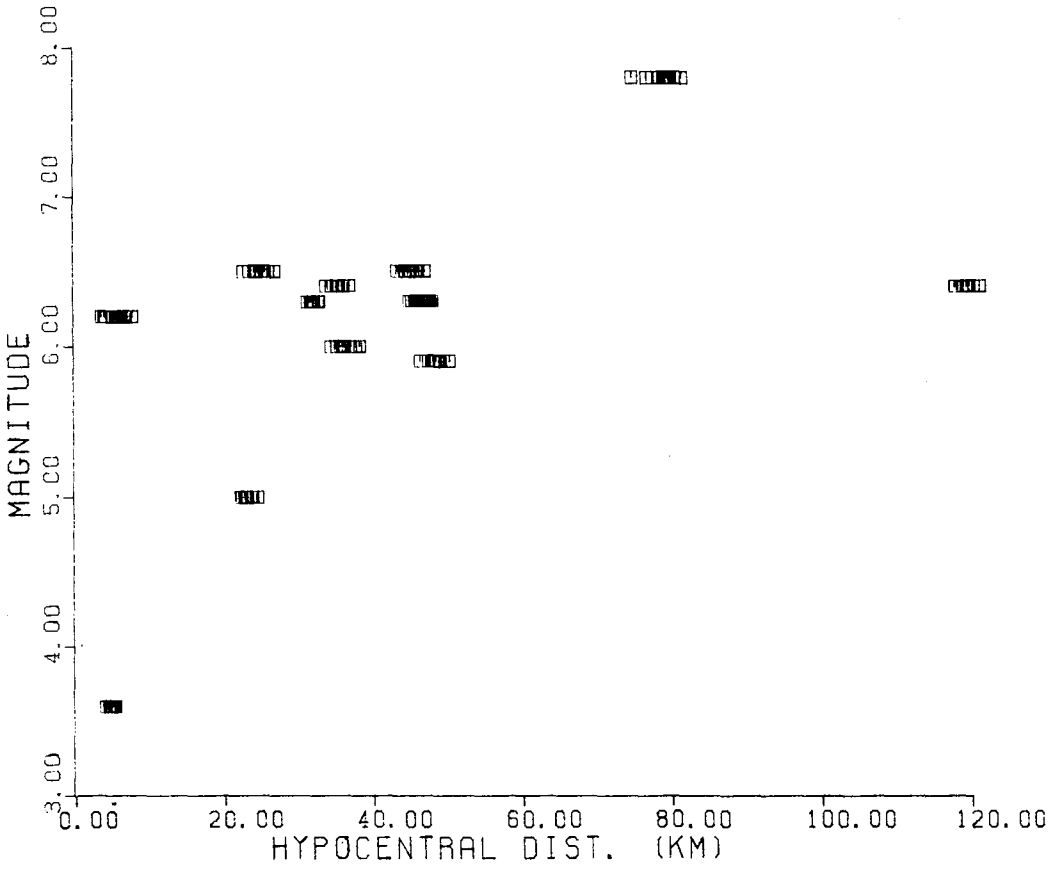

Figure 2.3 - Scattergram of observations in terms of magnitude and distance.

Table 2-2 - SMART 1 Array Recording Station Locations

Station	East Longitude	North Latitude	Elevation (m)
C00	121.45.52.98	24.40.25.52	6.10
I01	121.45.54.10	24.40.31.72	5.90
I02	121.45.57.72	24.40.30.10	5.50
I03	121.45.59.88	24.40.27.61	6.10
I04	121.46.00.16	24.40.24.08	6.10
I05	121.45.58.32	24.40.21.14	6.30
I06	121.45.54.55	24.40.19.40	6.60
I07	121.45.51.10	24.40.19.23	6.30
I08	121.45.48.60	24.40.20.91	6.20
I09	121.45.45.97	24.40.23.47	7.00
I10	121.45.46.00	24.40.26.75	7.00
I11	121.45.48.16	24.40.29.46	6.80
I12	121.45.50.91	24.40.31.79	6.40
M01	121.46.00.05	24.40.57.11	5.50
M02	121.46.17.94	24.40.53.05	4.40
M03	121.46.24.33	24.40.36.69	4.00
M04	121.46.28.09	24.40.18.20	4.50
M05	121.46.19.29	24.40.05.63	3.90
M06	121.46.03.72	24.39.54.45	4.30
M07	121.45.43.36	24.39.53.46	5.20
M08	121.45.30.10	24.40.01.34	7.40
M09	121.45.18.69	24.40.13.38	10.80
M10	121.45.20.53	24.40.30.10	7.60
M11	121.45.26.78	24.40.47.60	7.10
M12	121.45.42.92	24.40.57.28	5.90
O01	121.46.07.24	24.41.30.08	5.30
O02	121.46.41.25	24.41.13.63	4.90
O03	121.47.02.39	24.40.44.93	3.40
O04	121.47.02.24	24.40.13.12	2.40
O05	121.46.47.44	24.39.43.76	3.80
O06	121.46.14.91	24.39.23.34	4.80
O07	121.45.39.03	24.39.21.76	7.20
O08	121.45.06.47	24.39.33.94	18.10
O09	121.44.44.52	24.40.03.05	9.60
O10	121.44.43.58	24.40.40.25	13.40
O11	121.45.01.99	24.41.08.43	9.10
O12	121.45.32.03	24.41.27.52	6.50
E01	121.45.52.00	24.38.55.42	5.17
E02	121.45.39.61	24.37.49.69	9.72

Source-to-Station Distance

Hypocentral distance is taken to represent source-to-station distance. Focal depth and epicentral location are obtained from the regional network operated by the Institute of Earth Sciences, Taipei (Wen and Yeh, 1988).

There is inadequate information available to clearly define or compute closest distance to the rupture zone, as defined by Boore et al. (1981) and Campbell (1981). While there may be strong physical justification for such a distance definition, it requires exact knowledge of the multi-parametered source geometry, seldom known with sufficient certainty. Hypocentral distance is chosen over epicentral distance as a more meaningful representation of source-to-site distance.

Magnitude

Magnitude is defined as local magnitude (M_L) for magnitudes less than 6.6 and Surface Magnitude (M_s) for M_s 6.6 or above. This data base is not sensitive to the specific cut-off magnitude, since, for all values of M_L that are used in the analysis, the reported value of M_s is less than M_L. Also, as shown in Table 2-1, M_L is used for all events except for the November 14, 1986 earthquake of M_s 7.8.

Focal Mechanism

Of the earthquakes selected, four displayed a normal mechanism, two reverse, one reverse-oblique, and one normal-oblique (see Table 2-1). Since, focal mechanisms are not known for four events a scaling variable could not be used to decrease scatter. However, in Section 3.8 the possible correlations between the mean event residuals and source type are discussed.

Geology/Structure Type/Instrument Location/Instrument Type

These parameters do not vary across the recording stations and, therefore, are not included in the data set for the SMART-1 array. The geology for all stations used in the analysis is nearly identical. However, two neighboring stations (of different geologies) to the south of the array are utilized in the study of soil amplification (Section 3.9).

2.4 DATA PROCESSING

Data processing, including base line correction, filtering and integration, is performed using the approach described by Sunder (1981). The following input parameters are used for the analysis of individual accelerograms:

- Sample interval = 0.01 second
- Natural frequency of transducers = 50 Hertz
- Damping ratio of transducers = 0.8
- Corner frequencies of the trapezoidal band-passed filter = 0.07 Hz, 0.10 Hz, 25.0 Hz, and 30.6 Hz.

For each acceleration time-history, processed records consist of baseline and instrument corrected accelerograms in cm/sec^2, particle velocity in cm/sec, and displacement in centimeters. In addition, Fourier amplitude and phase spectra of the resulting time histories are calculated.

When integrating to obtain velocity and displacement time histories, there are a limited number of cases where the integration does not come to a reasonable convergence. For example, in many of these cases, the peak velocity or displacement value occurred near the end of the time history. This may be due either to long-period noise that is not filtered out or to compounding error in the integration. Therefore, these records are excluded from the analysis of PGV (if the peak velocity is in question) and from the analysis of PGD. Thus, while 234 stations are utilized for the analysis of vertical PGA, 224 and 190 are used for the PGV and PGD analyses, respectively.

2.5 UNIFORMITY ACROSS THE ARRAY

The closely-spaced strong motion recordings of the SMART 1 array provide an unusual opportunity to observe the variation of recordings over short distances for essentially identical site conditions and travel paths. Some of the figures from the Phase I Final Report (Niazi, 1986) are reproduced here, providing a visual indication of the variation of the records across the inner ring of the array. A detailed discussion is contained in that report.

As an example, Figure 2-4 presents the vertical accelerograms from the inner ring stations for the magnitude 6.4, May 10, 1983 earthquake (event number 22), 35.4 km from the center of the array. The time-histories are reproduced on a common time base, at the calculated epicentral distances. The peak accelerations are noted by the hollow circles, and the shaded band indicates the expected onset of the S-Phase. This comparison demonstrates similarities in the duration of strong-ground motion and the succession of energy packets across the array. However, there are substantial differences in the times of peak accelerations, with 7 of the 12 arriving prior to the expected onset of the S-Phase.

For the same earthquake, the discrete Fourier transforms of these acceleration time-histories are spatially displayed for the inner ring and central stations in Figure 2-5. The arrow represents the direction of the approach of the seismic waves from the preferred epicenter. These Fourier spectra show the energy content of the records generally concentrated in the frequency bands of 0.4-1.0 and 4-10 Hz, with the intervening band showing a relatively low energy content. Nevertheless, there can be significant variations in amplitude for a given frequency band over very short distances (e.g., stations I-09 and I-11).

The frequency content of the records is further explored in Figure 2-6, with a composite plot of the response spectra at 5% critical damping for the inner ring stations. The two bold lines represent the mean and plus one standard deviation value for these spectra. While there is variation of amplitude between stations, the shape of the spectra is strikingly uniform across the array. Also, the dispersion of the response spectra in general is tighter than that of the Fourier spectra.

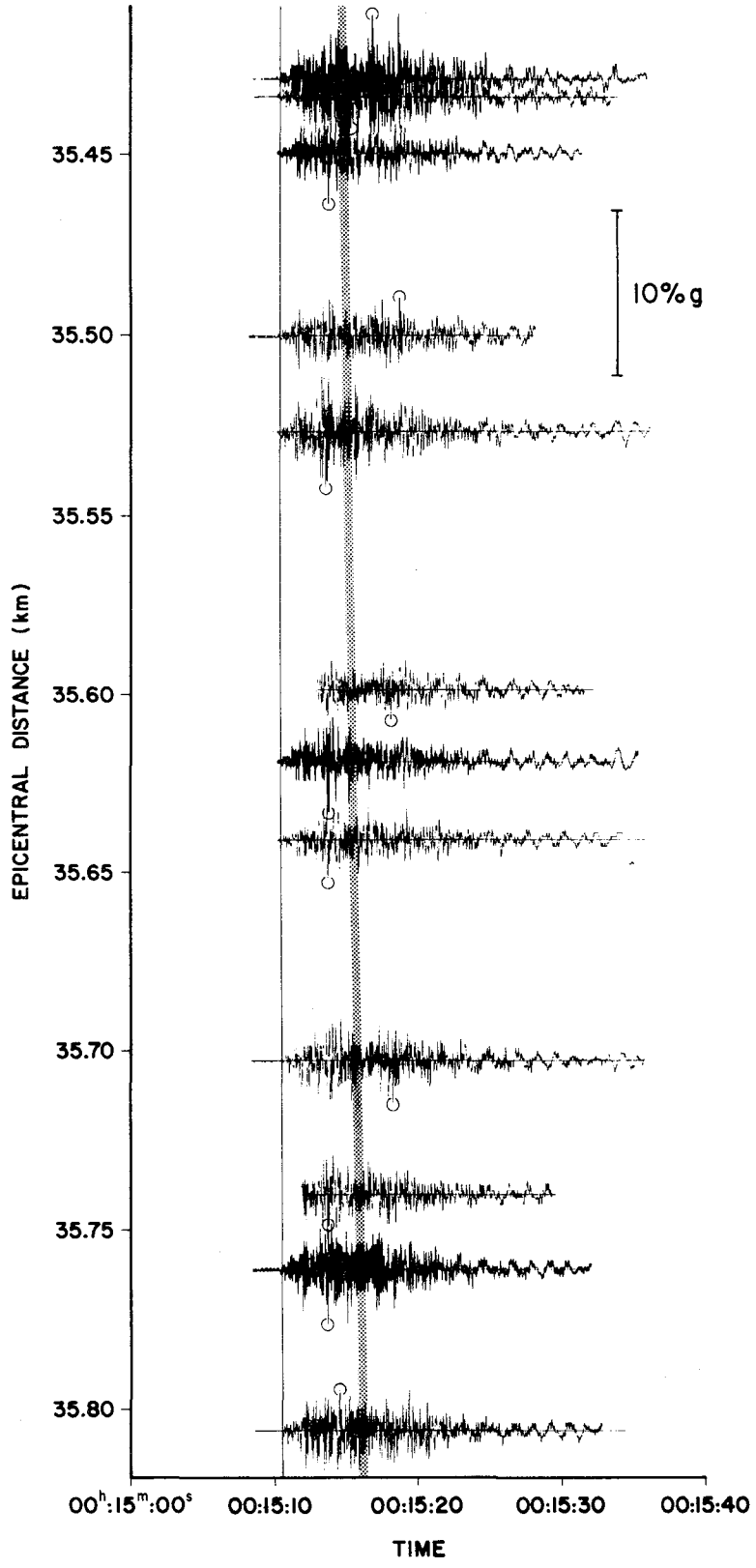

Figure 2.4 - Record section of the vertical accelerograms of May 10, 1983 earthquake (Event 22, M6.4) across the inner-ring stations. The maximum recorded PGA for each trace is marked by a hollow circle. The approximate time of the first arrival is shown by the the fine straight line with a slope of 250 m/sec. The thick shaded line corresponds to the approximate arrival band of the S phase.

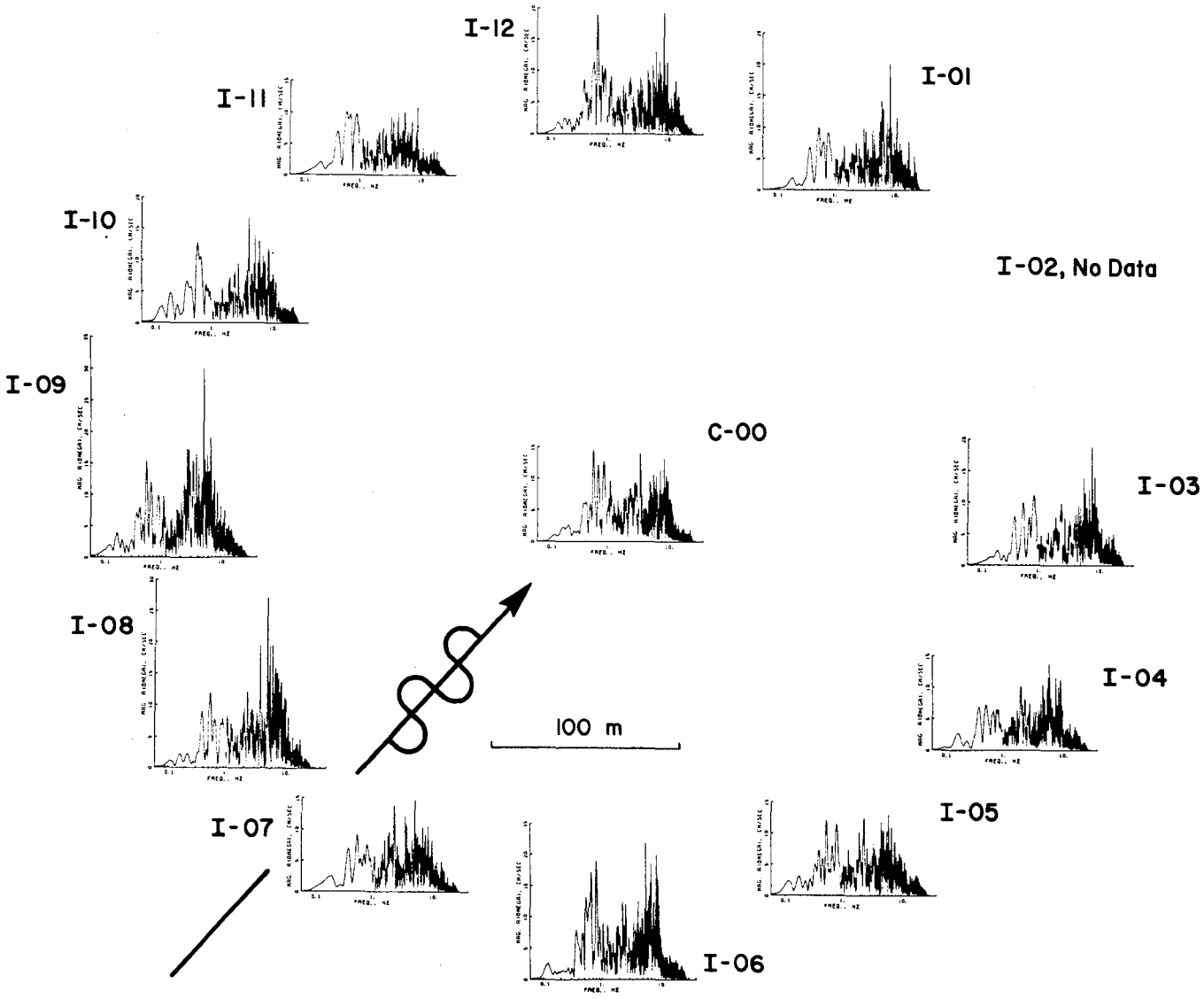

Figure 2.5 - The Fourier amplitude spectra of the observed acceleration time histories of the record section shown in Figure 2.4, drawn to a common scale. The arrow shows the direction of propagation.

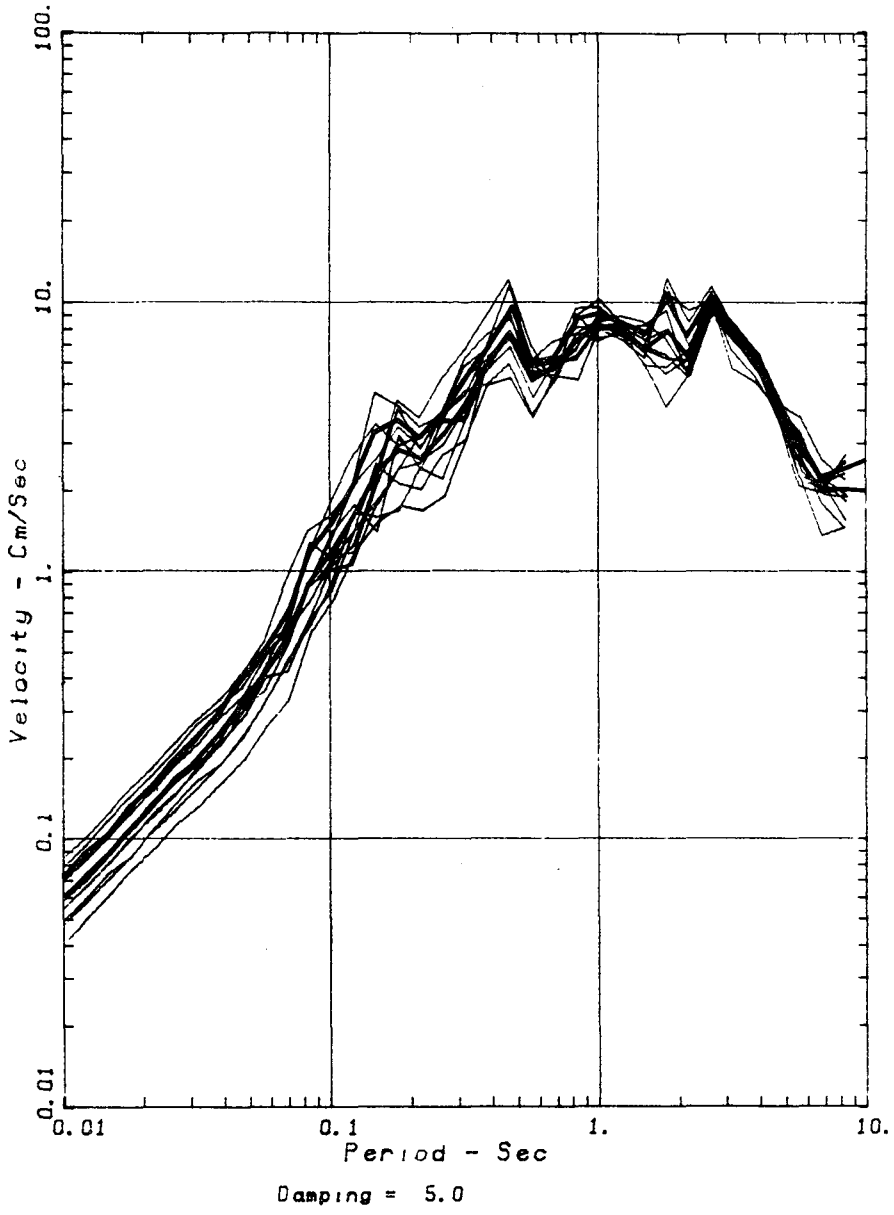

Figure 2.6 - Composite response spectra of the north-south component of the inner-ring accelerograms of Event 22. The pointwise mean and mean plus one standard deviation spectra are shown by bold traces.

3.0 ANALYSIS

3.1 NONLINEAR MODELLING OF GROUND-MOTION PARAMETERS

This study utilized the nonlinear attenuation equation of the form suggested by Campbell (1981)

$$\ln(Y) = a + bM + d \ln[R + c_1 e^{C_2 M}] \qquad (1)$$

where Y is Peak Ground Acceleration (PGA), Peak Ground Velocity (PGV), Peak Ground Displacement (PGD), or spectral amplitude, i.e., Pseudo Spectral Velocity (PSV). M is earthquake magnitude and R represents hypocentral distance in kilometers.

This functional form is selected because it is capable of modelling magnitude and distance saturation effects whenever supported by the data. The coefficient a scales the amplitude of ground motion at zero magnitude and distance. The coefficient b scales ground-motion amplitudes with magnitude. The coefficient d controls the attenuation rate of ground-motion amplitudes with distance at large distances. The C-term ($c_1 e^{C_2 M}$) allows magnitude scaling to be a function of distance in the near field. By setting $c_2 = 0$, equation (1) takes a less general or linear form which scales magnitude uniformly with distance. This latter form has been used in a number of ground-motion studies in recent years (Joyner and Boore, 1981; Donovan, 1982; and Campbell,1989).

Regression is performed using the nonlinear, multiple regression procedure of the SAS statistical software package (SAS, 1985).

In applying the regression procedure, the data is weighted by assigning an equal weight to recordings from each earthquake within each of ten distance bins. For vertical PGA, Table 3-1 gives the span of these bins and the number of recordings therein. Thus the earthquakes with a smaller number of recordings are not overwhelmed by those with a larger coverage. Also, this procedure gives additional weight to events recorded over multiple distance bins.

Table 3.1 - Distribution of vertical PGA within distance bins

Hypocentral Range of Distance Bins (km)	No. of Recordings	No. of Earthquakes in each Bin (*)
R < 2.5	0	0
2.5 ≤ R < 5.0	15	2
5.0 ≤ R < 7.5	24	2
7.5 ≤ R < 10.0	2	1
10.0 ≤ R < 14.1	0	0
14.1 ≤ R < 20.0	0	0
20.0 ≤ R < 28.3	38	1
28.3 ≤ R < 40.0	47	3
40.0 ≤ R < 56.6	68	3
56.6 ≤ R < 130.0	40	2

* An earthquake can have recordings in more than one distance bin.

Table 3.2 - Results of Regression Analysis on Peak Vertical Ground-Motion Parameters

Ground-Motion Parameter	a	b	c_1	c_2	d	σ	DMS %	No. of Obs. (*)
PGA (g)	-6.063	1.150	0.040	0.768	-1.219	0.553	81	234
PGV (cm/sec)	-3.963	1.368	0.117	0.701	-1.099	0.546	56	224
PGD (cm)	-4.088	1.152	0.269	0.658	-0.977	0.632	56	190

* The one rock site is excluded.

Table 3.3 - Results of Regression Analysis on Peak Horizontal Ground-Motion Parameters across Inner Ring

Ground-Motion Parameter	a	b	c_1	c_2	d	σ	DMS %	No. of OBs. (*)
PGA(g)	-6.625	1.164	0.011	0.902	-1.704	0.529	83	132
PGV(cm/sec)	-4.501	1.363	0.062	0.719	-0.958	0.544	51	127
PGD(cm)	-4.339	1.223	0.240	0.680	-1.020	0.668	57	104

* Regression performed on all earthquakes in data base, however, only stations of the inner ring and central station were included in the analysis.

3.2 PEAK VALUES OF THE VERTICAL COMPONENT

3.2.1 Regression Results

Regression on the full data set discussed in Section 2 (less the one station located on rock) results in the relationships given in Table 3-2, where parameters of equation (1) are given for the vertical component of PGA, PGV, and PGD.

In Table 3-2, σ refers to the standard deviation on ln(Y). Assuming a log-normal distribution, this value can be used to obtain the value of parameter Y corresponding to different probability levels. Specifically, ln(Y) at 84.1% probability (one sigma) may be obtained by multiplying the predicted median value by e.

DMS in Table 3-2 refers to the Degree of Magnitude Saturation, defined by Campbell (1981) as

$$DMS = (-c_2 d/b)*100 \qquad (2)$$

where the coefficients on the right side of the equation are determined by the regression analysis for equation (1).

DMS characterizes the saturation of the ground-motion parameter with magnitude, expressed as a percentage, in the near-source region. If DMS is 0% (no saturation), the ln(Y) scales uniformly with magnitude at all distances (i.e., the shape of the attenuation curve is independent of magnitude). If DMS is greater than zero, there is less scaling with magnitude as distance decreases. In the case of full saturation (DMS=100%) there is no scaling with magnitude at R=0 (i.e., Y is independent of magnitude at the hypocenter). Plots of ln(Y) as a function of distance and magnitude would show the lines converging as distance decreases.

Figures 3-1 to 3-3 plot the observed and predicted values of the peak values as a function of distance. The solid lines represent the median predictions for M = 5.5, 6.5 and 7.5, while the dashed lines represent the plus and minus one standard deviation curves. The individual data points are superimposed on the curves, demonstrating their distribution with respect to amplitude and distance. One can also see the spread in amplitudes for individual earthquakes (note that the center of the data has overlapping

events). Although the data points are coded by their magnitude band, the data are not normalized to a given magnitude and therefore do not display their variation from the predicted values.

The first noticeable characteristic of these plots is the relative convergence of the curves at short distances, representing a notable saturation of amplitude with magnitude at short distances. This is consistent with the values of DMS given in Table 3-2. Also the flattening of the curve with decreasing distance indicates saturation of amplitude with decreasing distance. In Table 3-2 this corresponds to a non-zero c_1 parameter.

The one standard deviation values, represented by the dotted and dashed lines, are modelled as constant with magnitude and distance. Therefore, the dotted lines are parallel to the respective median values (solid lines). In Figure 3-1, the increase in PGA in the far field for one standard deviation is comparable to that resulting from an additional half a unit of magnitude. However, since amplitude scales less with magnitude in the near field and the uncertainty does not (it is modelled to be constant), the increase in the near field is comparable to a whole degree of magnitude. This feature is seen to a lesser extent for PGV and PGD.

The results are also presented as a function of magnitude in Figures 3-4 to 3-6. The median predictions at distances of 3, 10, 30, and 50 kilometers are represented by the solid lines while the median plus one standard deviation values are represented by the dashed lines. A noticeable characteristic is that as magnitude increases there is less scaling with distance, since the lines pinch together at higher magnitudes. Thus, for a given magnitude, amplitudes increase more gradually as distance decreases and magnitude increases.

The relative scaling with distance is also apparent in Figures 3-4 to 3-6. The greater the spread between lines the greater the scaling of amplitude with changes in distance. Note that the spread decreases from PGA to PGV to PGD. This is expected, since the higher frequency PGA should attenuate faster (greater scaling with distance) than the lower frequency PGV and PGD.

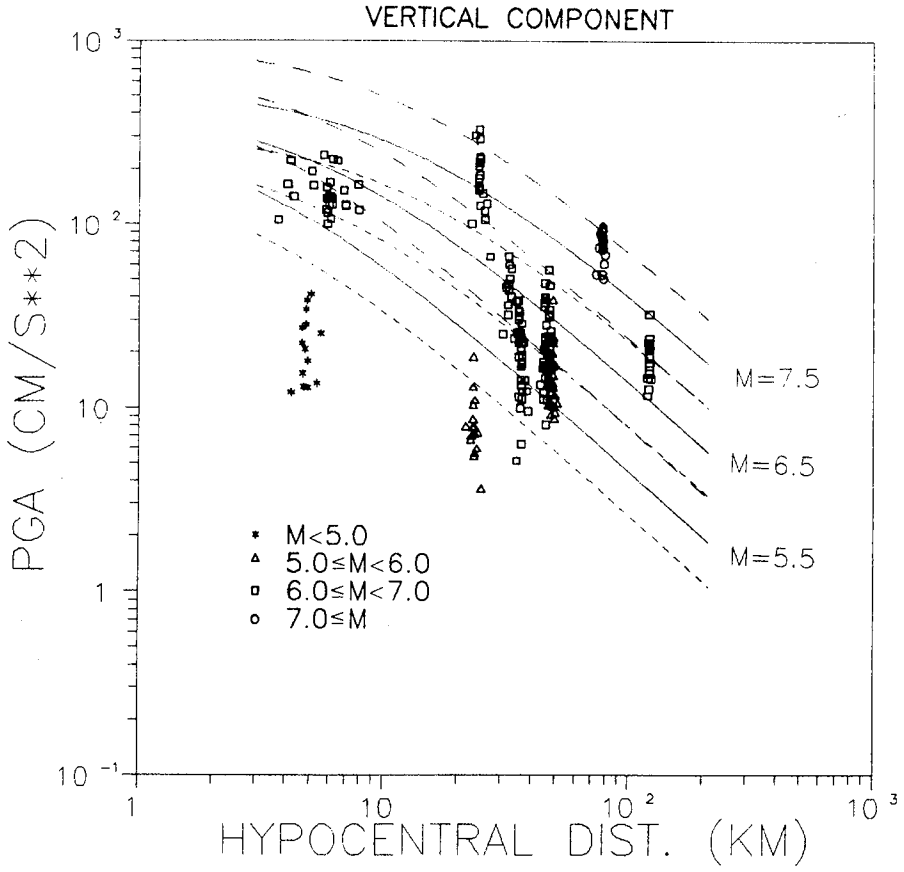

Figure 3.1 - Overlay of the observed vertical PGA and predicted attenuation curves at three magnitudes. Solid curves show median estimates, short and long dashes show minus and plus one standard deviation, respectively.

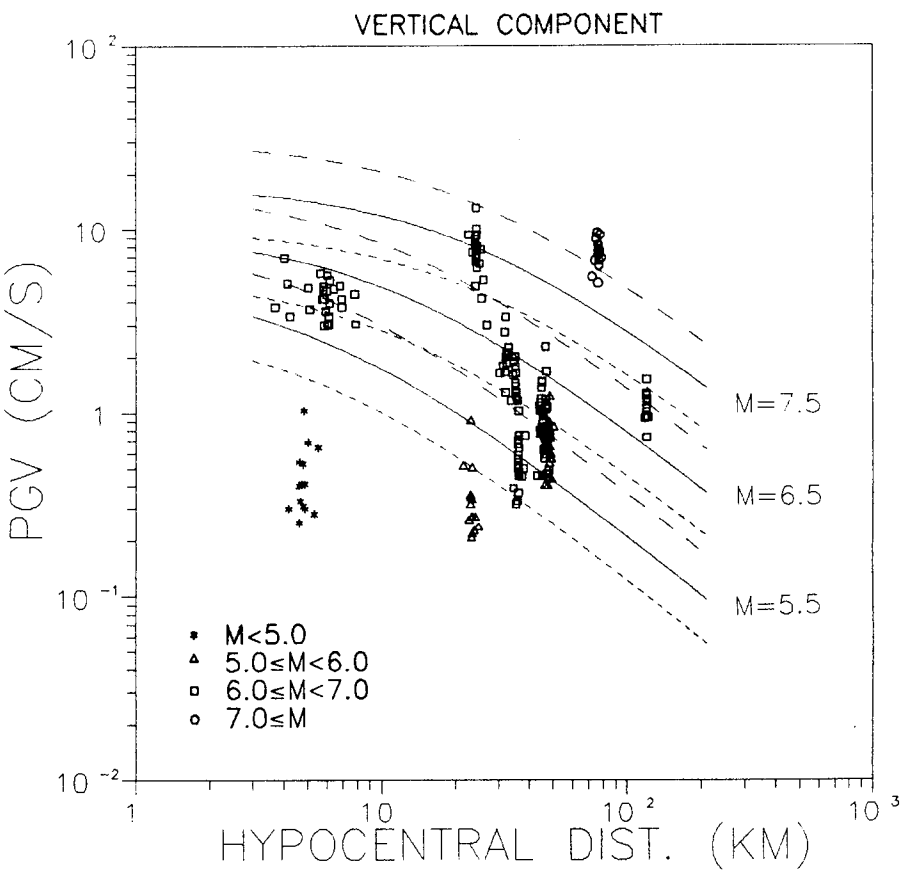

Figure 3.2 - Overlay of the observed vertical PGV and predicted attenuation curves at three magnitudes. Solid curves show median estimates, short and long dashes show minus and plus one standard deviation, respectively.

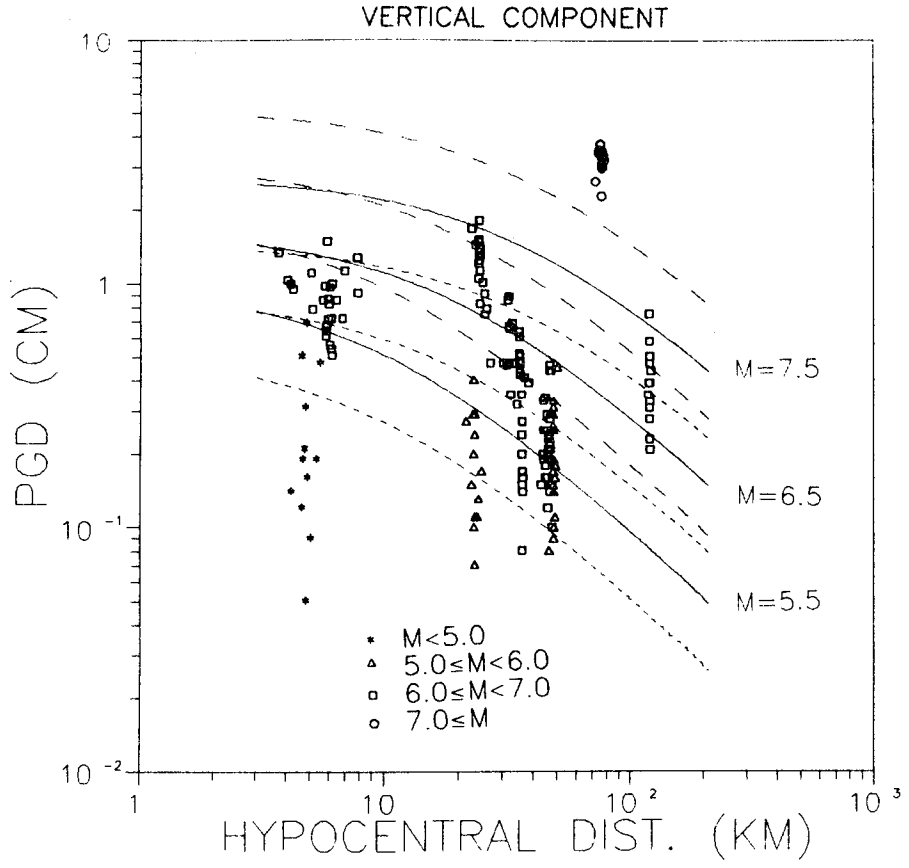

Figure 3.3 - Overlay of the observed vertical PGD and predicted attenuation curves at three magnitudes. Solid curves show median estimates, short and long dashes show minus and plus one standard deviation, respectively.

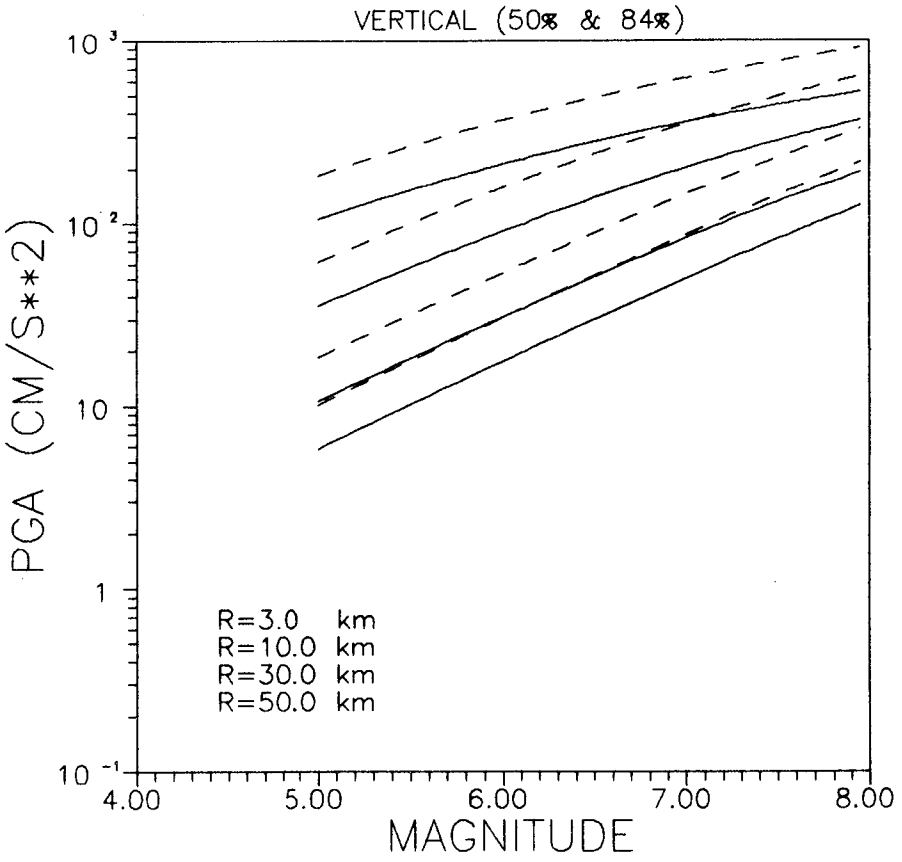

Figure 3.4 - Predicted vertical PGA at 50% and 84.1% probabilities for four specified hypocentral distances as a function of magnitude.

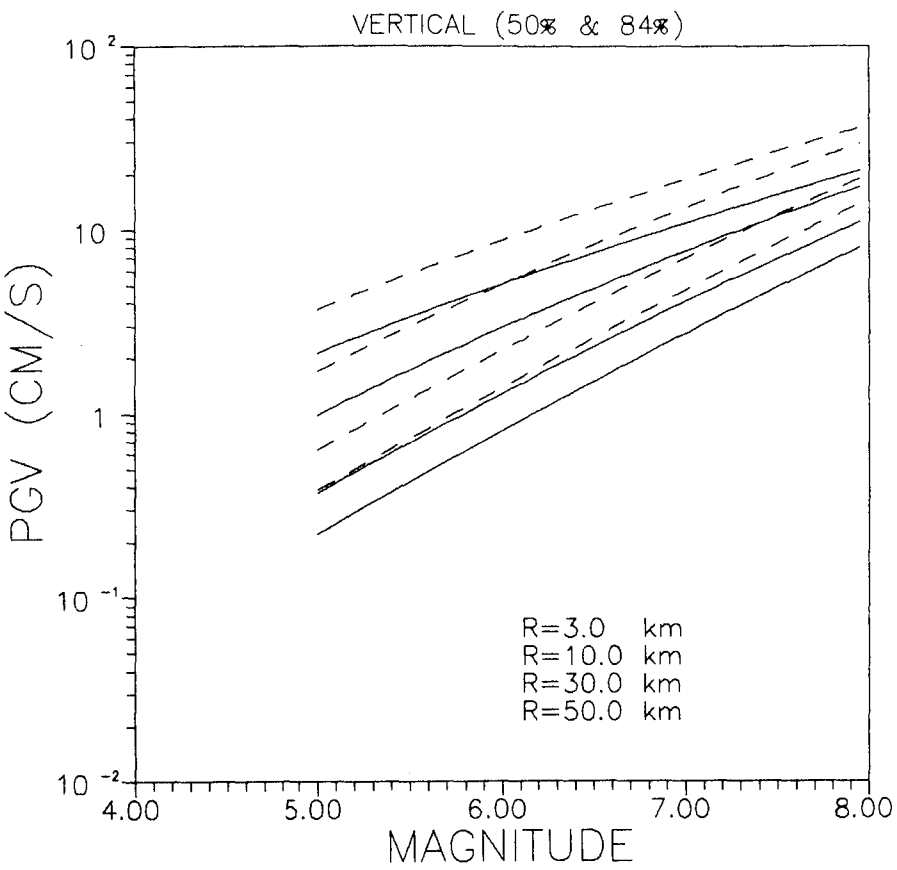

Figure 3.5 - Predicted vertical PGV at 50% and 84.1% probabilities for four specified hypocentral distances as a function of magnitude.

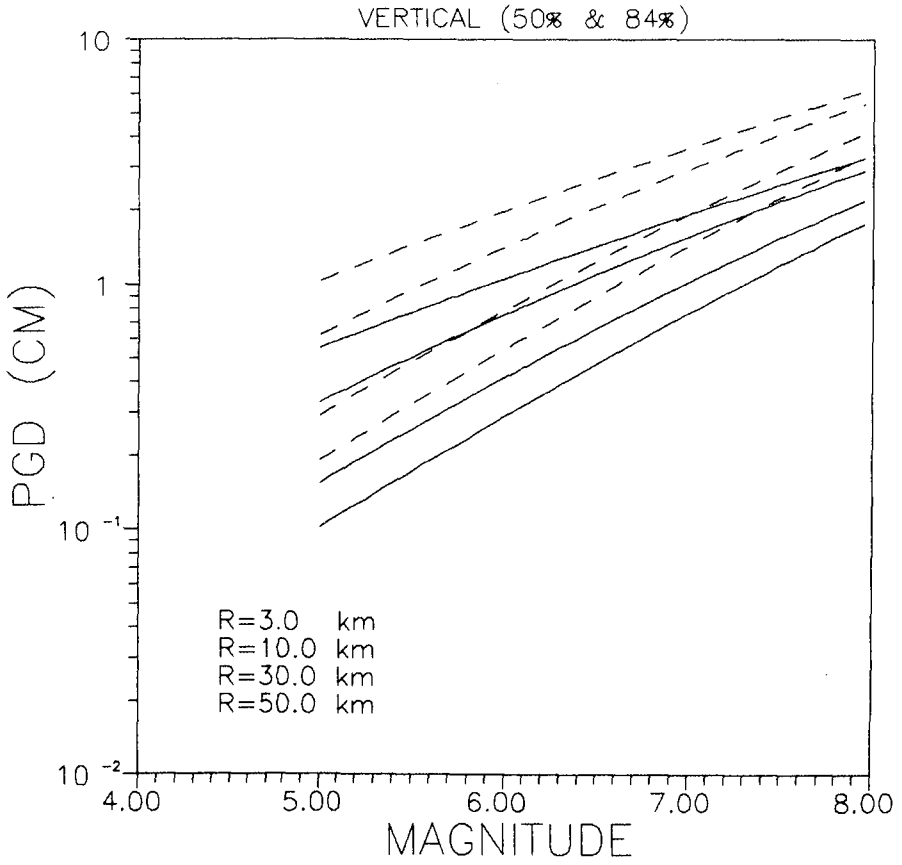

Figure 3.6 - Predicted vertical PGD at 50% and 84.1% probabilities for four specified hypocentral distances as a function of magnitude.

3.2.2 Discussion

Sensitivity to the Effect of Outer Stations

As discussed in Section 2.2, the data base includes the twelve station inner ring and the central station plus selected outer stations along the line of azimuth of the individual event. This provided a greater spread with distance for each earthquake. In order to evaluate the sensitivity of the results to the addition of these outer stations, regressions were conducted on the peak values using only the inner ring and central stations. The regression results are presented in Table 3-3 for vertical PGA, PGV, and PGD.

A comparison of Table 3-2 with Table 3-3, shows that the uncertainty is relatively unaffected by removing stations which are further away from each other. The uncertainty decreased by about 4% for PGA, stayed the same for PGV, and increased by about 6% for PGD. This is significant since these outer stations represent about 45% of the data base. Thus, it appears that the scatter of observations at adjacent locations (the inner ring has a radius of 200 meters) is as large as for stations placed farther apart (the outer ring has a radius of two kilometers) when other factors such as geology, structure type, and azimuth do not vary.

Comparing DMS for the two data sets shows that neither the magnitude saturation effect nor the magnitude scaling term b is affected by removing the outer stations. However, the distance parameter $\underline{d}$ decreased by about 12% for PGA with lesser changes for the other peak values. This indicates that the addition of the outer stations enhances the control of the far-field attenuation by increasing the spread of data with respect to distance for the individual earthquakes.

Comparison with Other Studies

Previous discussions of peak vertical ground motion have seldom gone beyond PGA (Donovan, 1982; Campbell, 1982; Abrahamson and Litehiser, 1989), and none have considered digital high quality data from a dense array with similar subsurface conditions. For horizontal PGA, a partial analysis of the SMART-1 data is reported by Tsai and Bolt (1983) and Loh (1984). These authors studied only four of the earthquakes and performed no direct regression on PGV and PGD. This study is therefore unique in this respect.

The model derived by Campbell (1982) for peak vertical acceleration (in g) is given below in terms of the log of acceleration in

$$\ln(Y) = -2.91 + .784M - 1.43 \ln(R+3.33e^{.108M})$$

The model derived by Donovan (1982) expressed in a form similar to equation (1) is given below for peak vertical acceleration in g:

$$\ln(Y) = -3.27 + 0.76M_L - 1.27 \ln[(R^2+7.0^2)^{1/2}]$$

When comparing the results of this study for peak vertical acceleration with those of Campbell and Donovan, it should be noted that there are differences in the definitions of distance used in these studies. This study defines R as hypocentral distance, while Campbell and Donovan employ alternate measures of significant distance. Campbell defines R as shortest distance to the fault rupture surface, while Donovan uses shortest distance to the surface projection of the fault plane.

With respect to magnitude, Donovan uses M_L, Campbell uses M_L for $M<6.0$ and M_s for $M\geq6.0$, while this study uses M_L for $M<6.6$ and M_s for $M\geq6.6$. Abrahamson and Litehiser adopted Campbell's definitions. Another notable difference is that those studies are based on worldwide near-field data whereas the present study is based on records from a single region.

The predicted values for peak vertical acceleration, for magnitudes 5.5, 6.5, and 7.5, are compared with those of Campbell (1982) and Donovan (1982) in Figure 3-7. The first notable difference is that this study displays slightly less peak amplitude close to the source. This is the opposite of what would be expected, since hypocentral distance models the recording (with a given amplitude) farther from the source, and therefore should predict larger amplitudes for a given distance. The second difference is that this model equation (1) displays greater saturation of ground-motion amplitudes with magnitude. Although this partially explains the lower amplitudes seen close to the source, it is also unexpected that the hypocentral modelling of distance should produce greater magnitude saturation than a significant distance model (see Section 3.7).

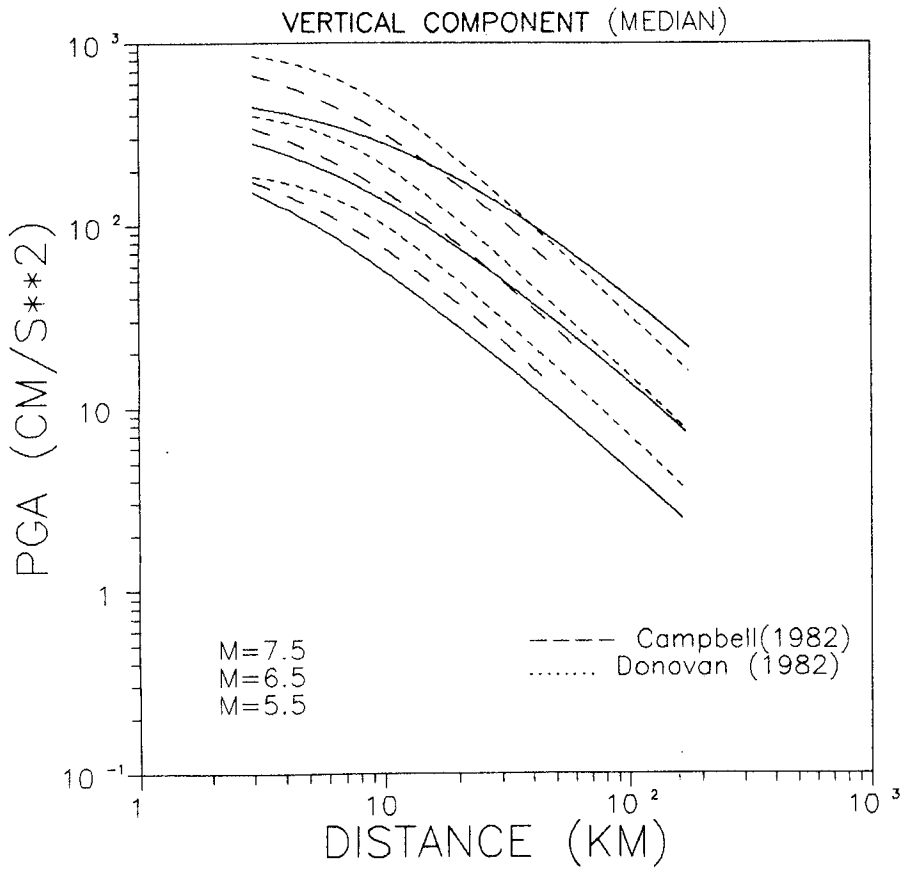

Figure 3.7 - Comparison of the predicted mean vertical PGA for this study (solid curves), and those of Campbell (1982) and Donovan (1982).

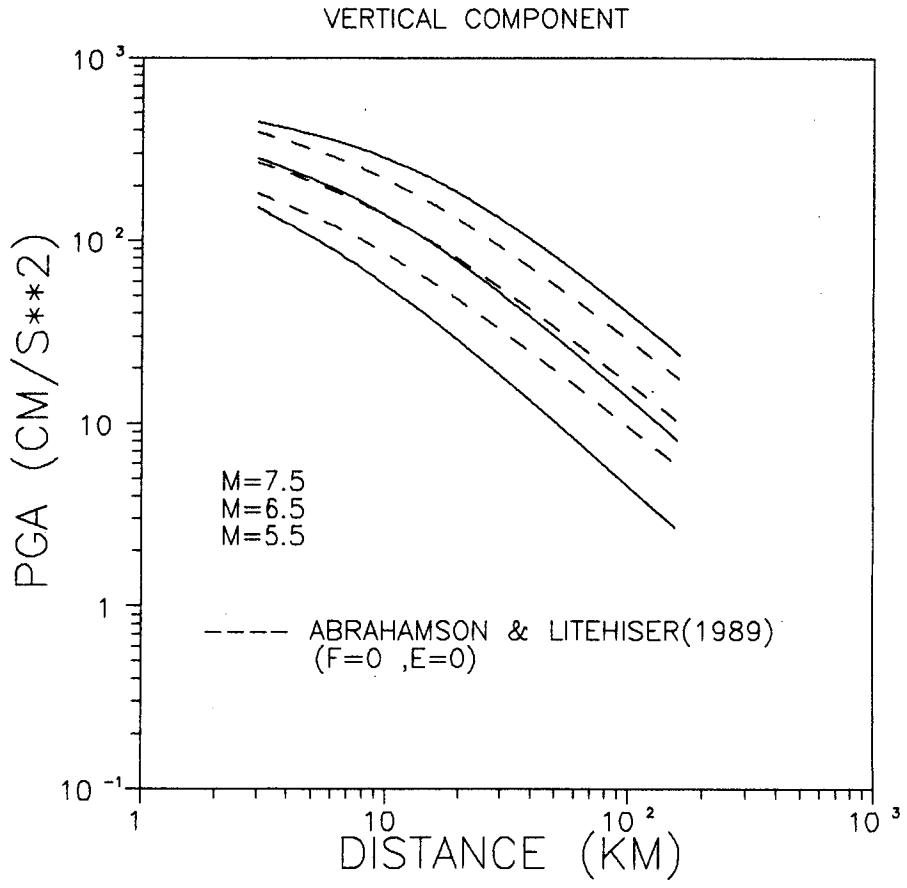

Figure 3.8 - Comparison of the predicted mean vertical PGA for this study (solid curves), and those of Abrahamson and Litehiser (1989). The latter estimates are for intraplate non-reverse sources.

This study also displays lower attenuation with distance than that of either Campbell or Donovan. This is demonstrated by the lower value for the distance parameter d and by the flatter slopes of the attenuation curves in Figure 3-7. This difference is rather surprising, since the reported crustal absorption rates (Q) for the Taiwan region (Chang and Yeh, 1983) are comparable to those of the western U.S. (Singh, 1981), at least in the 1 to 2 Hz frequency range.

Finally the present results show larger scaling with magnitude at hypocentral distances greater than about 30 kilometers. This is seen in the relative spread between curves in Figure 3-7 and by the relative size of the b term in the equations. However, the greater saturation of ground motion with magnitude significantly decreases the scaling with magnitude, in the near field.

The model derived by Abrahamson and Litehiser (1989) expressed as the natural log of peak vertical acceleration in g is given below for recordings on soil:

$$\ln (Y) = -2.65 + 0.564M - 1.096 \ln(R+e^{0.256M}) + 0.22F$$

where F is a scaling variable for fault type. This scaling variable adjusts the ground-motion amplitudes linearly with distance and magnitude and therefore does not affect the shape of the model.

Figure 3-8 compares the predictions from the present study with those of Abrahamson and Litehiser. Although at the center of the data, about magnitude 6.5, the predicted values are very similar, the Abrahamson and Litehiser equation is less sensitive to magnitude. This is evidenced by the widening differences with increasing and decreasing magnitude, in Figure 3-8,and by their smaller coefficient of b. The models scale similarly with distance in the far field (coefficient d), while that of the present study still shows greater magnitude saturation.

3.3 PEAK VALUES OF THE HORIZONTAL COMPONENT

3.3.1 Results

Regression on the full data set described in Section 2 (less the one station located on rock) resulted in the relationships given in Table 3-4. Results are given for the horizontal component of PGA, PGV, and PGD.

Note that two sets of analyses are included for the horizontal component: (1) Peak values recorded by individual horizontal components are treated as individual observations, and (2) the average of the two horizontal components for each record is considered a single observation. Comparing the equations for cases (1) and (2), we note that the two are almost identical. Plots of the results for PGA, PGV and PGD (Figure 3-9) also show no significant difference between the predicted values. However, when the two horizontal components are averaged in case (2), the standard deviation is reduced since the variation in amplitudes between the two components has been removed. Review of Table 3-4 indicates that the uncertainty is decreased by 7%, 6%, and 13% for PGA, PGV, and PGD, respectively. All further discussion is based on the mean of the horizontal components (i.e. case (2) in Table 3-4).

Figures 3-10 to 3-12 plot these predictions as a function of distance for magnitudes 5.5, 6.5 and 7.5. The plus and minus one standard deviation values are given by the dashed lines.

Results for the average horizontal peak values are also displayed as a function of magnitude in Figures 3-13 to 3-15. They display similar characteristics to the corresponding plots for the vertical component, see Section 3.2.1. However, the prediction curves for PGD demonstrate a greater degree of magnitude saturation than those for PGV or PGA, the opposite of what is seen for the vertical component (also, compare Tables 3-3 and 3-4).

Table 3.4 - Results of Regression Analysis on Peak Horizontal Ground-Motion Parameters Across the Entire Array

Ground-Motion Parameter	a	b	c_1	c_2	d	σ	DMS %	No. of Obs.
Case 1 - Individual components,								
PGA(g)	-5.610	0.951	0.349	0.478	-0.818	0.497	41	474
PGV(cm/sec)	-4.216	1.575	0.235	0.487	-1.089	0.569	34	468
PGD(cm)	-4.952	1.644	0.114	0.676	-1.387	0.805	57	424
Case 2 - Mean of the two components,								
PGA(g)	-5.502	0.934	0.411	0.452	-0.814	0.462	39	236
PGV(cm/sec)	-4.164	1.576	0.210	0.510	-1.097	0.537	36	232
PGD(cm)	-4.468	1.589	0.133	0.660	-1.411	0.790	59	189

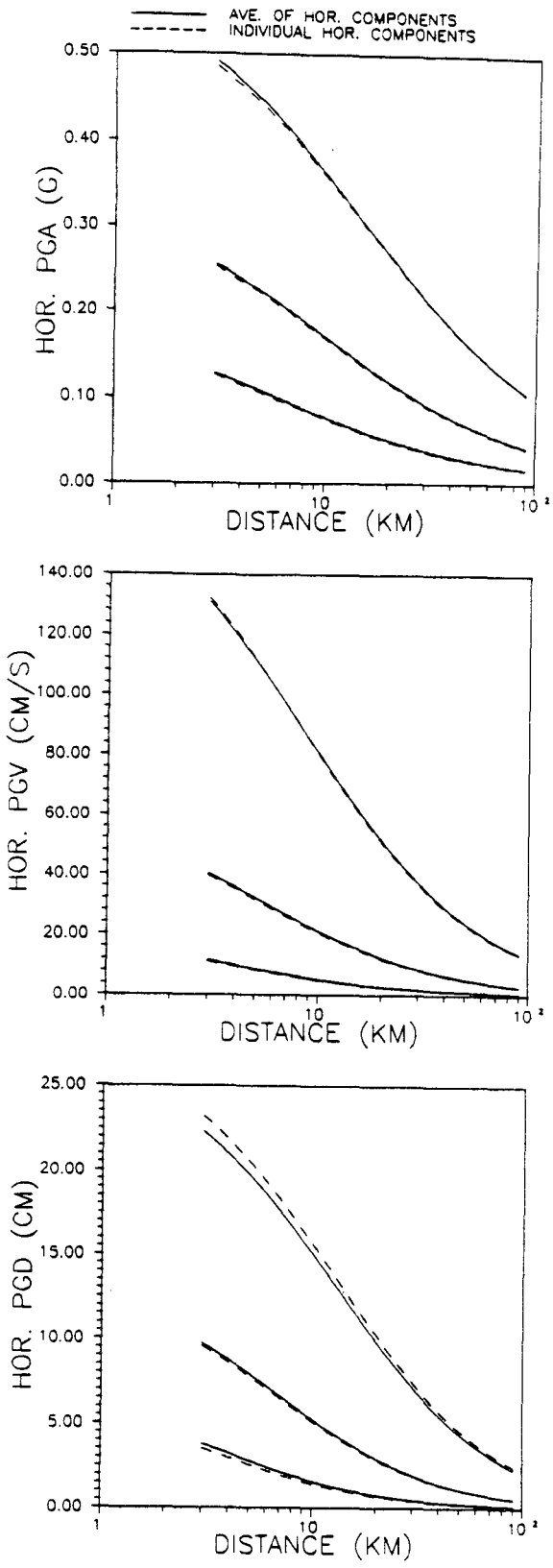

Figure 3.9 - Comparison of the prediction for horizontal PGA, PGV and PGD when regression is applied to the mean of the two components (solid curves) or to the individual components (dashed curves). Predictions are for M7.5 6.5 and 5.5, respectively for all three ground-motion parameters.

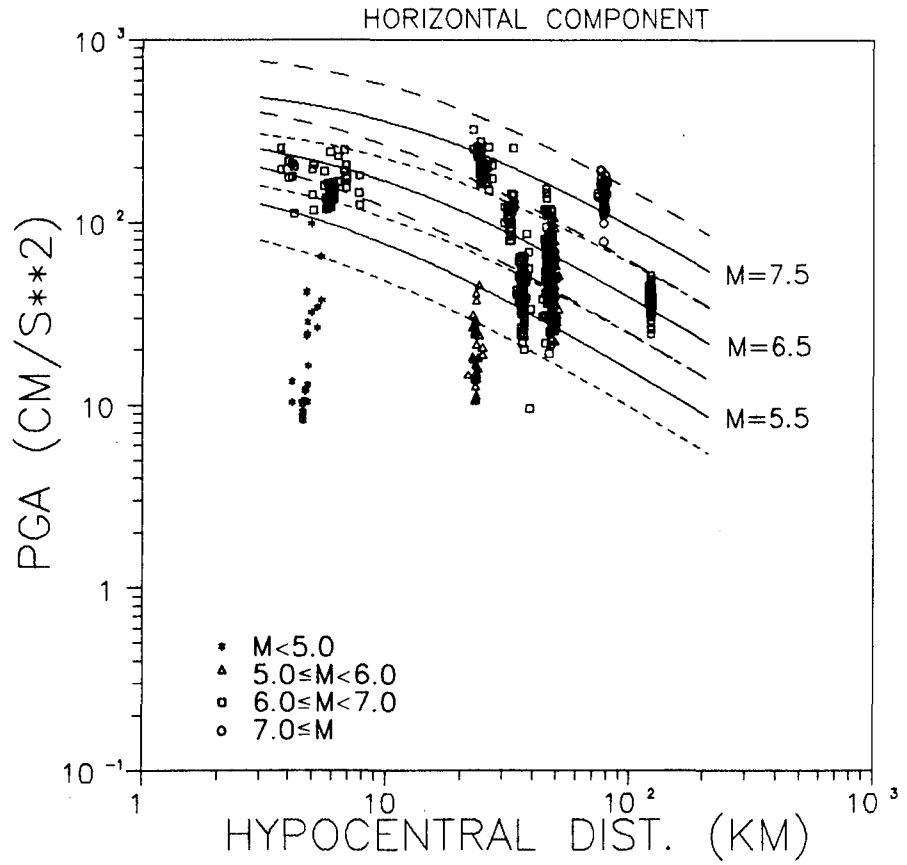

Figure 3.10 - Overlay of the observed horizontal PGA and predicted attenuation curves at three magnitudes. Solid curves show median estimates, short and long dashes show minus and plus one standard deviation, respectively.

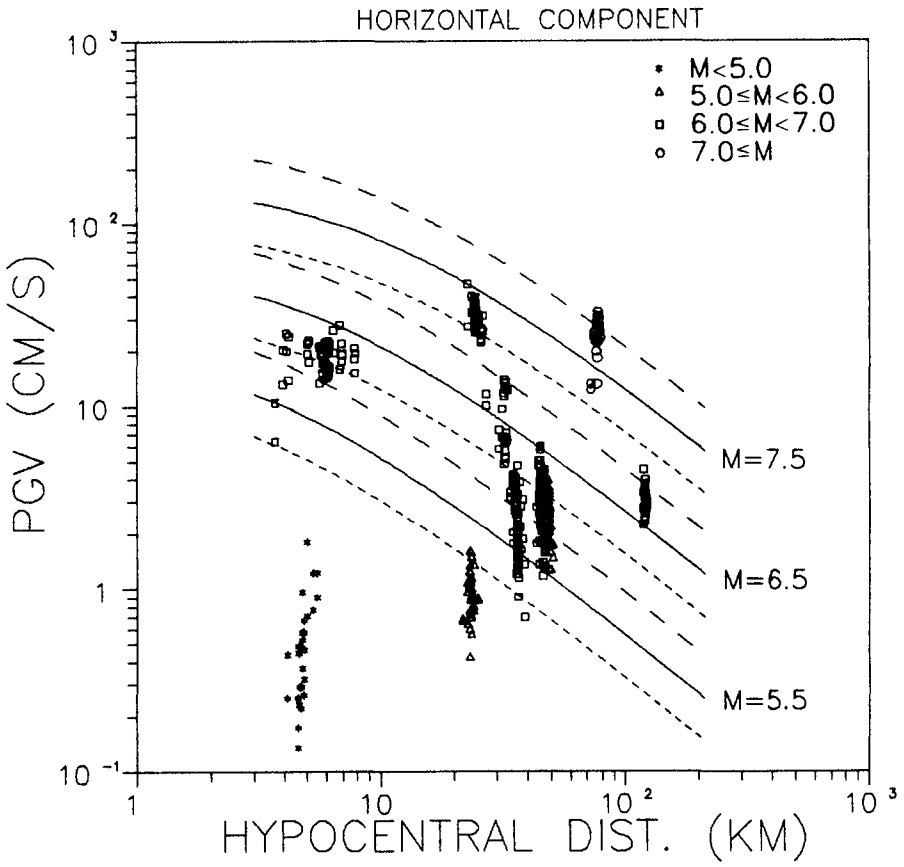

Figure 3.11 - Overlay of the observed horizontal PGV and predicted attenuation curves at three magnitudes. Solid curves show median estimates, short and long dashes show minus and plus one standard deviation, respectively.

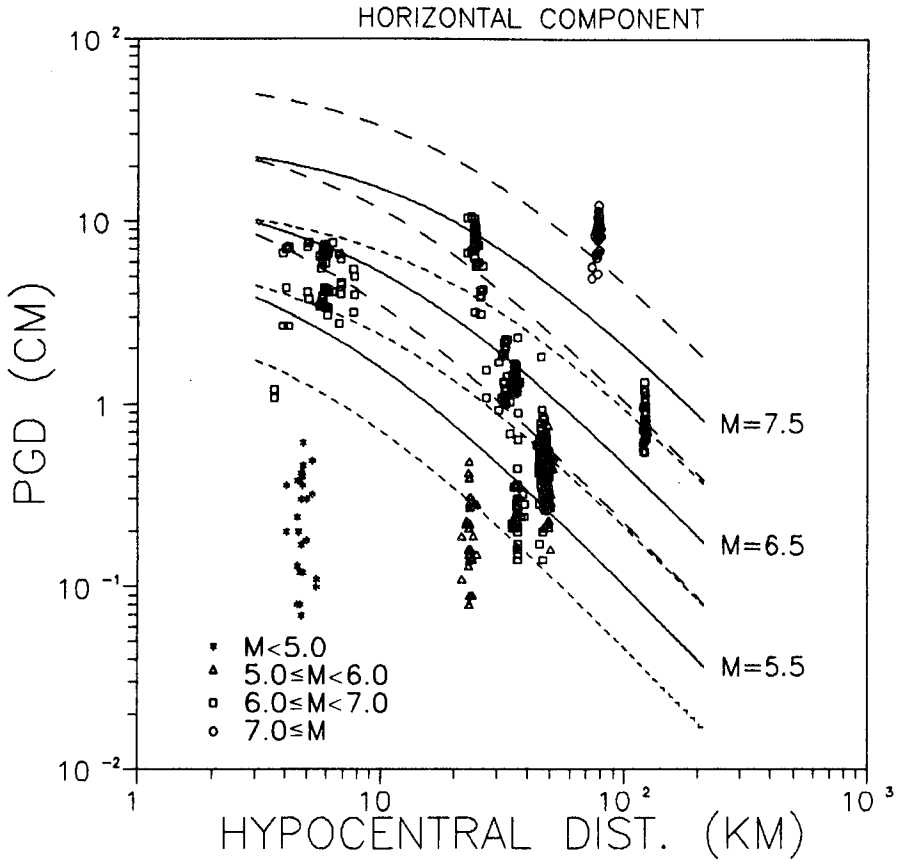

Figure 3.12 - Overlay of the observed horizontal PGD and predicted attenuation curves at three magnitudes. Solid curves show median estimates, short and long dashes show minus and plus one standard deviation, respectively.

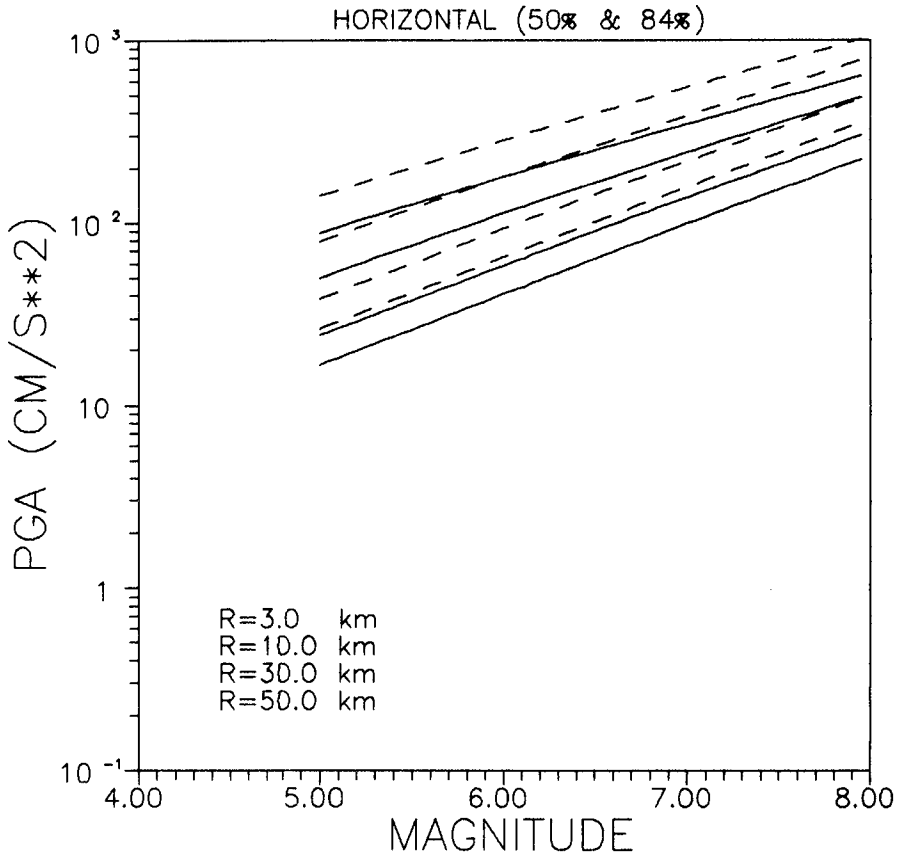

Figure 3.13 - Predicted horizontal PGA at 50% and 84.1% probabilities for four specified hypocentral distances as a function of magnitude.

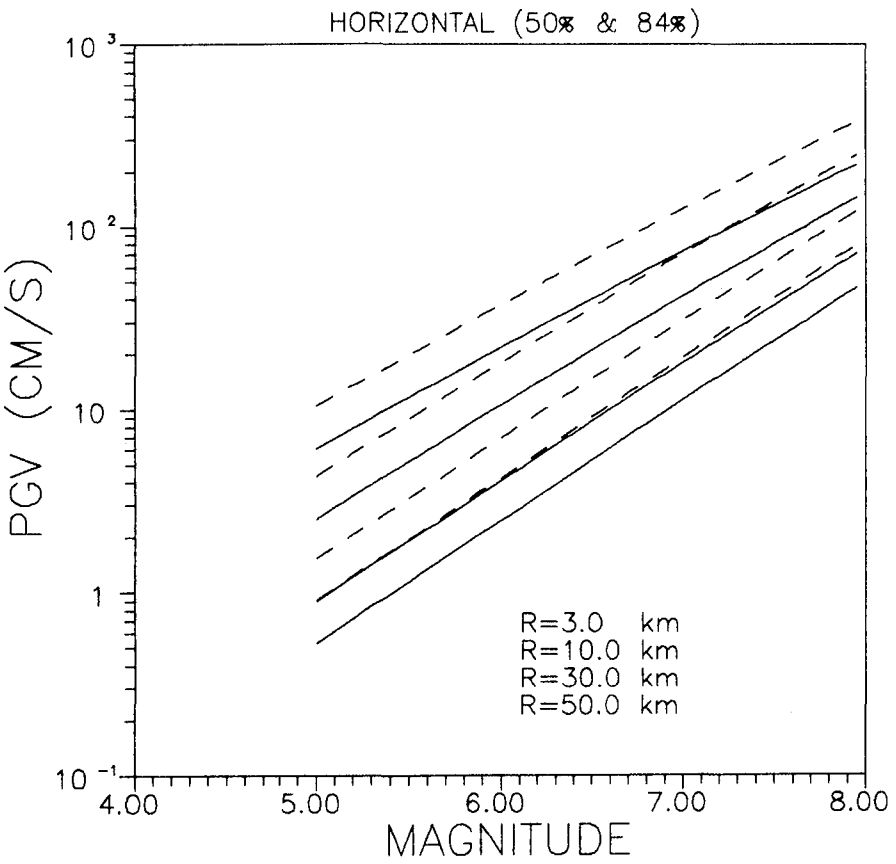

Figure 3.14 - Predicted horizontal PGV at 50% and 84.1% probabilities for four specified hypocentral distances as a function of magnitude.

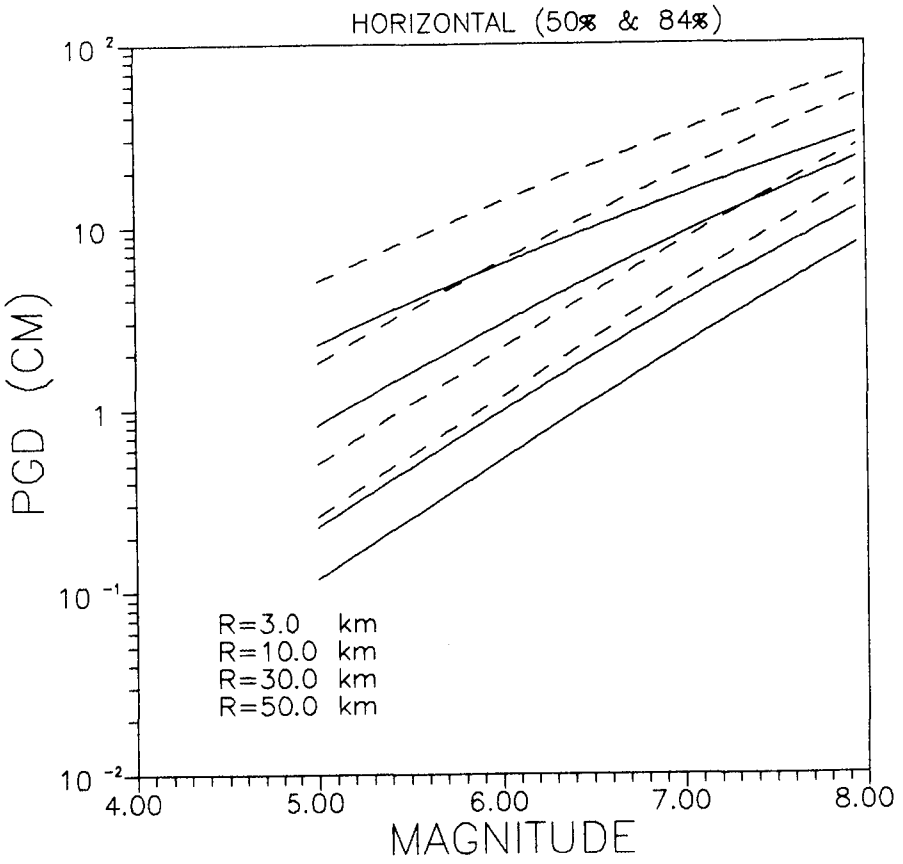

Figure 3.15 - Predicted horizontal PGD at 50% and 84.1% probabilities for four specified hypocentral distances as a function of magnitude.

3.3.2 Discussion

Comparison with Vertical Component

An interesting trend is observed with respect to far-field attenuation, represented by the coefficient d.

Horizontal PGA exhibits lower attenuation (d=-0.81) than does the vertical component (d=-1.22), which has a higher frequency content than the horizontal. This is expected, since it is thought that higher frequency energy is absorbed faster than the lower frequencies.

A similar trend is observed when comparing different peak parameters of the vertical component. The coefficient d decreases from PGA to PGV to PGD, indicating decreasing attenuation with decreasing frequency. Again, this would normally be expected, since the higher frequency PGA should attenuate faster than PGV and PGD, associated with decreasing predominant frequencies. This trend is graphically displayed in Figures 3-4 to 3-6. The greater the spread between lines the greater the scaling of amplitude with distance. Note that the spread decreases from PGA to PGV to PGD.

However, an opposite trend is observed when comparing Figures 3-13 to 3-15 for the horizontal component. The spread between the predicted values increases from PGA to PGV to PGD, indicating that the longer period PGD attenuates more rapidly than the higher frequency PGA. This is also seen in Table 3-4, since the coefficient d increases from PGA to PGV to PGD. This is rather unexpected, since, for a constant Q, attenuation should decrease with decreasing frequency (as seen by the regression results reported by McGuire, 1977; Cornell et al., 1979; Hasegawa et al., 1981; Nuttli and Hermann, 1984). It is interesting, however, to note that a trend similar to the one observed for the far-field coefficient of attenuation for horizontal PGA has also been reported by Boore et al. (1980) for small earthquakes (M5.0-5.7) at close-in distances(5-30 km). At this time, there is no definite explanation for this phenomenon. However, this effect could be due to either

- different behavior of Q_α and Q_β with respect to frequency, or

- coupling between high frequency Lg and other forms of seismic energy. Since the propagation of Lg is geologically controlled, this effect would then be region specific.

This unexpected unexpected trend, observed for the horizontal component, is also seen in the values of DMS. Vertical PGA show 81% saturation decreasing to 56% for PGV and PGD, while horizontal PGA and PGV shows only 39% and 36% saturation increasing to 59% for PGD. These are also opposing trends with respect to frequency, since magnitude saturation is thought to be a function of frequency content (see Section 3.7 for further discussion).

Comparison with Other Studies - PGA

Results for horizontal PGA (Table 3-4) are compared with those of Campbell (1981) and Joyner and Boore (1981). The model derived by Campbell is given below for the natural log of PGA in g:

$$\ln(PGA) = 1.016 + 0.868M - 1.09 \ln(R + 0.0606e^{0.7M})$$

The model derived by Joyner and Boore is in a different functional form, as given below for the log of PGA in g:

$$\log(PGA) = -1.02 + 0.249M - \log r - 0.00255r$$

$$\text{where } r = (d^2 + 7.3^2)^{1/2}$$

where d is distance.

When comparing the results of this study for peak horizontal acceleration with those given above, it should be noted that there are differences in the definitions of distance used in these studies. Campbell defines R as shortest distance to the fault rupture surface, while Joyner and Boore use shortest distance (d) to the surface projection of the rupture. This study, on the other hand, defines R as hypocentral distance. With respect to magnitude, Campbell uses M_L for $M<6.0$ and M_s for $M\geq6.0$, while this study uses M_L for $M<6.6$ and M_s for $M\geq6.6$. Joyner and Boore use moment magnitude. Another notable difference is that the earlier studies are based on worldwide near-field data,

whereas the present study is based on records from a single region. Finally, while this study and that of Campbell regress on the mean of the horizontal components, Joyner and Boore report on the maximum horizontal. The maximum horizontal may be approximated by increasing the median prediction by 13% (Campbell, 1981).

The predicted values for peak horizontal acceleration, for magnitudes 5.5, 6.5, and 7.5, are compared to those of Campbell (1981) and Joyner and Boore (1981) in Figure 3-16. As with vertical PGA, a notable difference is that this study displays slightly lower peak amplitudes close to the source. This is the opposite of what would be expected, since hypocentral distance models the recording (with a given amplitude) further from the source, and therefore should predict larger amplitudes for a given distance.

Another difference is that this study displays significantly less far-field attenuation than the other studies. This can be seen by the more gradual slope of the predicted values with increasing distance (Figure 3-16). Also, Campbell's coefficient for d (far-field slope) is -1.09 while in this study is only -0.814. The coefficient d on equation (1) cannot be compared with that of Joyner and Boore, since they effectively set the far-field coefficient of attenuation to one and let their distance term fit the far-field slope. (Note that in Joyner and Boore (1981), the coefficient d represents shortest distance and not far-field attenuation coefficient).

Finally the plots show that Joyner and Boore found no saturation with magnitude, while Campbell found higher saturation than the present study. (88% vs. 39%, as seen in Table 3-4 and Campbell, 1981).

Comparison with other studies - PGV

Campbell (1984) and Joyner and Boore (1981) report the following equations for the attenuation of horizontal Peak Ground Velocity (PGV) in cm/sec.

Campbell's equation is given in terms of the natural log of PGV for the mean of the horizontal components:

$$\ln (PGV) = -0.798 + 1.02M - 1.26 \ln (R + 0.0150e^{0.812M})$$

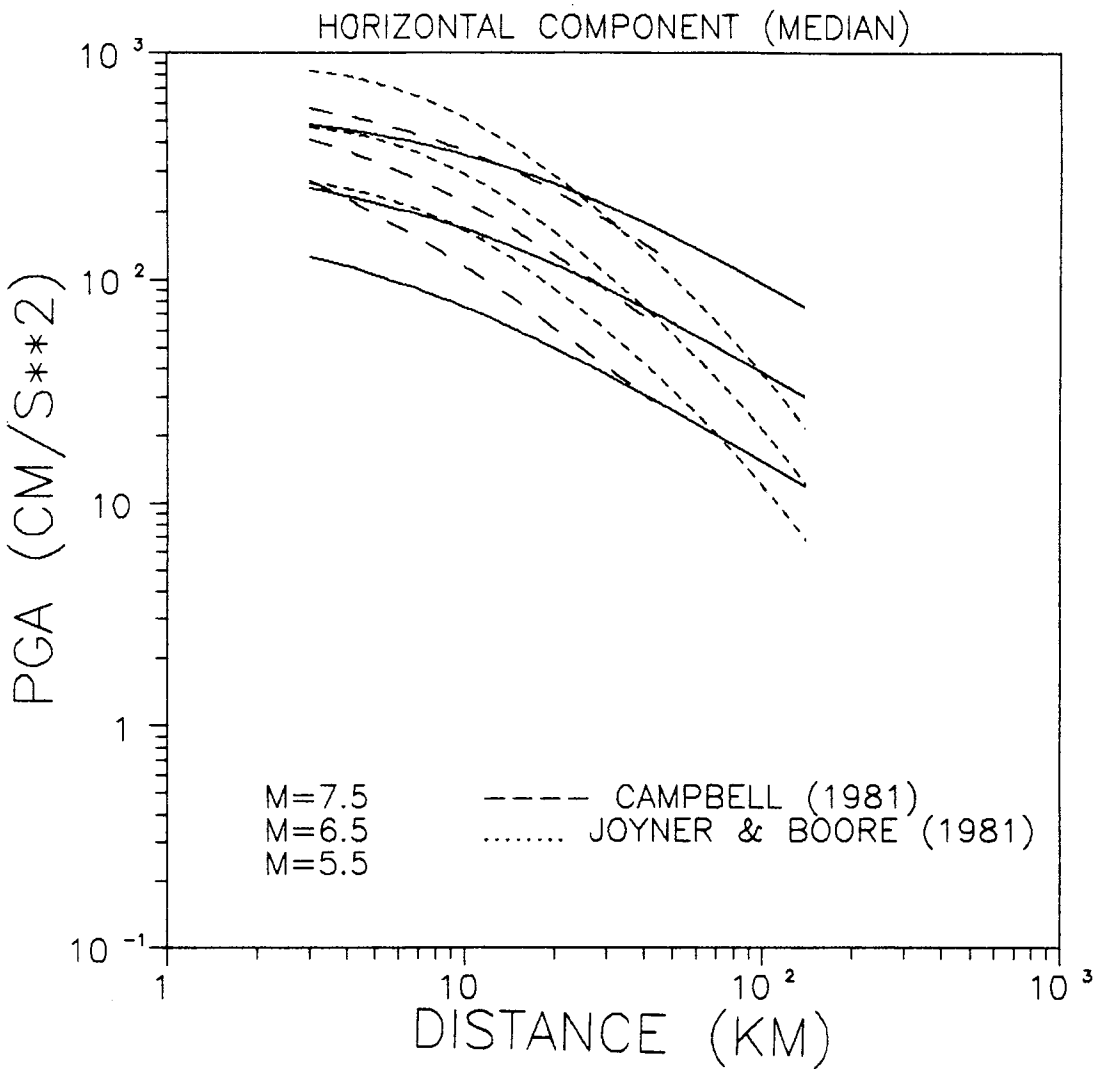

Figure 3.16 - Comparison of the predicted mean horizontal PGA for this study (solid curves), and those of Campbell (1981) and Joyner and Boore(1981).

The model derived by Joyner and Boore (1981) is in a different functional form, as given below. For the maximum horizontal component:

$$\log (PGV) = -0.67 + 0.489M - \log r - 0.00256r$$

$$\text{where } r = (d^2+4.0^2)^{½}$$

The same differences exist between the studies with respect to definition of distance and magnitudes (see discussion of PGA, Section 3.2.2). Again, as for PGA, this study shows less attenuation with distance in the farfield. Also, while Joyner and Boore found no saturation with magnitude and this study found only 36%, Campbell found that PGV saturated 100% with magnitude. Finally comparison of the magnitude scaling coefficient (b) indicates that this study shows greater scaling (b=1.58) with magnitude than that found by Campbell (b=1.02). Converting the Joyner and Boore coefficient from $\log_{10}$ to natural log, their relationship shows $b_{ln} = 2.303 * 0.489 = 1.126$; greater than Campbell to value but less than that of this study.

3.4 RESPONSE SPECTRA

Response spectra at 5% damping are calculated for the full data set at the following periods:

$T_{(sec.)}$ = 0.03, 0,04, 0.05, 0.075, 0.10, 0.111, 0.15, 0.20, 0.286, 0.30, 0.40, 0.50, 0.60, 0.70, 0.80, 1.0, 1.5, 2.0, 3.0, 4.0, 5.0, 7.0, and 10.0.

The attenuation characteristics of the spectra are analyzed making use of the same functional form (Campbell, 1981) that was applied to the analysis of peak ground-motion values. Thus,

$$\ln(PSV) = a + bM + d \ln[R + c_1 e^{C_2 M}] \qquad (3)$$

where PSV is Pseudo Relative Velocity in cm/sec.

Regression analysis is performed for each spectral ordinate. As with the analysis of peak values, the one rock station in the data base is excluded from the analysis in order to

preserve the condition of similar site geology. The same weighting procedure is also applied. In this way, attenuation relationships are developed for both the vertical and the average horizontal value at each spectral ordinate. Regression results are presented for the vertical component in Table 3-5 and for the mean horizontal component in Table 3-6.

Note that the magnitude saturation parameter c_2 is equal to zero in the mid frequency range. For a few periods this parameter is constrained to be zero, as noted by the asterisk in the tables. This is done primarily to eliminate physically meaningless results at these periods (DMS > 100) where amplitude would decrease with increasing magnitude at zero distance. Also, these periods bordered the frequency range where the calculated value of c_2 is zero (DMS = 0; no magnitude saturation) and one of them had DMS near zero. The uncertainty is not affected by constraining c_2 to zero, as seen in the tables (the unconstrained cases are given at the bottom of the tables). This indicates that the constrained regression fits the data equally well. The results of these constrained cases are used in subsequent discussions of the spectral results.

Using these attenuation relationships, response spectra at 5% critical damping are plotted for magnitudes 5.0, 6.0, and 7.0 for the median predicted values of both the vertical and mean horizontal components (Figures 3-17 to 3-22). These spectra are given for source-to-site distances of 3, 10, 30 and 50 kilometers. Plots of the vertical median plus one standard deviation spectra are displayed in Figures 3-23 to 3-25.

Predicted values for response spectral ordinates at 5% damping are presented in an alternate format in Figures 3-26 to 3-33. For selected periods, predicted values of PSV are plotted versus magnitude for distances equal to 3, 10, 30, and 50 kilometers. The convergence of the lines with increasing magnitudes indicates saturation of PSV with magnitude. The further apart the lines, the more PSV scales with distance. These figures will be referred to in subsequent discussion.

Table 3.5 - Results of Regression Analysis on Pseudo Relative Velocity (PSV), Vertical Components *

Period (sec.)	a	b	c_1	c_2	d	σ	DMS %
0.03	-4.106	1.144	0.046	0.769	-1.294	0.546	87
0.04	-2.835	1.074	0.052	0.753	-1.395	0.552	98
0.05	-2.148	1.054	0.050	0.752	-1.438	0.562	102
0.075	-2.955	1.232	0.0309	0.805	-1.339	0.568	88
0.10	-3.598	1.339	0.017	0.878	-1.223	0.582	80
0.111	-4.072	1.405	0.0015	1.256	-1.166	0.614	104
0.150	-4.398	1.474	0.0013	1.346	-1.085	0.609	99
0.20	-3.732	1.319	5.408	0**	-0.968	0.614	0
0.286	-4.463	1.425	6.276	0	-0.958	0.617	0
0.30	-4.842	1.449	5.188	0	-0.908	0.622	0
0.40	-6.504	1.629	0.00009	1.673	-0.783	0.510	80
0.50	-7.234	1.890	0.00053	1.545	-1.004	0.559	82
0.60	-6.487	1.645	0.0769	0.686	-0.858	0.591	36
0.70	-6.585	1.696	0.0832	0.727	-0.904	0.553	39
0.80	-6.923	1.749	0.0512	0.759	-0.897	0.547	39
1.00	-6.497	1.701	0.049	0.755	-0.946	0.616	42
1.50	-6.171	1.800	0.0633	0.825	-1.117	0.716	51
2.00	-5.920	1.722	0.114	0.751	-1.085	0.709	47
3.00	-5.281	1.733	0.245	0.679	-1.326	0.703	52
4.00	-4.151	1.537	0.436	0.647	-1.299	0.678	55
5.00	-3.574	1.318	0.358	0.674	-1.105	0.726	57
7.00	-3.181	1.006	0.281	0.669	-0.788	0.693	52
10.00	-3.461	1.013	0.342	0.661	-0.858	0.632	56

* Regressions were performed on all earthquakes in the data base for all stations except the rock site (N=234).

** This value is assigned. The calculated value of 0.000004, resulted in an unacceptable value of 124% for DMS. Also note that at two other periods (0.05 and 0.111 sec), saturation is slightly exceeded.

Table 3.6 - Results of Regression Analysis on Pseudo Relative Velocity (PSV), Horizontal Components *

Period (sec.)	a	b	c_1	c_2	d	σ	DMS %
0.03	-3.833	0.939	0.188	0.596	-0.843	0.455	53
0.04	-2.887	0.910	0.122	0.710	-0.940	0.451	73
0.05	-2.162	0.922	0.145	0.729	-1.050	0.444	83
0.075	-2.092	0.883	0.072	0.767	-0.878	0.468	76
0.10	-1.747	0.699	0.609	0**	-0.582	0.505	0
0.111	-1.401	0.701	2.724	0**	-0.615	0.510	0
0.15	-0.116	0.836	18.495	0	-0.955	0.504	0
0.20	-1.285	1.035	15.444	0	-0.902	0.537	0
0.286	-2.614	1.290	9.181	0	-0.941	0.508	0
0.30	-2.865	1.346	8.284	0	-0.965	0.517	0
0.40	-3.756	1.523	7.225	0	-0.975	0.462	0
0.50	-4.297	1.620	7.712	0	-0.984	0.523	0
0.60	-5.203	1.719	5.227	0	-0.946	0.543	0
0.70	-5.653	1.800	4.779	0	-0.961	0.533	0
0.80	-5.825	1.881	5.125	0	-1.051	0.581	0
1.00	-6.435	2.033	2.900	0	-1.183	0.597	0
1.50	-7.352	2.124	0.016	0.753	-1.176	0.662	42
2.00	-6.928	2.067	0.025	0.748	-1.240	0.678	45
3.00	-6.950	2.201	0.070	0.733	-1.450	0.775	48
4.00	-5.825	2.057	0.142	0.690	-1.559	0.713	52
5.00	-4.520	1.788	0.180	0.683	-1.485	0.652	57
7.00	-4.049	1.551	0.161	0.685	-1.306	0.669	57
10.00	-4.859	1.621	0.155	0.691	-1.339	0.664	57
Original Cases with c_2 Uncons-trained							
0.10	-2.226	0.871	0.00024	1.583	-0.713	0.503	130
0.111	-1.475	0.727	1.355	0.143	-0.636	0.511	13

* Regressions were performed on all earthquakes in the data base for all stations except the rock site (N=236).

** This value is assigned. Note the unconstrained c_2 results listed at the bottom.

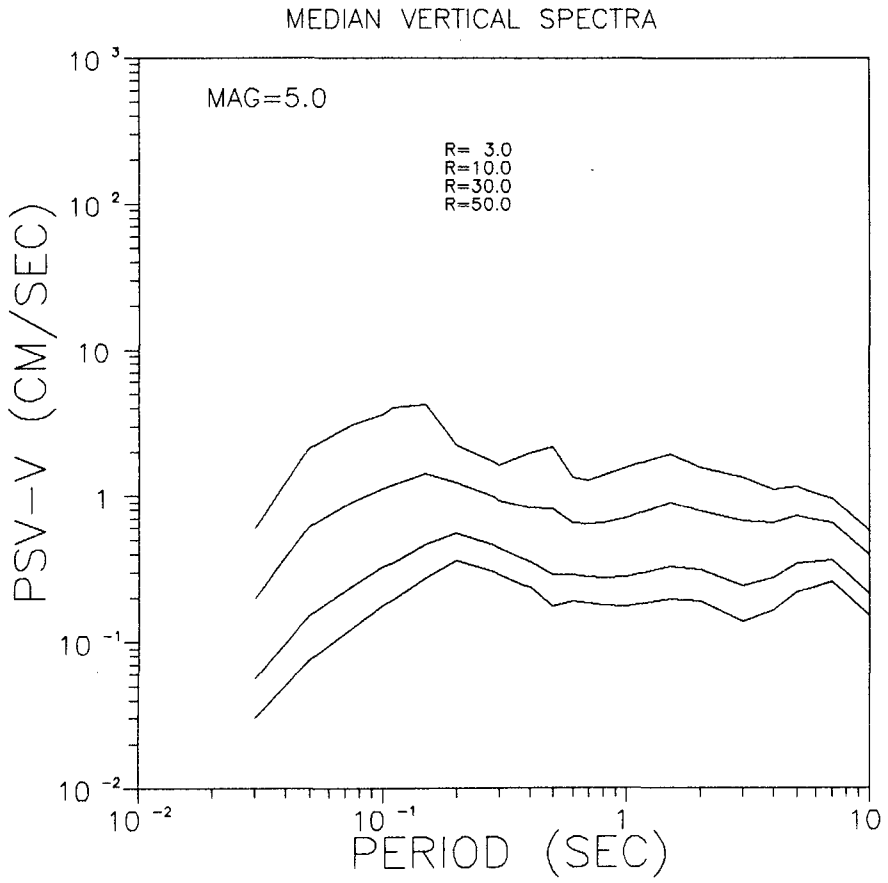

Figure 3.17 - Pointwise predicted mean vertical response spectra at 5% critical damping for M5 at four hypocentral distances of 3, 10, 30 and 50 km.

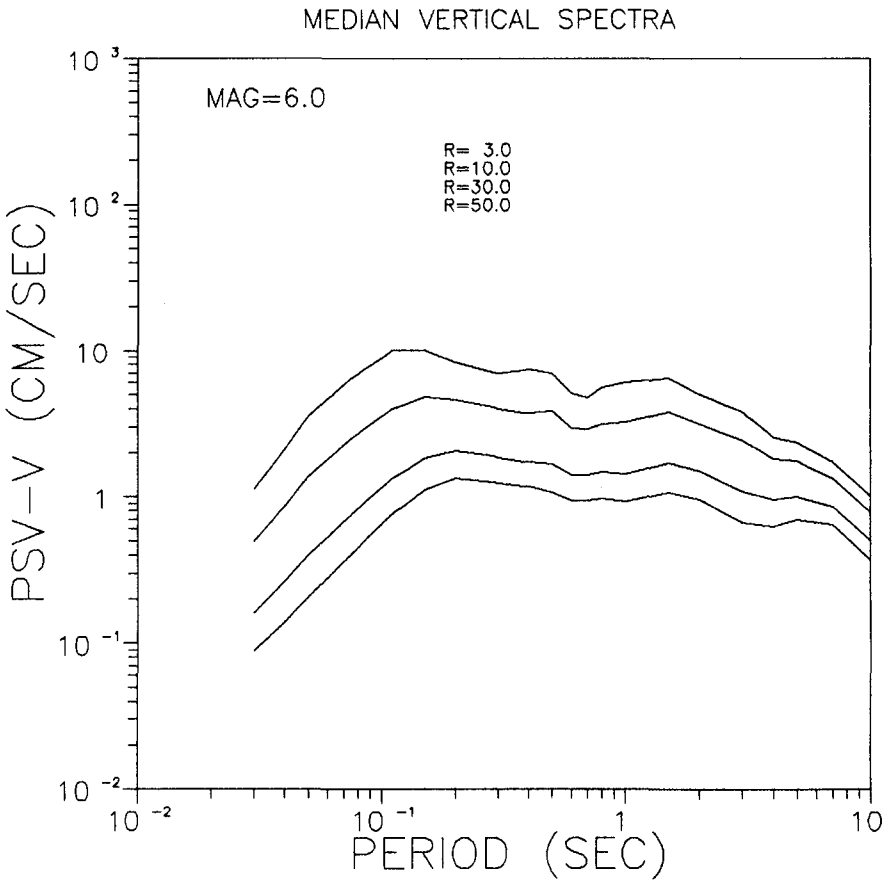

Figure 3.18 - Pointwise predicted mean vertical response spectra at 5% critical damping for M6 at four hypocentral distances of 3, 10, 30 and 50 km.

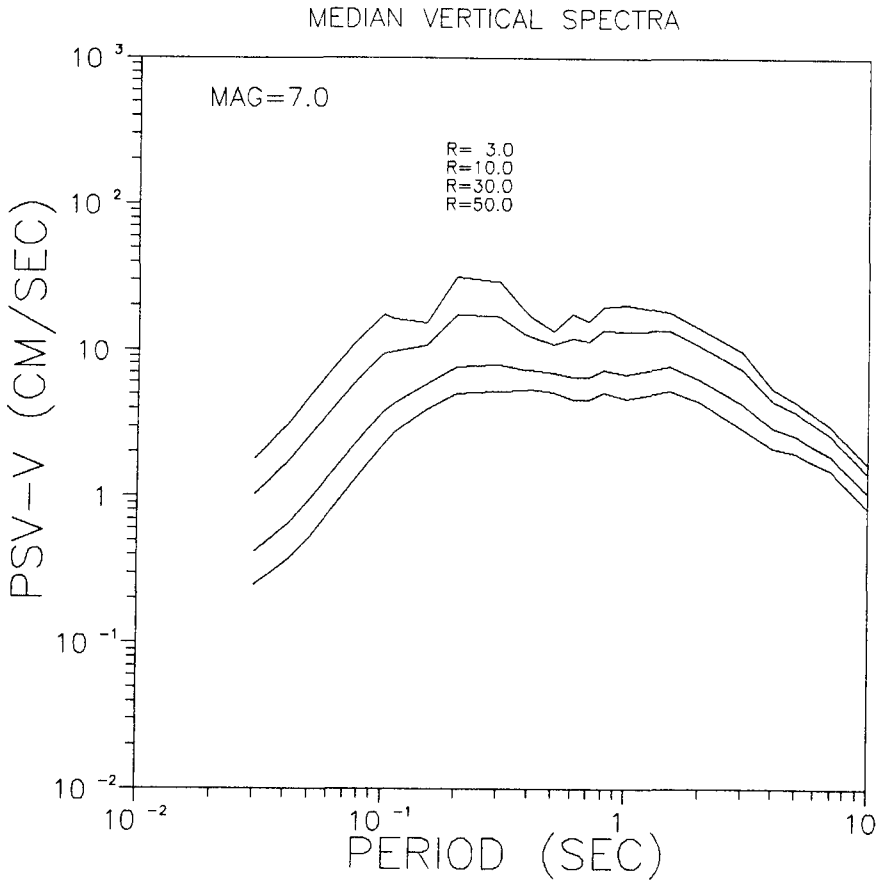

Figure 3.19 - Pointwise predicted mean vertical response spectra at 5% critical damping for M7 at four hypocentral distances of 3, 10, 30 and 50 km.

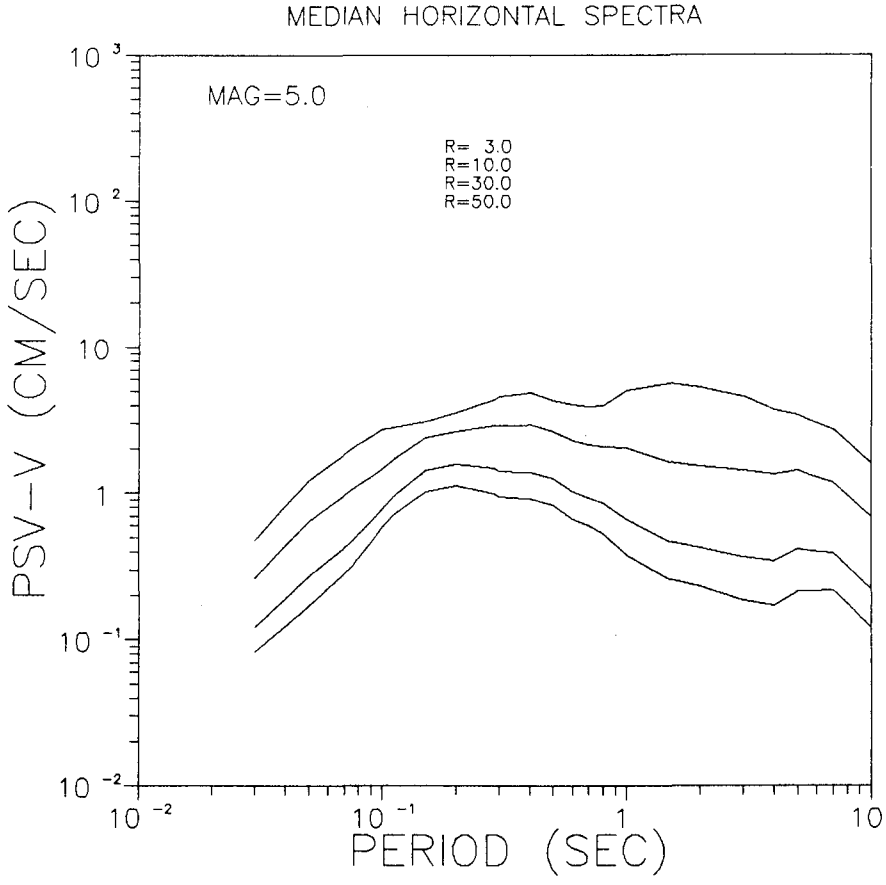

Figure 3.20 - Pointwise predicted mean horizontal response spectra at 5% critical damping for M5 at four hypocentral distances of 3, 10, 30 and 50 km.

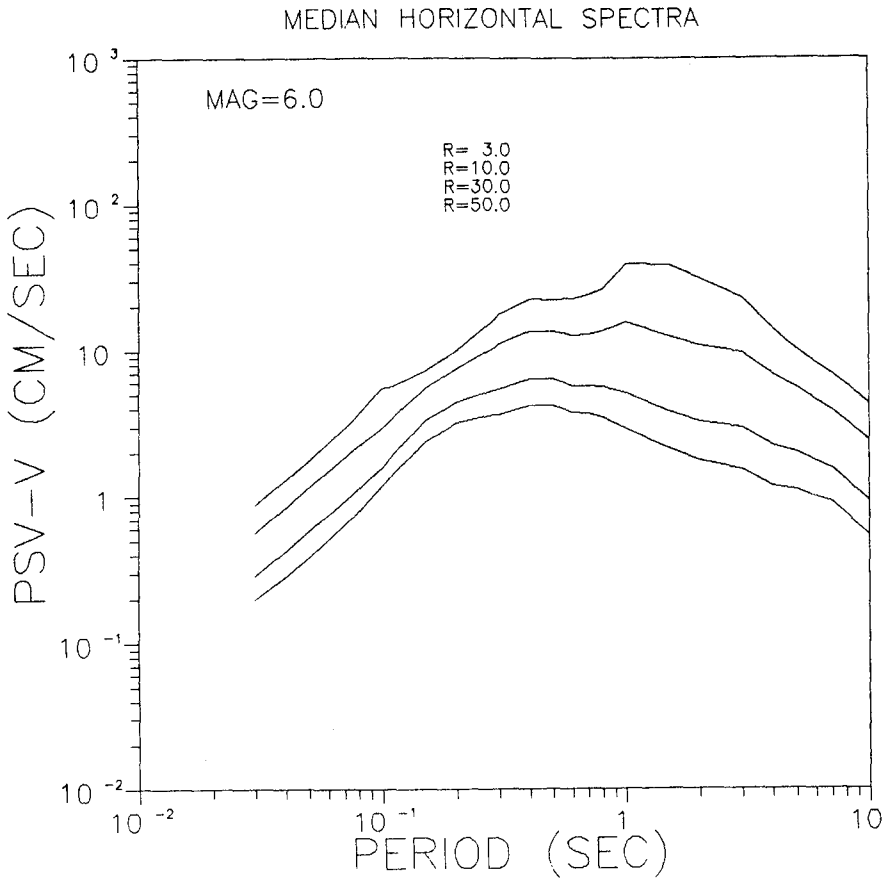

Figure 3.21 - Pointwise predicted mean horizontal response spectra at 5% critical damping for M6 at four hypocentral distances of 3, 10, 30 and 50 km.

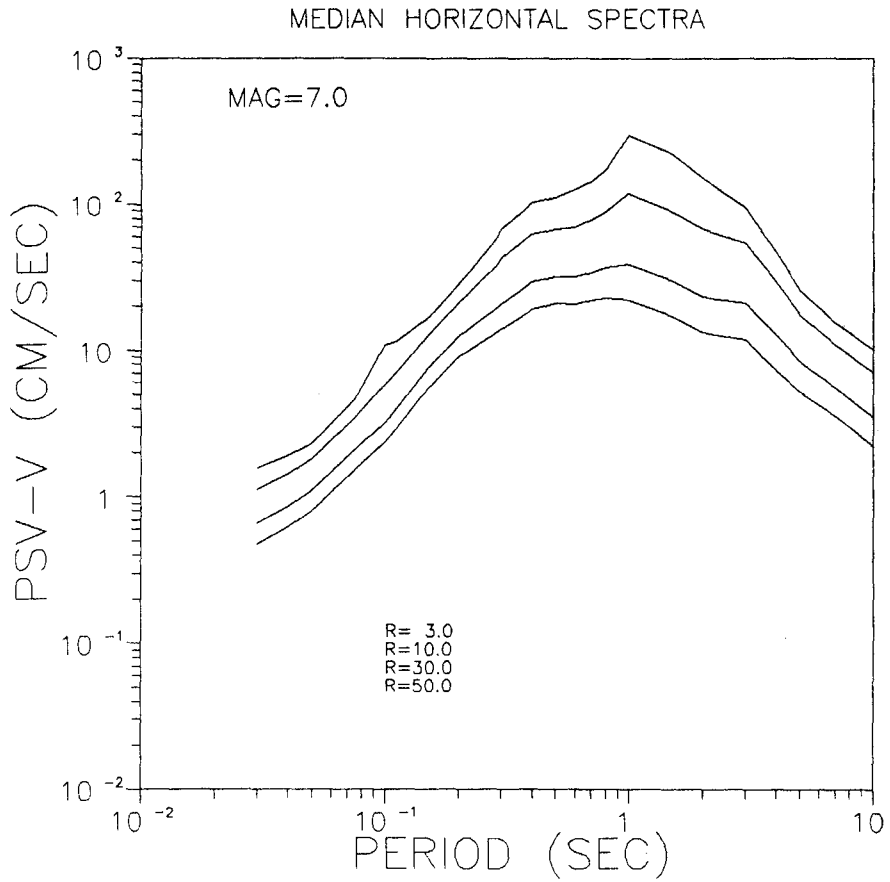

Figure 3.22 - Pointwise predicted mean horizontal response spectra at 5% critical damping for M7 at four hypocentral distances of 3, 10, 30 and 50 km.

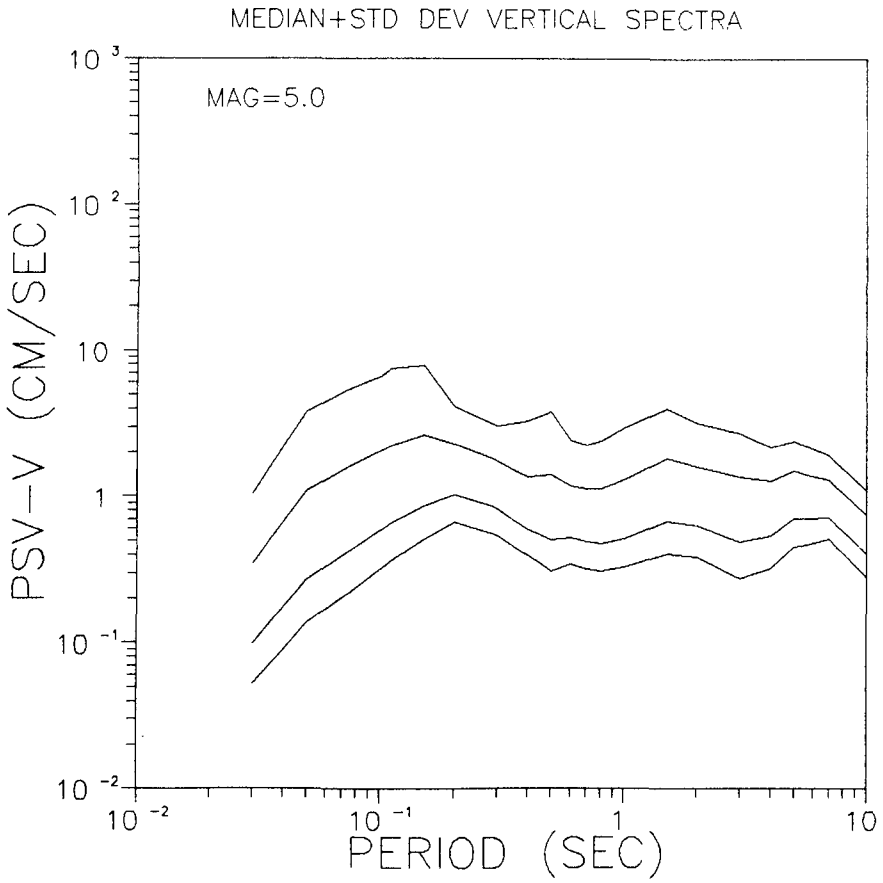

Figure 3.23 - Pointwise predicted vertical response spectra (84.1% probability) at 5% critical damping for M5 at four hypocentral distances of 3, 10, 30 and 50 km.

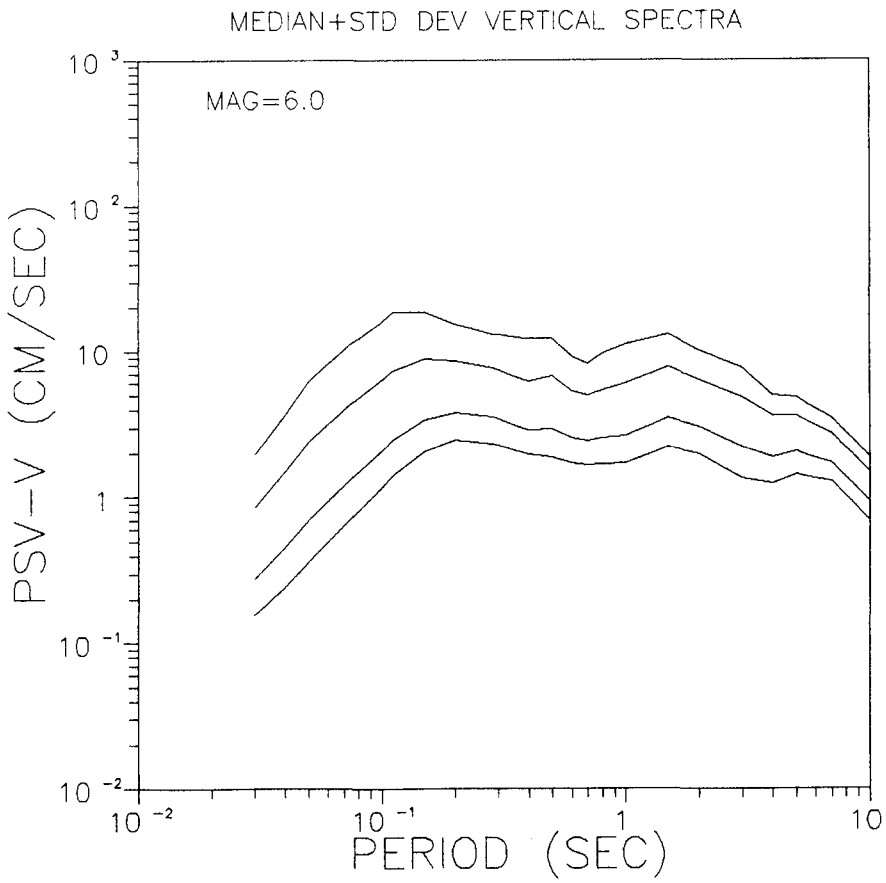

Figure 3.24 - Pointwise predicted vertical response spectra (84.1% probability) at 5% critical damping for M6 at four hypocentral distances of 3, 10, 30 and 50 km.

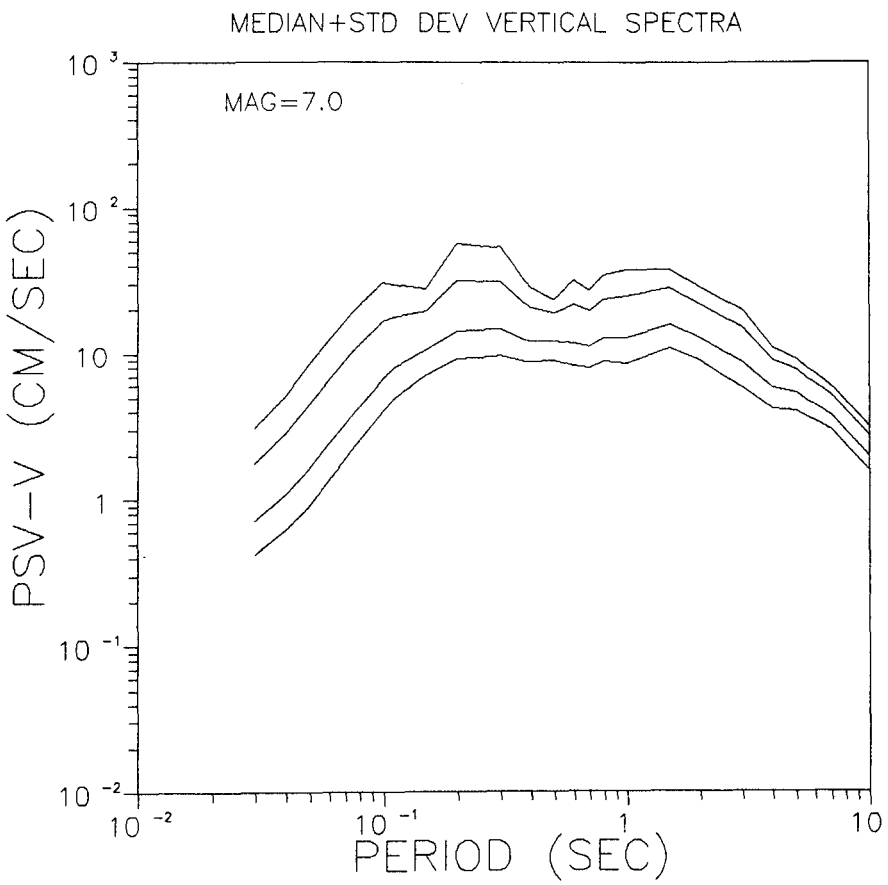

Figure 3.25 - Pointwise predicted vertical response spectra (84.1% probability) at 5% critical damping for M7 at four hypocentral distances of 3, 10, 30 and 50 km.

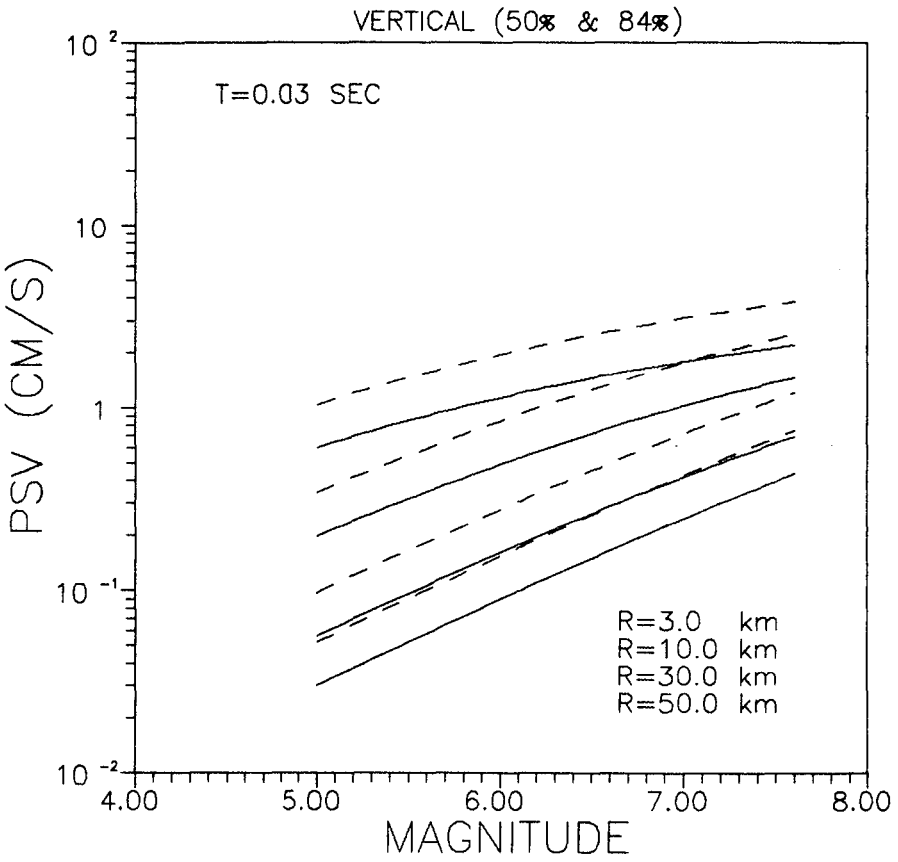

Figure 3.26 - Predicted vertical spectral amplitude at 0.03 sec period for 50% and 84.1 probabilities at four specified hypocentral distances as a function of magnitude.

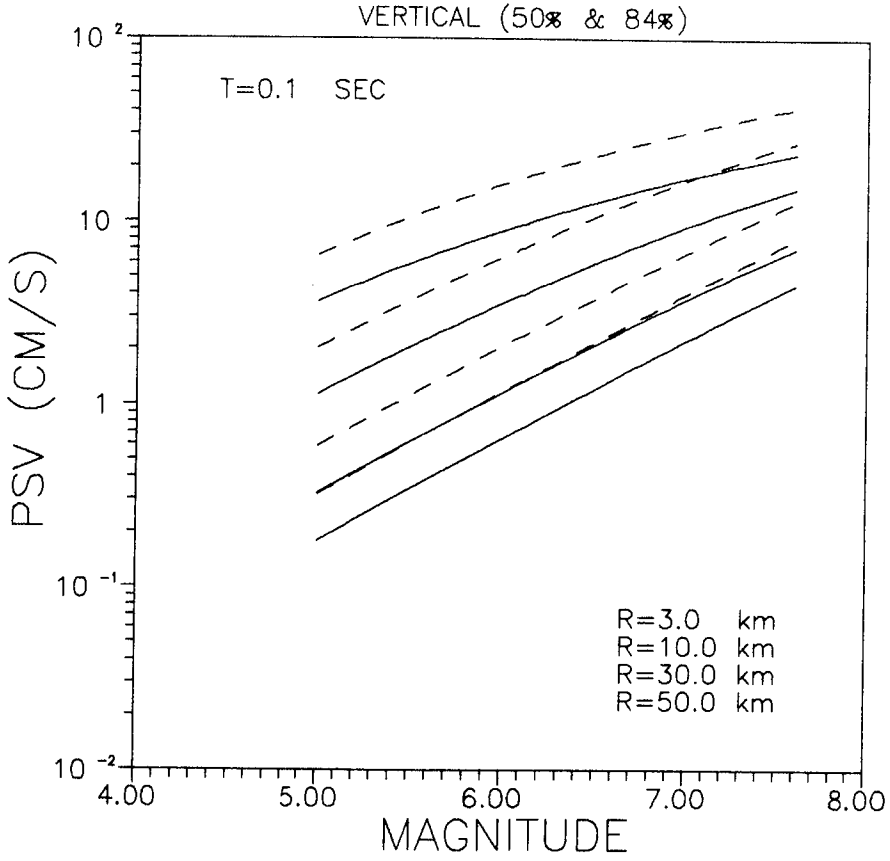

Figure 3.27 - Predicted vertical spectral amplitude at 0.10 sec period for 50% and 84.1 probabilities at four specified hypocentral distances as a function of magnitude.

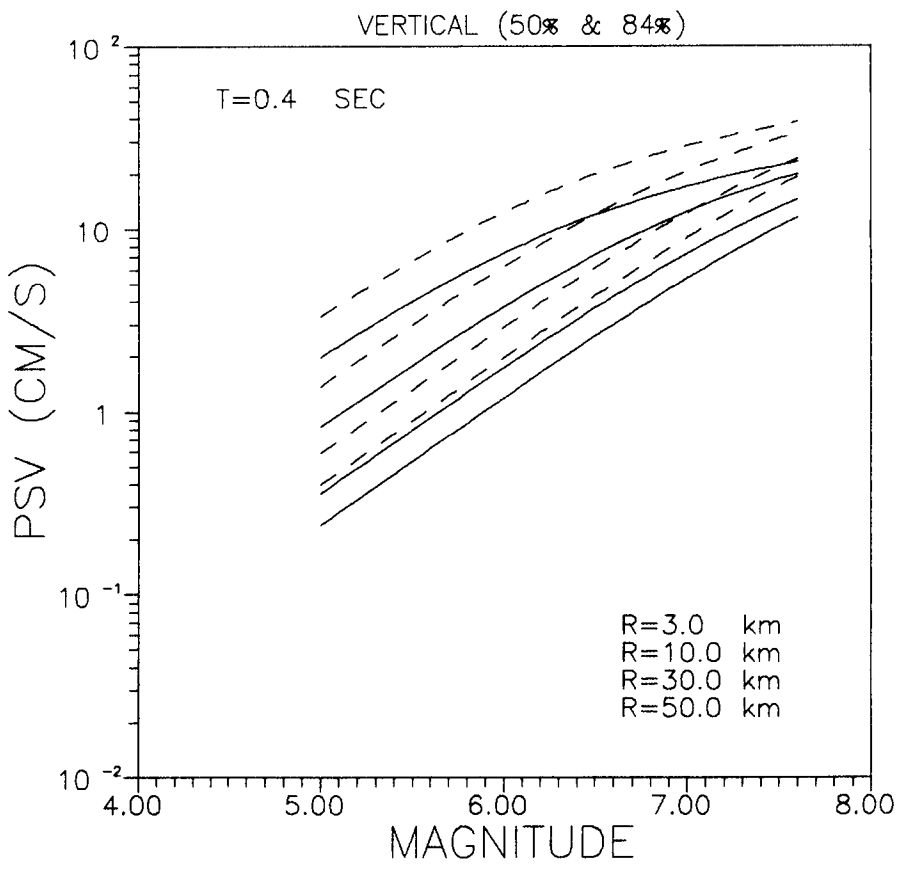

Figure 3.28 - Predicted vertical spectral amplitude at 0.40 sec period for 50% and 84.1 probabilities at four specified hypocentral distances as a function of magnitude.

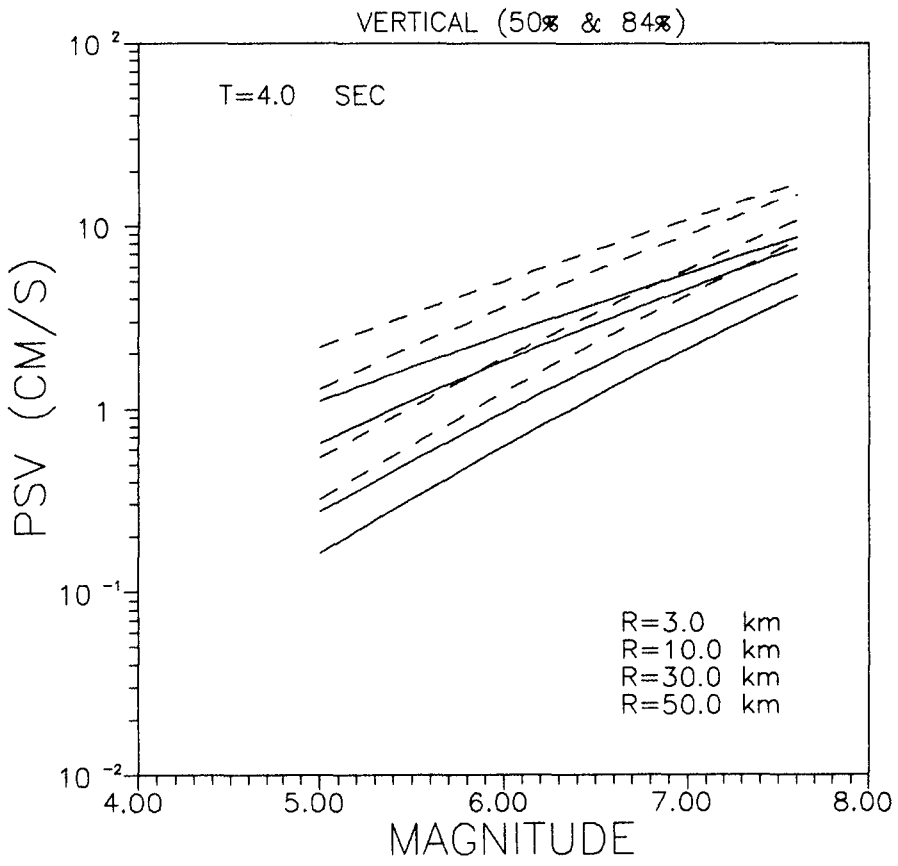

Figure 3.29 - Predicted vertical spectral amplitude at 4.0 sec period for 50% and 84.1 probabilities at four specified hypocentral distances as a function of magnitude.

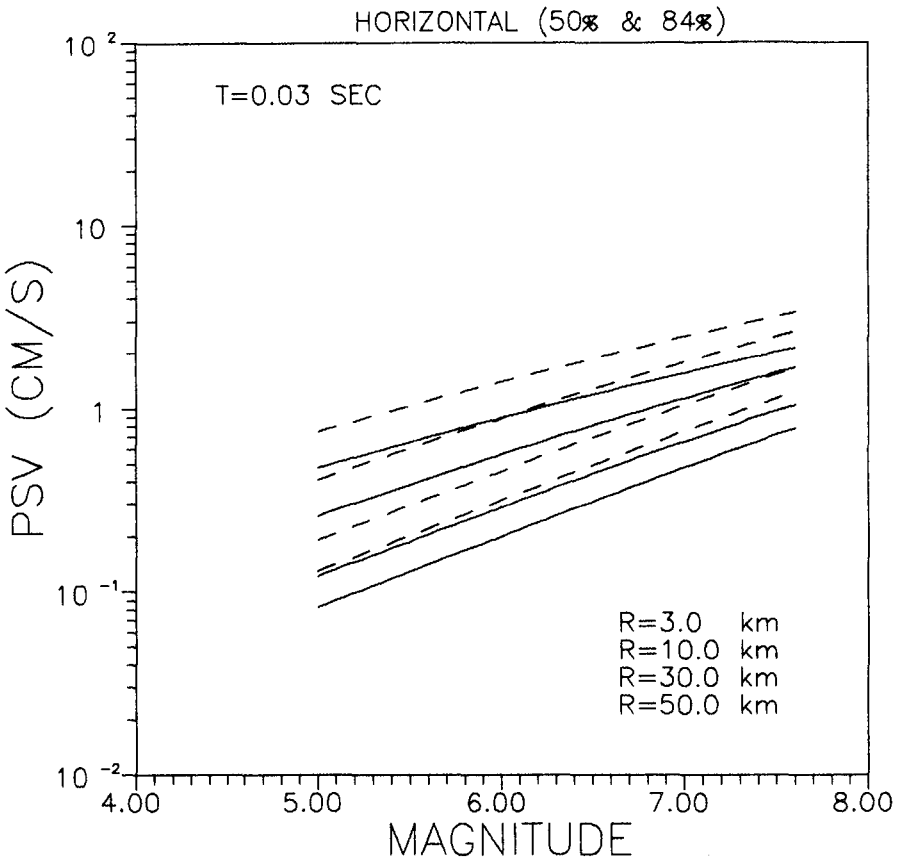

Figure 3.30 - Predicted horizontal spectral amplitude at 0.03 sec period for 50% and 84.1 probabilities at four specified hypocentral distances as a function of magnitude.

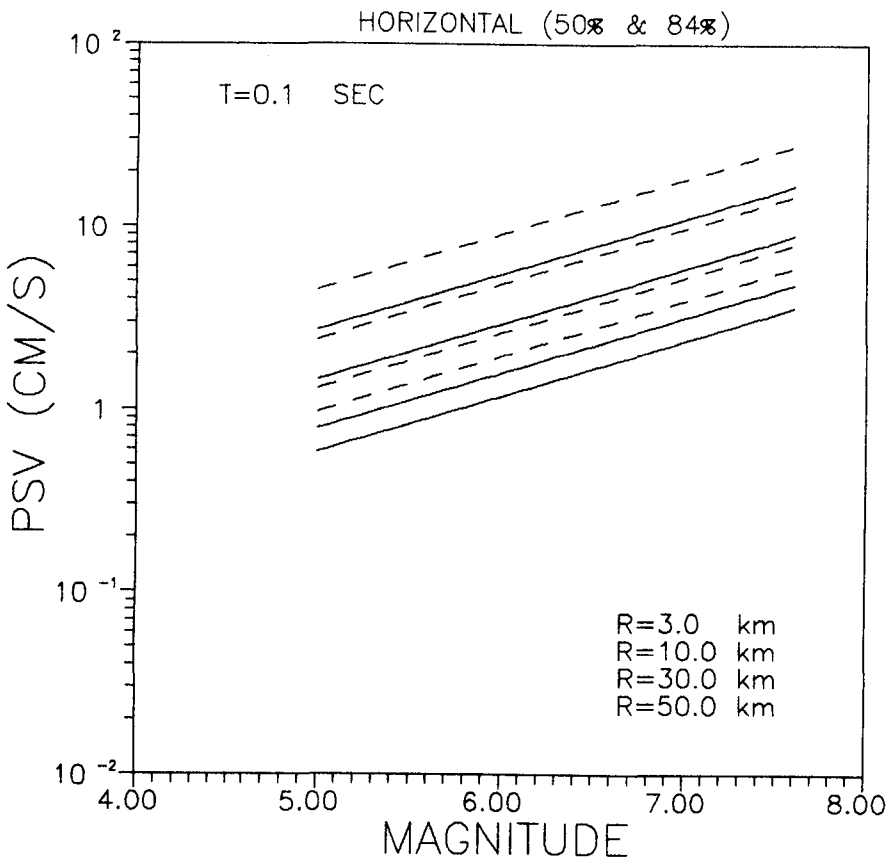

Figure 3.31 - Predicted horizontal spectral amplitude at 0.10 sec period for 50% and 84.1 probabilities at four specified hypocentral distances as a function of magnitude.

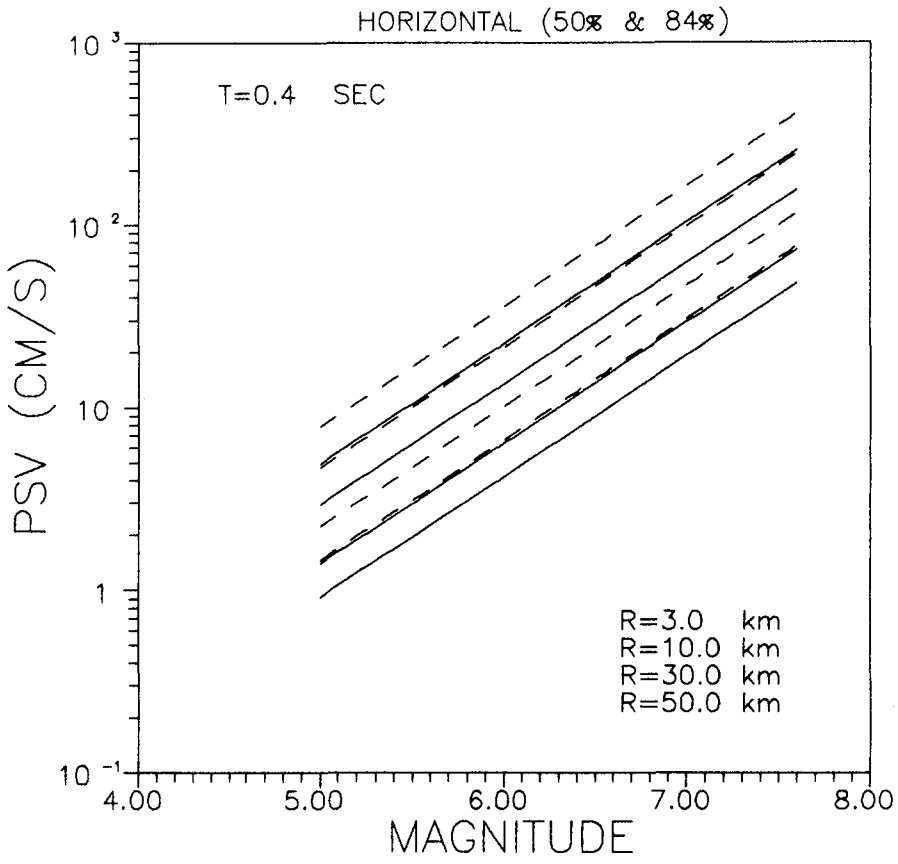

Figure 3.32 - Predicted horizontal spectral amplitude at 0.40 sec period for 50% and 84.1 probabilities at four specified hypocentral distances as a function of magnitude.

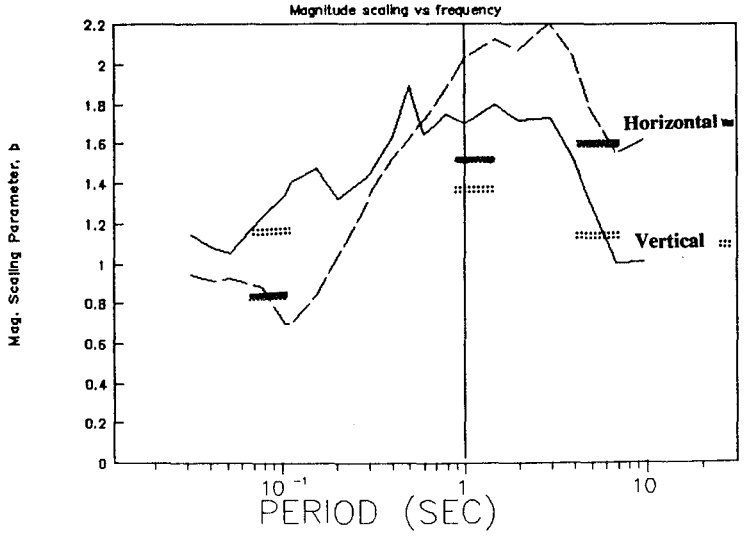

Figure 3.34 - Comparison of the magnitude scaling parameter, b, for vertical and horizontal spectral ordinates as a function of period. The estimates of parameter b obtained from the regression analyses of peak ground observations are also shown by the shaded bands in the period range corresponding to PGA, PGV, and PGD.

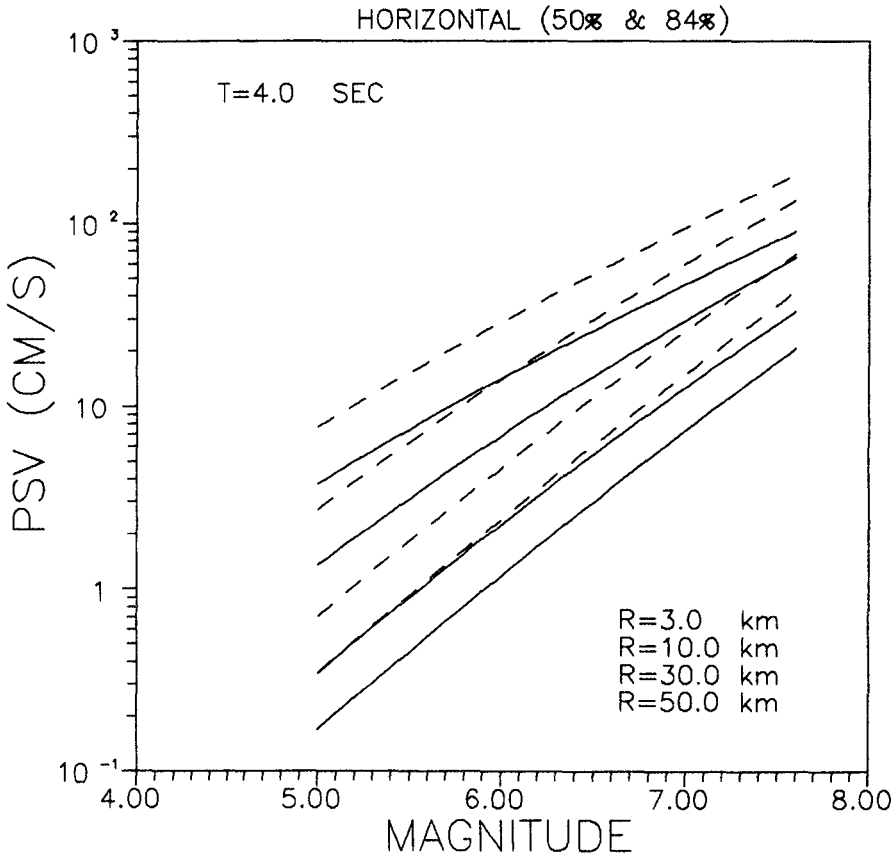

Figure 3.33 - Predicted horizontal spectral amplitude at 4.0 sec period for 50% and 84.1 probabilities at four specified hypocentral distances as a function of magnitude.

3.4.1 Limitations in the Data

Our discussion of the analysis of response spectral ordinates must be tempered by limitations inherent in the data with respect to long-period noise and distribution of the data with respect to magnitude. These are discussed below.

Effect of Long-Period Noise

In processing the data, the low cut-off frequency of the band-pass filter is set at ten seconds to reduce the effect of long-period noise. If the filter is applied at shorter periods (e.g., one second), the information on spectral ordinates beyond that frequency would effectively be lost. However, there may be considerable information available in that frequency range. The limitations with respect to long-period noise below are discussed further.

In Figure 3-22, which displays horizontal spectra for magnitude 7.0, there appears to be minimal long-period noise. However, the spectra for magnitudes 6.0 and 5.0, respectively, show increasing flatness or drift beyond the one second ordinate. This is probably associated with increasing noise, as magnitude and the signal-to-noise ratio decreases. Indeed, there is minimal low frequency energy generated by magnitudes as low as 5.0.

The vertical spectra show the same trend with decreasing magnitude. The vertical spectra for magnitude 7.0 shows the possible influence of noise beginning at the three second ordinate (Figure 3-19).

Distribution of the Data with respect to Magnitude

Since the bulk of the data is in the magnitude 6.0 to 7.0 range, the results for magnitude 6.0 and 7.0 are well constrained. However, despite the high quality digital data and uniform recording conditions, there is insufficient data below magnitude six for obtaining well constrained results at magnitude 5.0.

3.4.2 Results of Response Spectra Analysis

This section discusses three elements of the analysis of spectral ordinates.

Far-Field Attenuation

In Table 3-5, the far-field coefficient d tends to diminish as frequency increases. This is graphically displayed in Figures 3-17 to 3-19 by the convergence of the vertical response spectra at long periods. As discussed in Section 3.3.2, this is expected, since scaling with distance should decrease with decreasing frequency. However, the horizontal component displays the same counter-intuitive trend that was seen with the peak values. In Table 3-6, the far-field coefficient d tends to increase with decreasing frequency, indicating a larger scaling with distance as frequency decreases. This is graphically displayed in Figures 3-20 to 3-23, where the response spectra diverge at long periods.

Magnitude Scaling

Scaling with magnitude is represented by the coefficient b in equation (1). Since b represents scaling of the natural log of the ground-motion parameter, an increase of 1 in the value of b will increase the scaling of the ground-motion parameter by 2.7 times ($e^{1.0}=2.7$). For example, b=2.033 for the one second horizontal spectral ordinate, and b=0.871 for the 0.1 second ordinate. Since 2.033 - 0.871 = 1.162, PSV for the one second ordinate scales 3.16 times as much for each unit increase in magnitude than does PSV for the 0.1 second ordinate ($e^{1.16}=3.20$).

The values of b are given in Tables 3-5 and 3-6 and plotted with respect to period in Figure 3-34. For the horizontal component, the values of b are nearly constant at periods below 0.1 second and increase almost monotonically as period increases from 0.1 to 3 seconds. This trend is also observed by Joyner and Boore (1982) from 0.1 to 2 seconds. To a lesser extent, the vertical component displays the same trend.

This increase of magnitude scaling with increasing wavelength is intuitively appealing, since longer period energy is produced by larger portions of the source. For example, high frequency PGA is thought to be generated by small segments of the rupture zone (Hanks and Johnson, 1976). Thus, as more of the source is seen by the wave being studied, the larger the scaling should be relative to the size of the source.

The reverse trend is seen as b decreases beyond the three second ordinate. This is also observed by Joyner and Boore (1982).

Figure 3-34 also displays the values for coefficient b for the peak parameters, at the frequency bands believed to best represent them. Horizontal PGA scales comparably with PSV at the 0.1 second period, while vertical PGA scales about 30% less than vertical PSV at this period. For both components, PGV scales 40-50% less with magnitude than PSV in the one to two second range. PGD scales comparably with PSV in the six to ten second range.

Relative Attenuation at Different Frequencies

In order to explore how attenuation of PSV varies with frequency, three spectral ordinates are selected at periods of 0.1, 0.7 and 1.5 seconds. For these periods, the ratio of amplitude is computed at selected magnitudes for distances 0 to 50 km to the amplitude at 10 km (PSV,M,R,T/PSV,M,10,T), thus the ratio is constrained to be one at 10 km. These normalized amplitudes are plotted in Figures 3-35 to 3-37 for magnitudes 5.0, 6.0 and 7.0.

These plots show that at distances less than about twenty kilometers the slope of the curves for the higher frequency spectral ordinate is greater than that of the lower frequencies. This indicates more rapid attenuation of high frequency motion at short distances. However, beyond about twenty kilometers, the slope of the lines for the three periods are roughly the same, indicating more or less uniform attenuation with frequency. These curves can also be used to scale spectral information (for any distance less than 50 kilometers) from available data elsewhere.

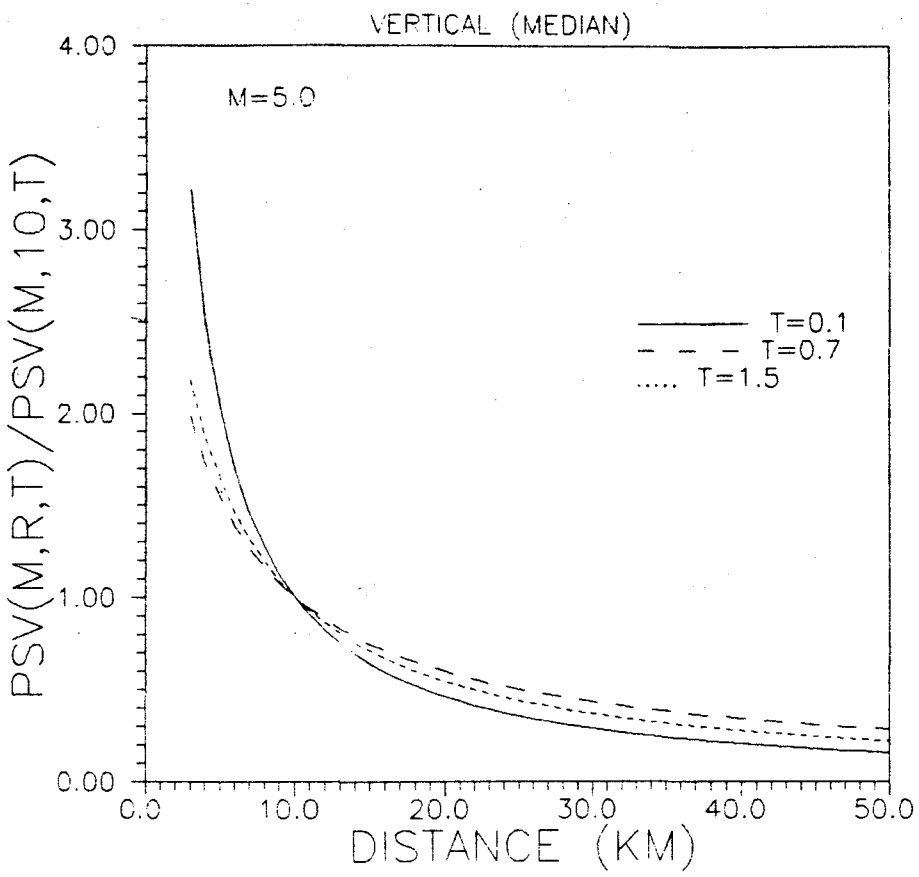

Figure 3.35 - Attenuation of the predicted vertical mean spectral ordinates (normalized to 10 km) at three periods of 0.1, 0.7 and 1.5 sec for M5.

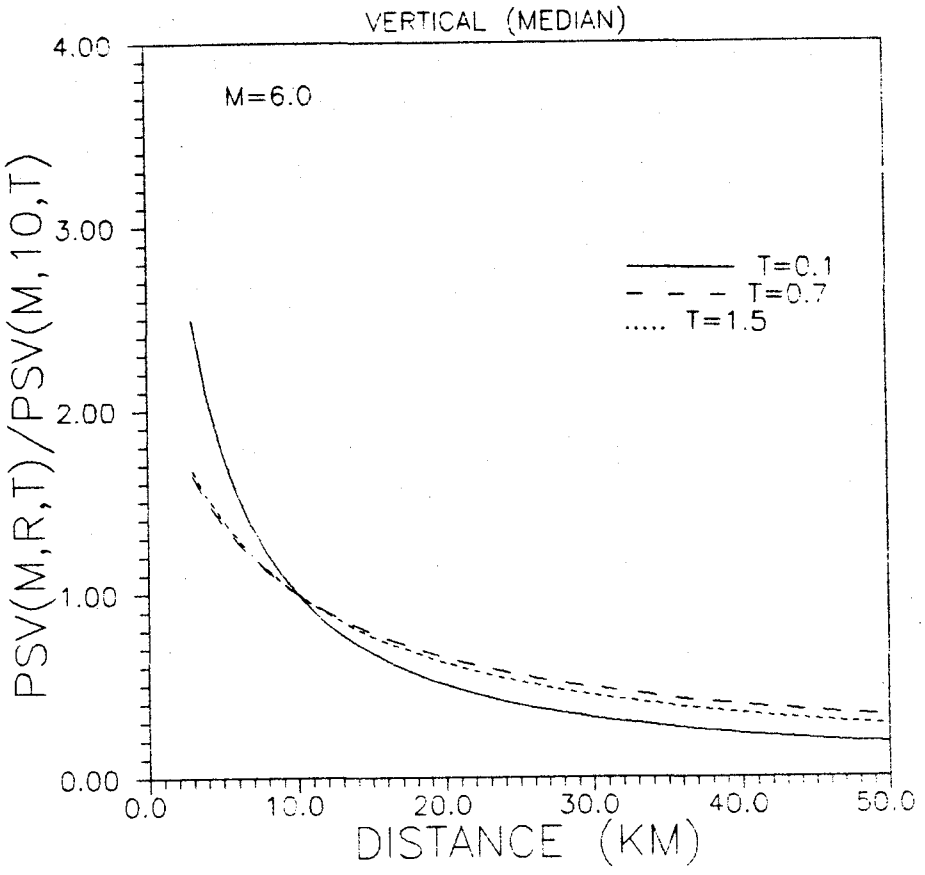

Figure 3.36 - Attenuation of the predicted vertical mean spectral ordinates (normalized to 10 km) at three periods of 0.1, 0.7 and 1.5 sec for M6.

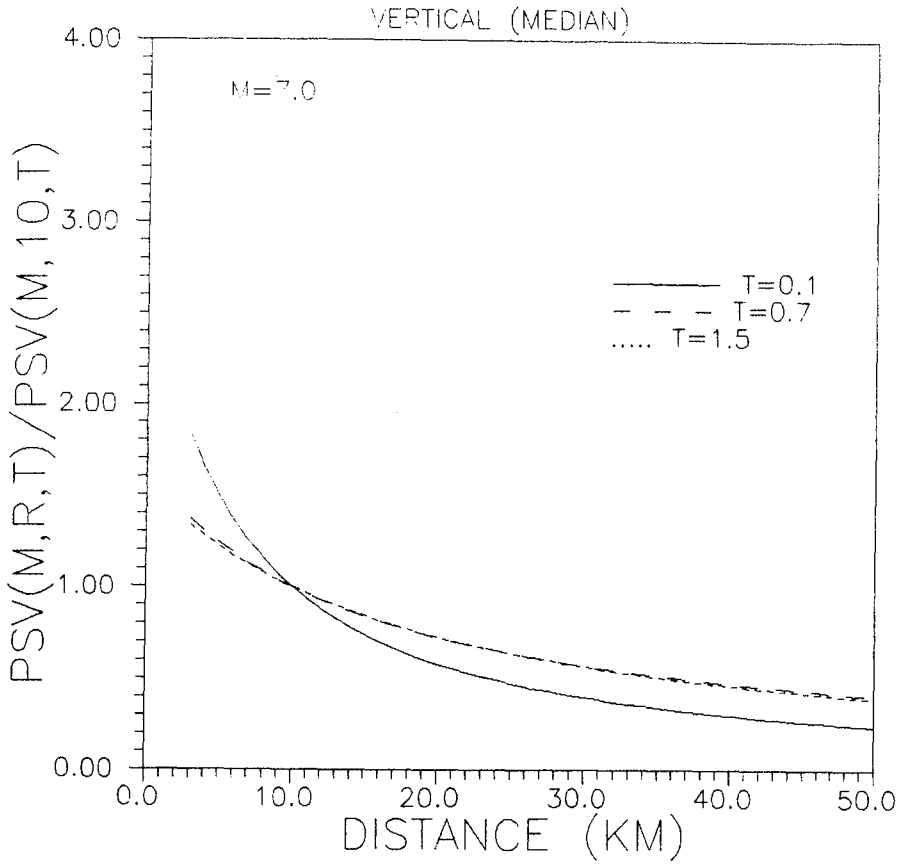

Figure 3.37 - Attenuation of the predicted vertical mean spectral ordinates (normalized to 10 km) at three periods of 0.1, 0.7 and 1.5 sec for M7.

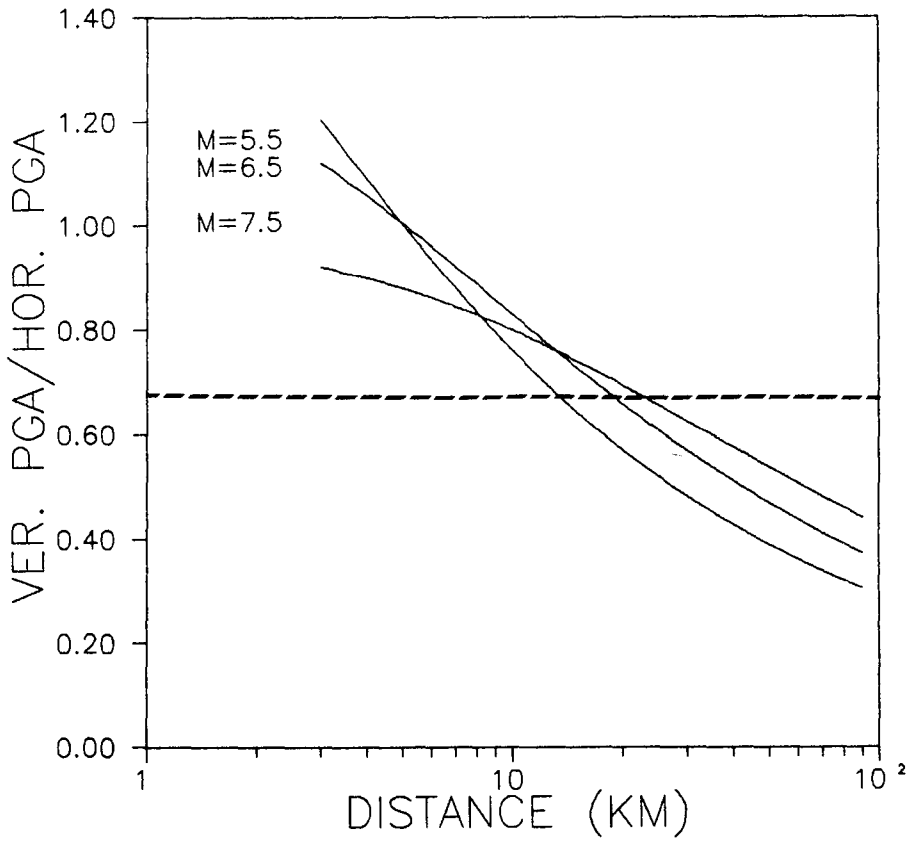

Figure 3.38 - Predicted ratio of vertical to horizontal PGA as a function of distance for three magnitudes M5.5, 6.5, and 7.5.

3.5 RATIO OF VERTICAL TO HORIZONTAL GROUND MOTION

The ratios of the vertical component of ground motion to the average horizontal component are presented in Figures 3-38 to 3-41. Figure 3-38 graphically displays the ratio for PGA. Figures 3-39 to 3-41 presents results for both the median spectral ordinates and peak values (PGA, PGV, and PGD) for magnitudes 5.0, 6.0 and 7.0 at hypocentral distances of 3, 10, 30, and 50 kilometers.

This study found that the ratio of the vertical to horizontal component is sensitive to frequency content, distance, and magnitude. Furthermore, the ratio significantly exceeds 2/3 (commonly used in engineering applications) in the nearfield of large earthquakes and is much less than 2/3 in the farfield of those events. Specific observations are as follows:

The limitations in the data, discussed in Section 3.4, also apply to this discussion. Specifically, the predominance of long-period noise increases as the magnitude and signal-to-noise ratio decreases. Therefore, the reliability of the ratios are diminished for

- magnitude 5.0 beyond one second
- magnitude 6.0 beyond three seconds
- magnitude 7.0 beyond five seconds
- PGD at the lower end of the magnitude range.

PGA

Figure 3-38 plots the ratio of vertical to horizontal PGA against hypocentral distance for magnitude 5.5 and 6.5. The ratio exceeds 2/3 at distances less than 25 km and exceeds unity within 5 km. Also, at distances greater than 30-50 km, the ratio is less than 1/2. These findings for the SMART 1 array are consistent with those of Campbell (1982) for a worldwide data base.

Amplitude vs. Frequency

Figures 3-39 to 3-41 demonstrate that the ratio of vertical to horizontal ground motion is much higher for PGA and high frequency spectral ordinates in the nearfield than it is in the farfield or for low frequency ordinates. This trend is consistent with the fact that the frequency content of the vertical component of ground motion is greater than that for the horizontal (Housner, 1970). Since the near-field ground motion can be rich in high frequency and higher frequencies attenuate more rapidly (Housner, 1970), the predominantly low frequency energy of the horizontal component is left to control the ground motion in the farfield.

Amplitude vs. Distance

The sensitivity of the ratio to distance changes with frequency. The ratios are larger for both high frequency energy at short distances and low frequency energy at long distances. For example, in Figures 3-39 to 3-41 the high frequency spectral ordinates ($T<0.3$ second) have significantly higher ratios at three kilometers than they do at 30 or 50 kilometers. Conversely, the lower frequency ($T>1.0$ sec) spectral ordinates have slightly higher ratios at 30 and 50 kilometers than at three or ten kilometers.

The predictions of peak ground-motion parameters are also consistent with those of spectral ordinates for high frequency PGA; a ratio of 1.18 at three kilometers and a ratio of 0.428 at 50 kilometers is predicted for a magnitude 6.0 . The converse is again apparent for low frequency PGD with a ratio of 0.548 at 50 kilometers ($M=6$) and only 0.172 at three kilometers. The ratio of mid-period PGV is relatively stable with respect to distance.

Sensitivity to Magnitude

As magnitude increases, the ratio in the high frequency range ($f>10$ Hz) also increases. Indeed, at 14 Hz. and 3 kilometers, the predicted value of vertical PSV is 1.5 times that of the horizontal value for a magnitude 5.0. This ratio increases to 2.0 for a magnitude of 6.0 and to 2.35 for a magnitude of 7.0.

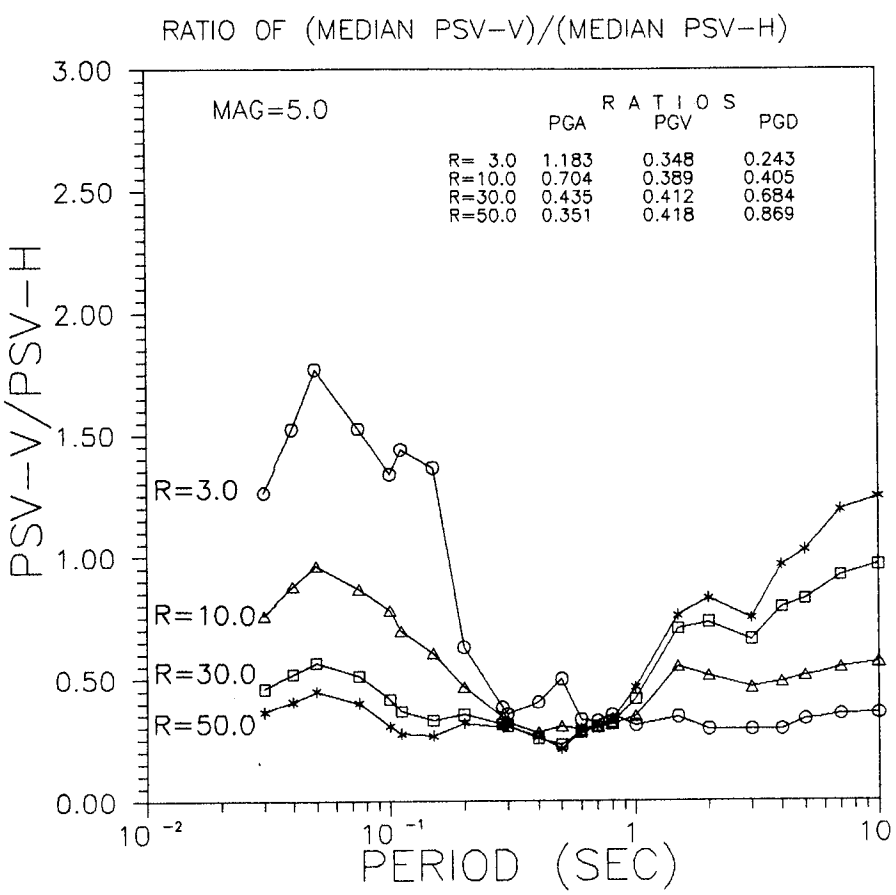

Figure 3.39 - Predicted ratio of vertical to horizontal response spectra for M5 at four hypocentral distances 3, 10, 30 and 50 km. Predictions for PGA, PGV, and PGD ratios at the same four distances are listed in the inset.

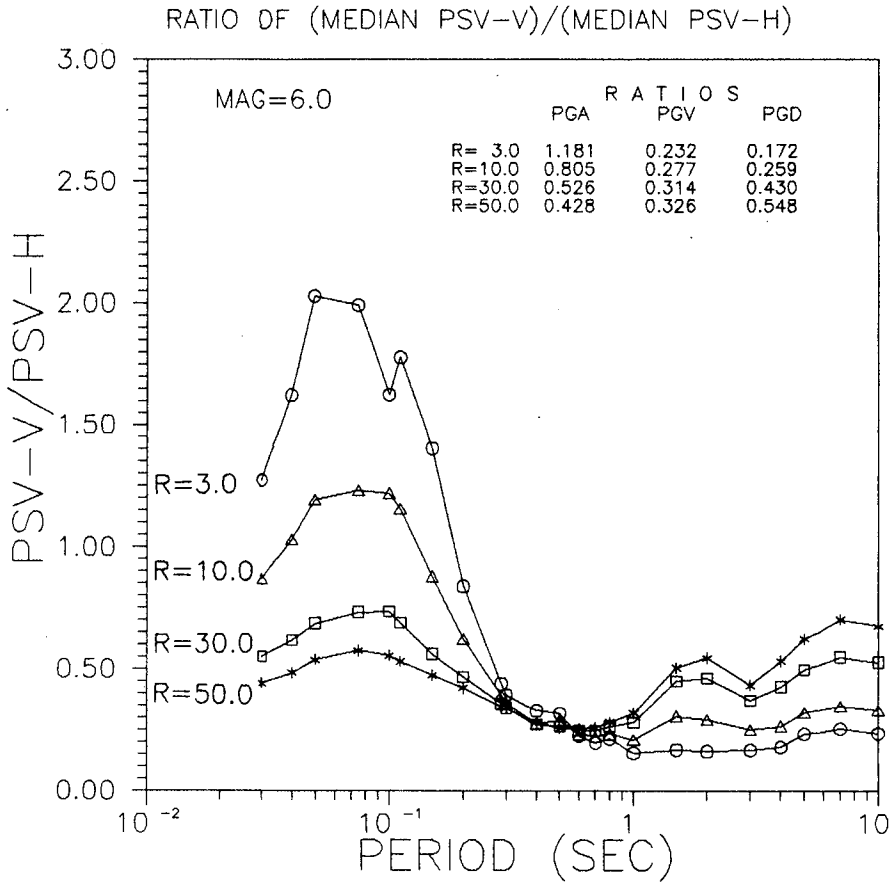

Figure 3.40 - Predicted ratio of vertical to horizontal response spectra for M6 at four hypocentral distances 3, 10, 30 and 50 km. Predictions for PGA, PGV, and PGD ratios at the same four distances are listed in the inset.

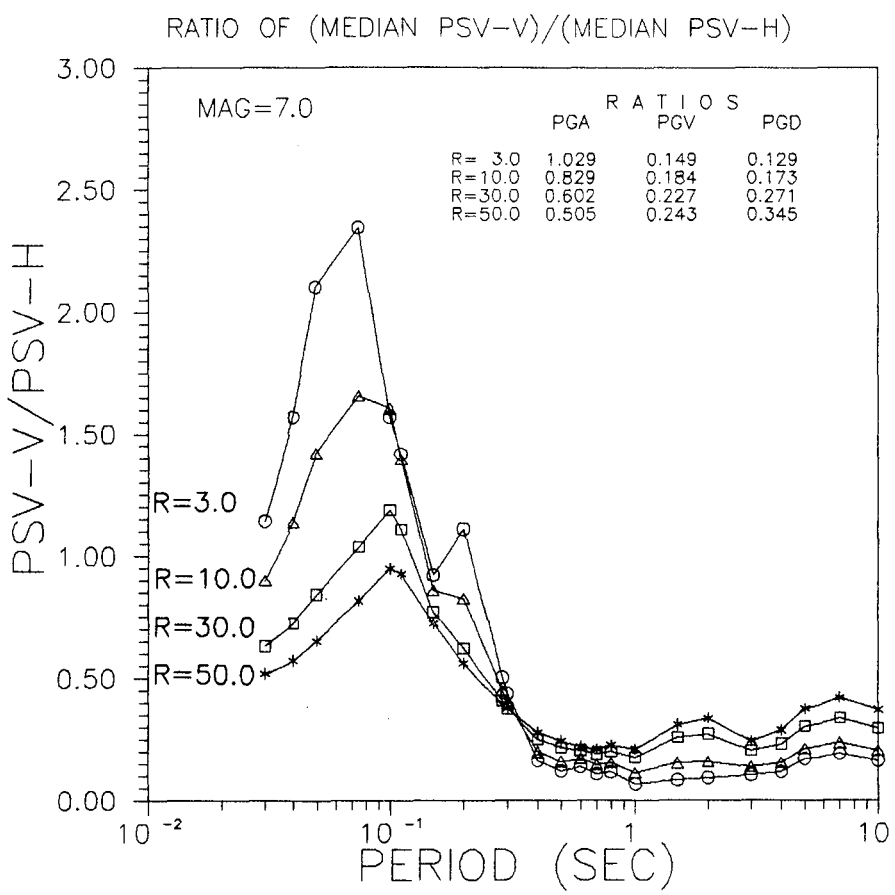

Figure 3.41 - Predicted ratio of vertical to horizontal response spectra for M7 at four hypocentral distances 3, 10, 30 and 50 km. Predictions for PGA, PGV, and PGD ratios at the same four distances are listed in the inset.

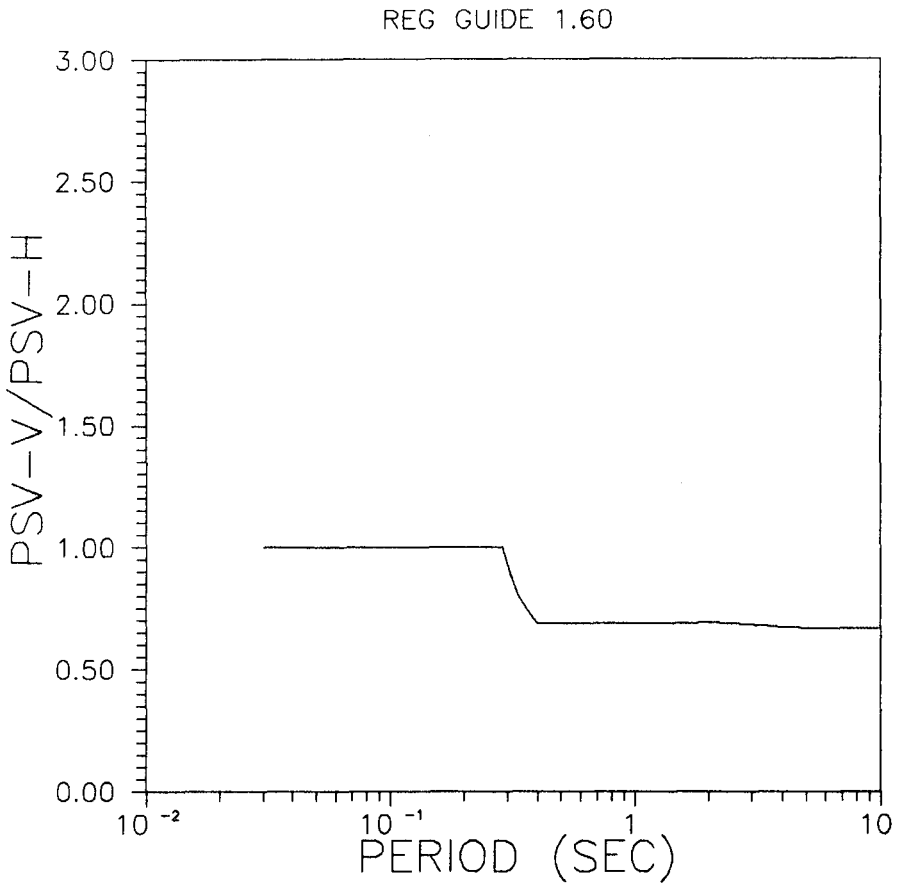

Figure 3.42 - Ratio of vertical to horizontal response spectra as predicted by Regulatory Guide 1.60 for all magnitudes and distances. The drop in spectral ratio from 1.0 to 2/3 occurs between 0.286 and 0.4 sec.

These results indicate that, at distances less than ten kilometers, vertical ground motion controls the high frequency excitation and that low frequency excitation is controlled by the horizontal motion. The cross-over frequency lies between 5 and 10 Hz.

The ratio does not increase with magnitude for PGA, nor are the ratios as high as those observed for the spectral ordinates above 10 Hz. This may indicate that PGA is associated with a broader frequency band. The ratios for PGA correspond to those of the spectral ordinates at about 5 to 7 Hz. Note that ratios for PGV are consistent with those for the one second spectral ordinates.

Other observations with respect to the ratios will be discussed in subsequent sections.

3.6 COMPARISON TO REGULATORY GUIDE 1.60

U.S. Nuclear Regulatory Guide 1.60 (R.G. 1.60) has been used for almost two decades to define the design spectra for critical structures in the United States. This section first discusses the guidance of R.G. 1.60 and then compares it with the results of this study.

3.6.1 Regulatory Guide 1.60

R.G. 1.60 defines the shape of both the horizontal and vertical design spectra at 84.1 percent probability level. The 84th percentile value of horizontal PGA serves as the anchorage point at 33 Hz. The 84th percentile value is recommended by Newmark, Blume and Kapur (1973) and adopted by the regulatory guide because, "...it is considered desirable to use the mean plus one standard deviation value, or the 84.1% probability level, as the design spectrum probability level" (Newmark, Blume and Kapur, 1973). The regulatory guide does not scale the vertical spectrum with respect to vertical PGA, but anchors it to horizontal PGA at 33 Hz.

The regulatory guide does not specify a ratio of vertical to horizontal PGA. However, Newmark, Blume and Kapur (1973) recommend the use of the 2/3 ratio. The regulatory guide, however, does define the ratio of the vertical to horizontal response spectra to be 2/3 at frequencies below 2.5 Hz (0.4 sec) and unity above 3.5 Hz (0.286 sec), with the ratio varying between those frequencies. The variation of the ratio with respect to frequency is graphically displayed in Figure 3-42.

The regulatory guide does not specify changes in the spectra (or ratios) with respect to magnitude or distance. However, the guide states that their recommended spectra do not apply to sites "relatively close" to an earthquake epicenter. Thus, the results of this study extend to the region for which the regulatory guide is silent, i.e., the very near-source region. The following section presents a comparison between the results of this study and the recommendations of the guide.

3.6.2 Comparison of Spectra

In order to compare the empirical results with the recommended design spectra of R.G. 1.60, the vertical and horizontal response spectra at 5% critical damping are compared with the guide's spectra in Figures 3-43 to 3-51. These figures display the 84th percentile response spectra (comparable to the regulatory guide) at 3 and 50 kilometers for magnitudes 5.0, 6.0, and 7.0.

Figures 3-43 to 3-48 plot the predicted horizontal and vertical spectra. The R.G. 1.60 vertical and horizontal spectral shape is then anchored to the zero period amplitude (ZPA) of the horizontal spectra (at 84.1% probability). This allows an assessment of the conservatism of R.G. 1.60 with respect to the spectra, since the guide recommends anchoring both horizontal and vertical spectra to horizontal PGA. An additional set of figures similar to 3-43 to 3-48 in which the R.G. 160 spectra are anchored to the zero period median amplitude (i.e., at 50% probability) of horizontal spectra was also constructed but not reproduced in this report. The high frequency exceedance discussed herein is intensified in such figures.

In Figures 3-43 to 3-45, the horizontal spectra are enveloped by the regulatory guide except at high magnitudes between about 0.15 and 2.0 seconds. In this range, the near-field spectra significantly exceed the regulatory guide. This result reflects the lack of magnitude saturation found in this frequency range for the horizontal component (see Section 3-7). While for this study the 3 km line is at the limit of the data, this same trend is observed at 50 km, supporting the findings for the very nearfield.

Joyner and Boore (1982) also found the regulatory guide unconservative (for a magnitude 7.5) in the very nearfield from 0.2 to 3.0 seconds and slightly unconservative between 0.5 and 4.0 seconds at about 40 km.

In Figures 3-46 to 3-48, the vertical spectra exceed that of the regulatory guide in the high frequency range, in the very nearfield. However, the regulatory guide appears very conservative with respect to this study beyond about 0.25 second. It is also conservative at all frequencies for distances greater than about 50 kilometers.

In Figures 3-49 to 3-51, both spectra are anchored to vertical PGA, allowing a direct comparison of spectral shape.

3.6.3 Comparison of Ratios

The ratios of vertical to horizontal PSV of the 84th percentile response spectral ordinates were computed for comparison with the regulatory guide. Figures 3-52 to 3-54 display ratios of the 84th percentile response spectra and 84th percentile peak values for magnitudes 5.0, 6.0 and 7.0 at distances of 3, 10, 30, and 50 kilometers. The ratio recommended by the regulatory guide is indicated by a dashed line.

This study predicts a ratio far exceeding that of the regulatory guide at periods below about 0.2 second. The exceedance increases as magnitude increases and as distance decreases. The ratios for 84th percentile PGA also exceed unity in the very nearfield.

This study also predicts ratios exceeding that of the regulatory guide at periods greater than one second for a magnitude of 5.0. However, the results for such low magnitudes are not well constrained by the data and are controlled by noise in the long-period range. Furthermore, the lower magnitudes are not of interest for engineering considerations.

One major conclusion is that the spectral ratios of the regulatory guide are conservative at periods longer than about 0.20 second. This is especially noticeable for the larger magnitude earthquakes, which are of primary engineering significance. Figure 3-54 shows spectral ratios for magnitude 7.0 roughly half that of the regulatory guide beyond 0.2 second.

The conservatism of the 2/3 ratio for PGA is also upheld for distances exceeding 30 kilometers. However, the 2/3 ratio appears unconservative in the very nearfield.

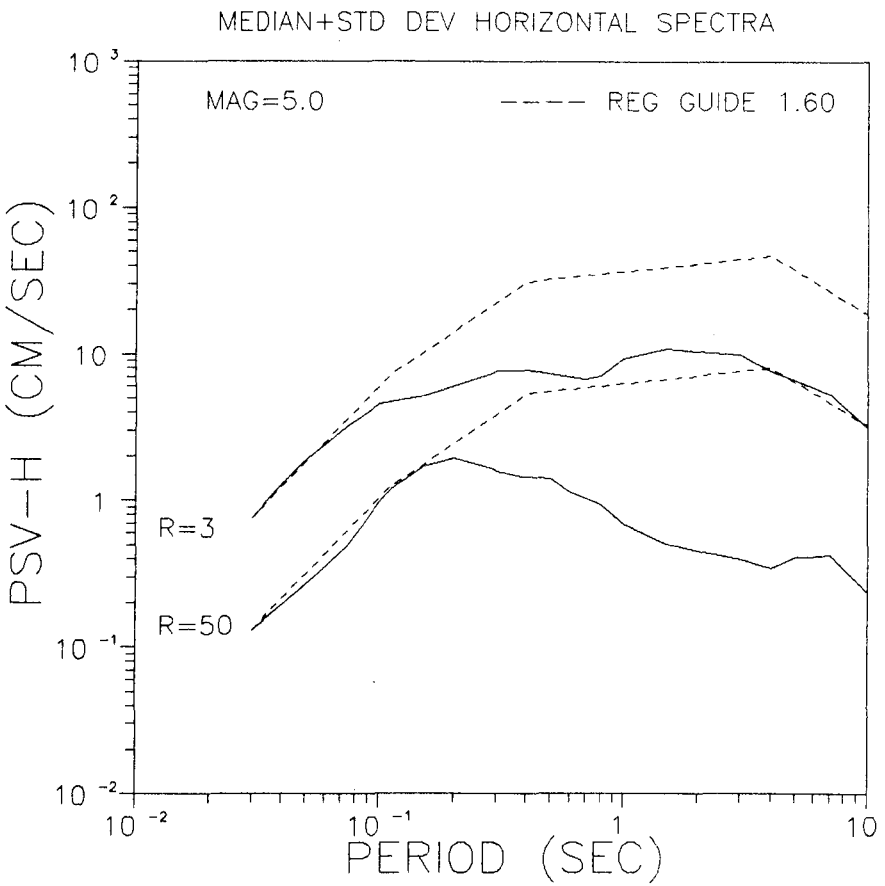

Figure 3.43 - Comparison of predicted horizontal response spectra (84.1% probability) for M5 at 3 and 50 km distances with Reg. Guide 1.60 predictions.

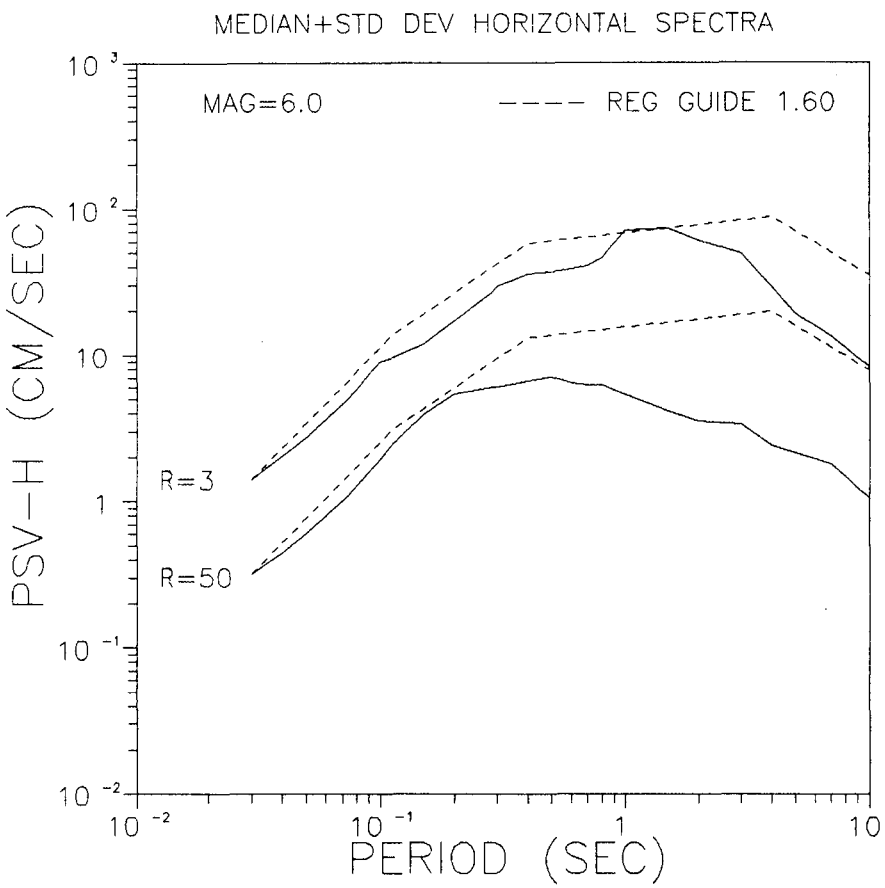

Figure 3.44 - Comparison of predicted horizontal response spectra (84.1% probability) for M6 at 3 and 50 km distances with Reg. Guide 1.60 predictions.

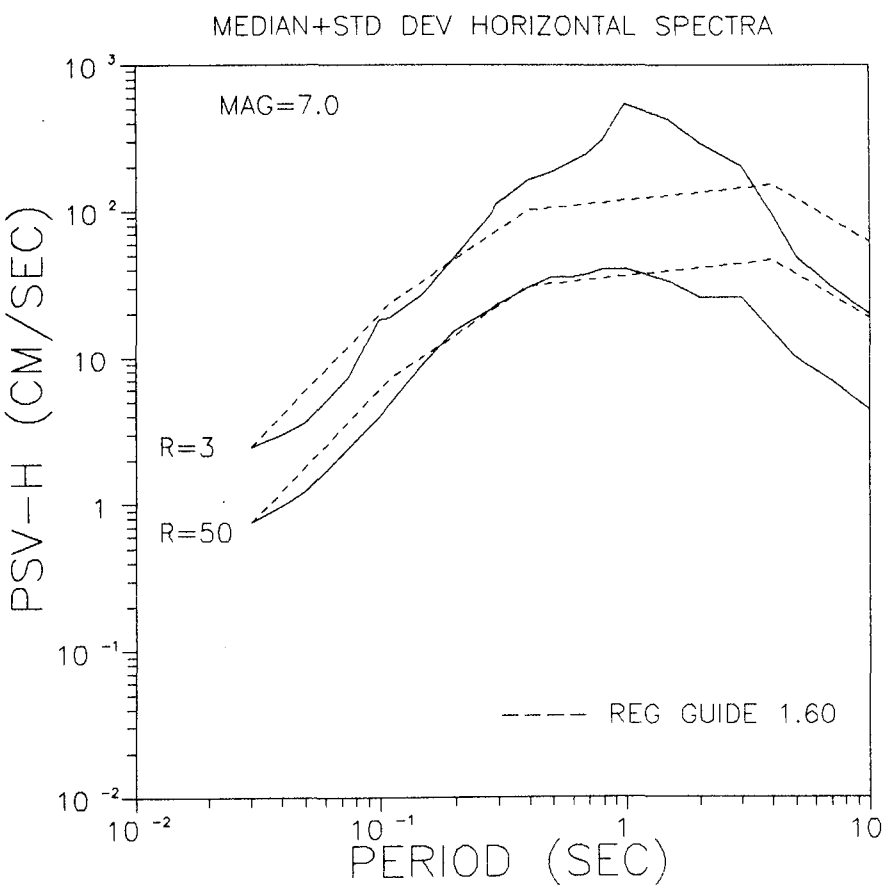

Figure 3.45 - Comparison of predicted horizontal response spectra (84.1% probability) for M7 at 3 and 50 km distances with Reg. Guide 1.60 predictions.

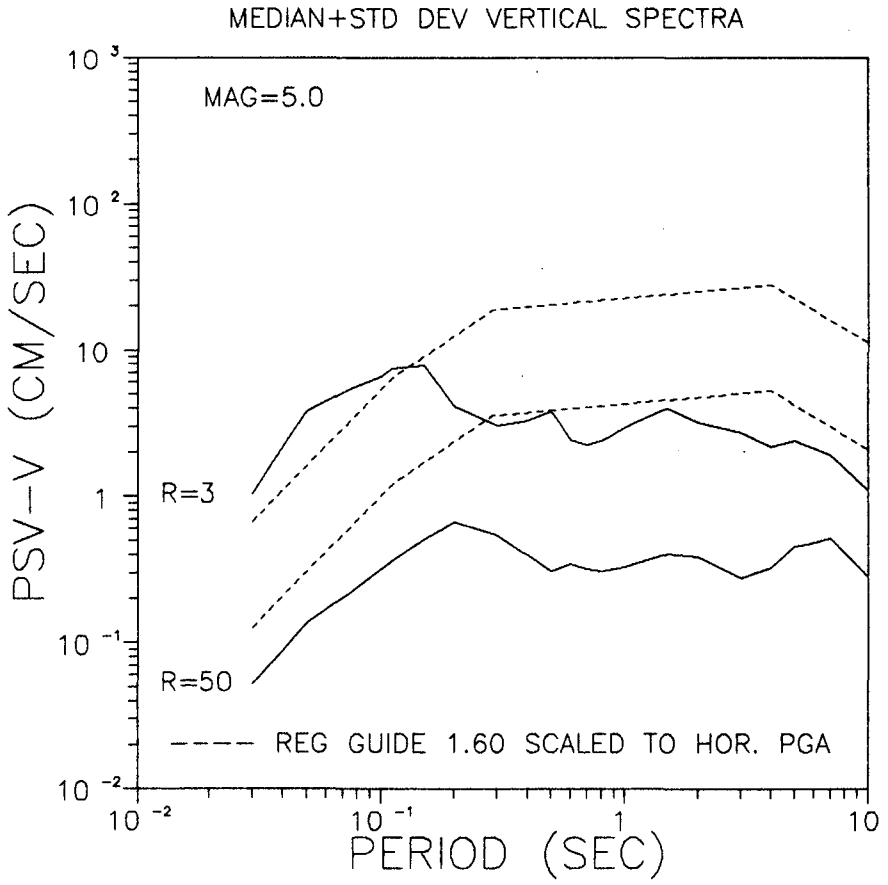

Figure 3.46 - Comparison of predicted vertical response spectra (84.1% probability) for M5 at 3 and 50 km distances with Reg. Guide 1.60 vertical spectra anchored to horizontal PGA.

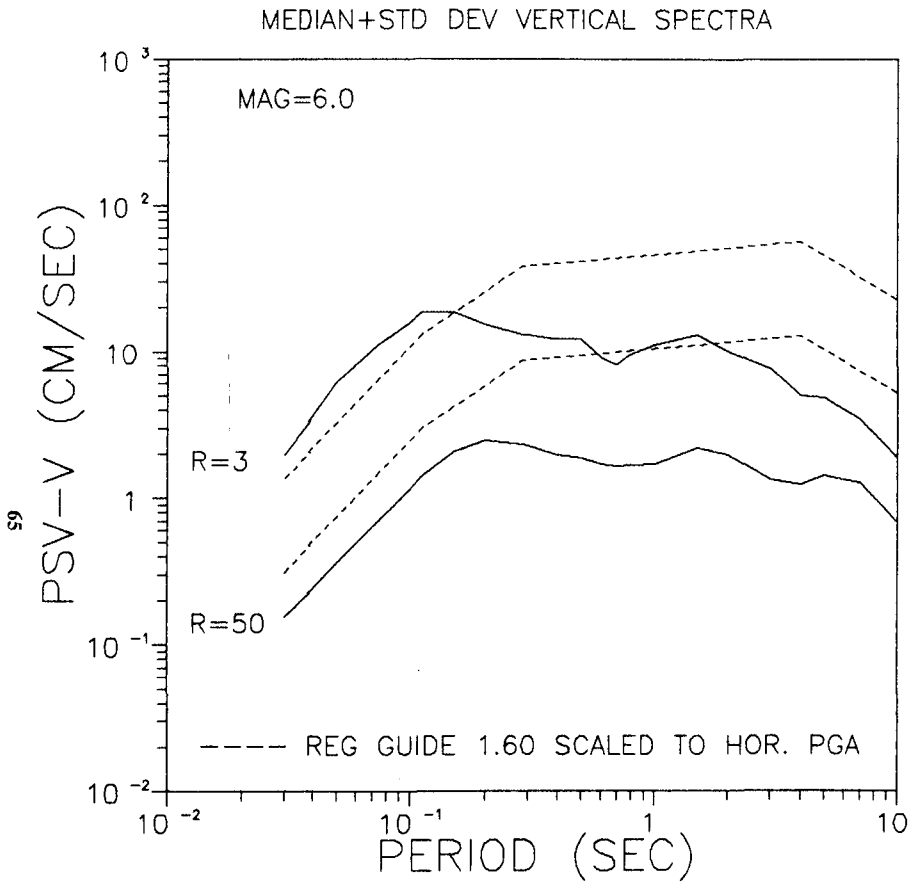

Figure 3.47 - Comparison of predicted vertical response spectra (84.1% probability) for M6 at 3 and 50 km distances with Reg. Guide 1.60 vertical spectra anchored to horizontal PGA.

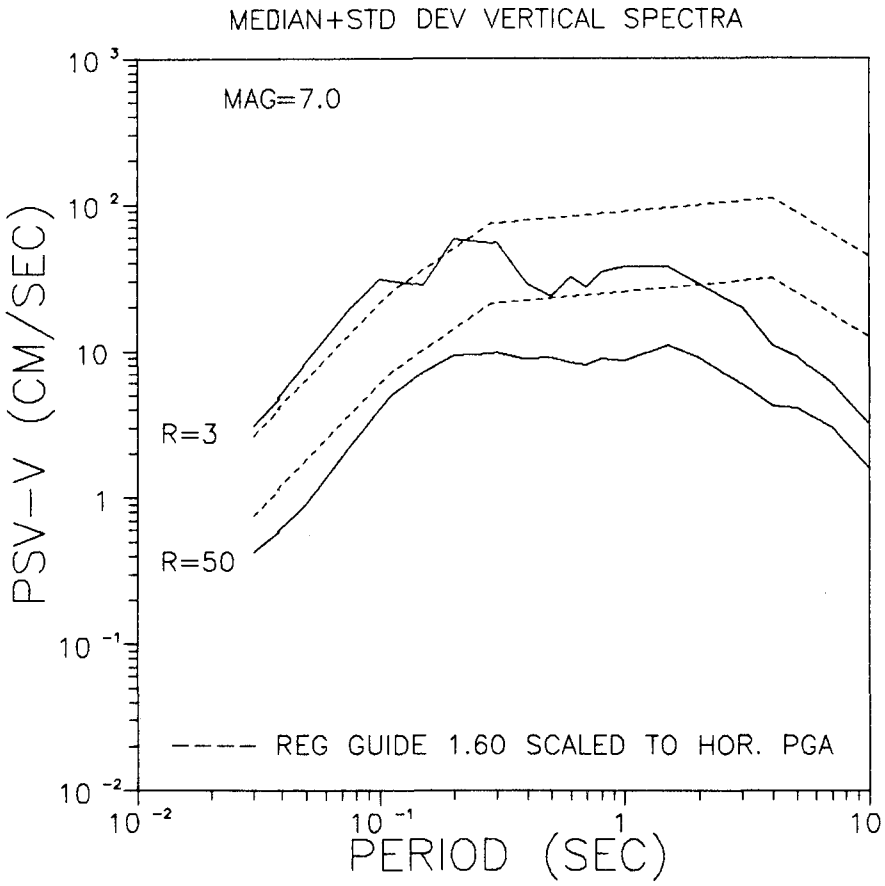

Figure 3.48 - Comparison of predicted vertical response spectra (84.1% probability) for M7 at 3 and 50 km distances with Reg. Guide 1.60 vertical spectra anchored to horizontal PGA.

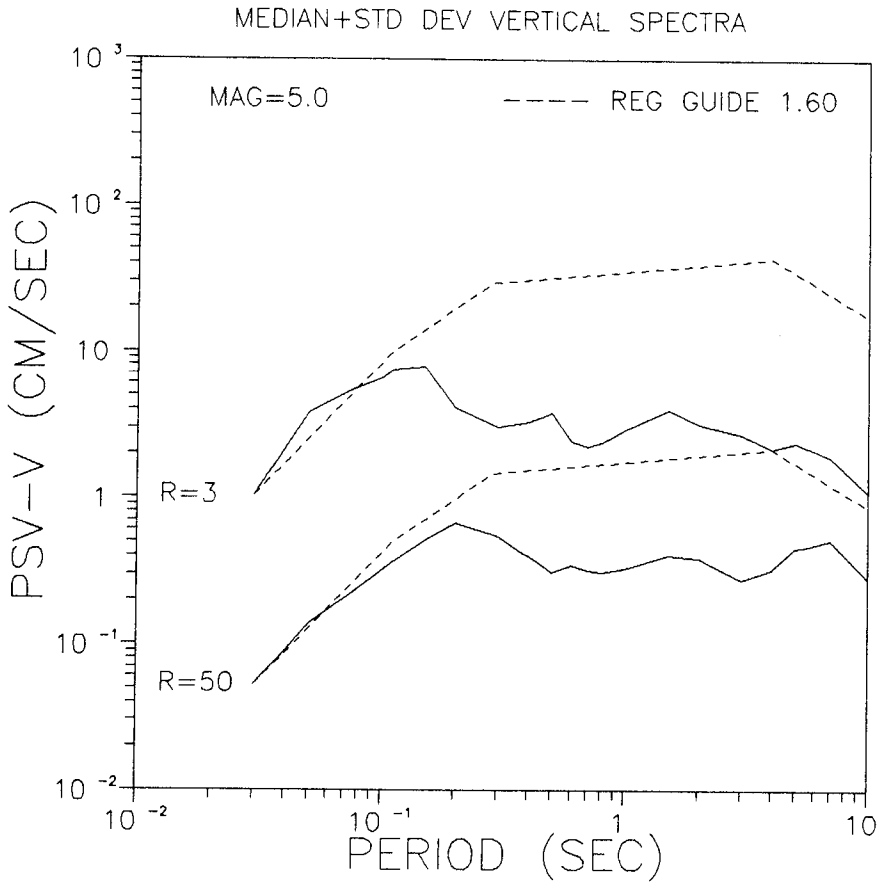

Figure 3.49 - Comparison of predicted vertical response spectra (84.1% probability) for M5 at 3 and 50 km distances with Reg. Guide 1.60 vertical spectra anchored to vertical PGA.

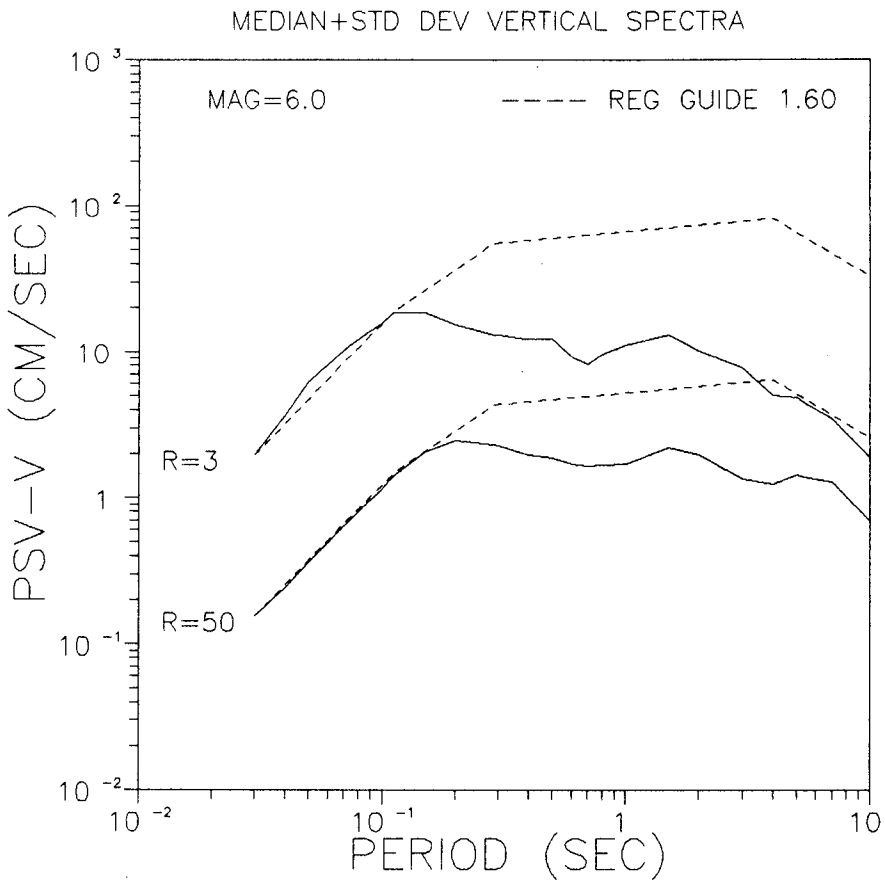

Figure 3.50 - Comparison of predicted vertical response spectra (84.1% probability) for M6 at 3 and 50 km distances with Reg. Guide 1.60 vertical spectra anchored to vertical PGA.

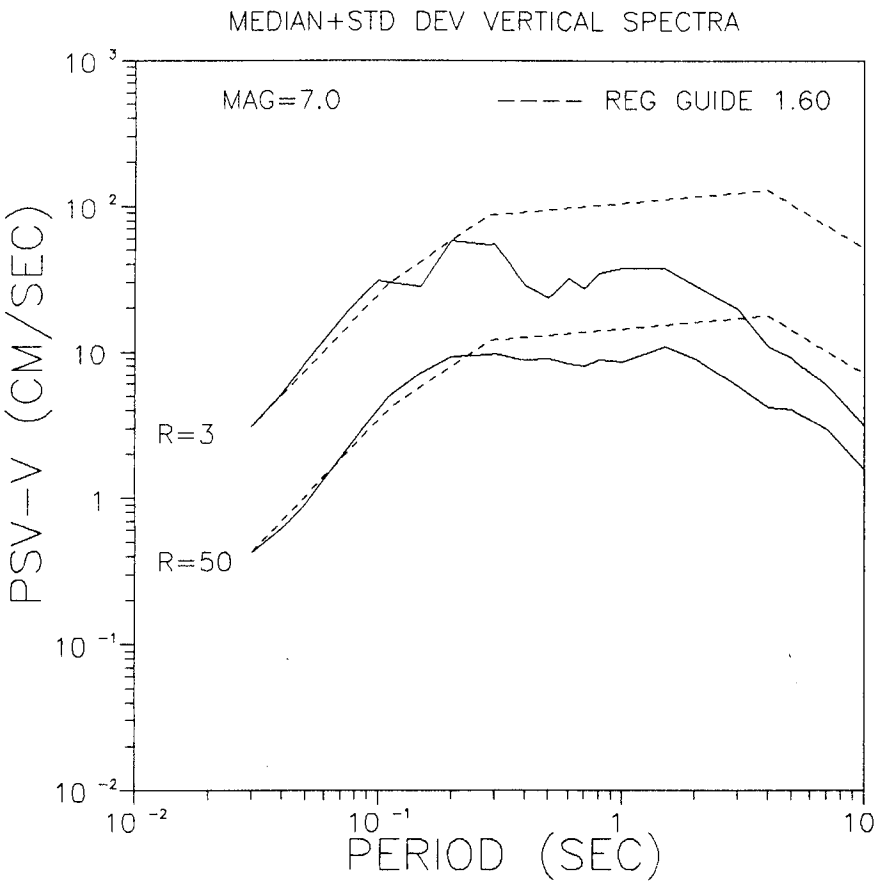

Figure 3.51 - Comparison of predicted vertical response spectra (84.1% probability) for M7 at 3 and 50 km distances with Reg. Guide 1.60 vertical spectra anchored to vertical PGA.

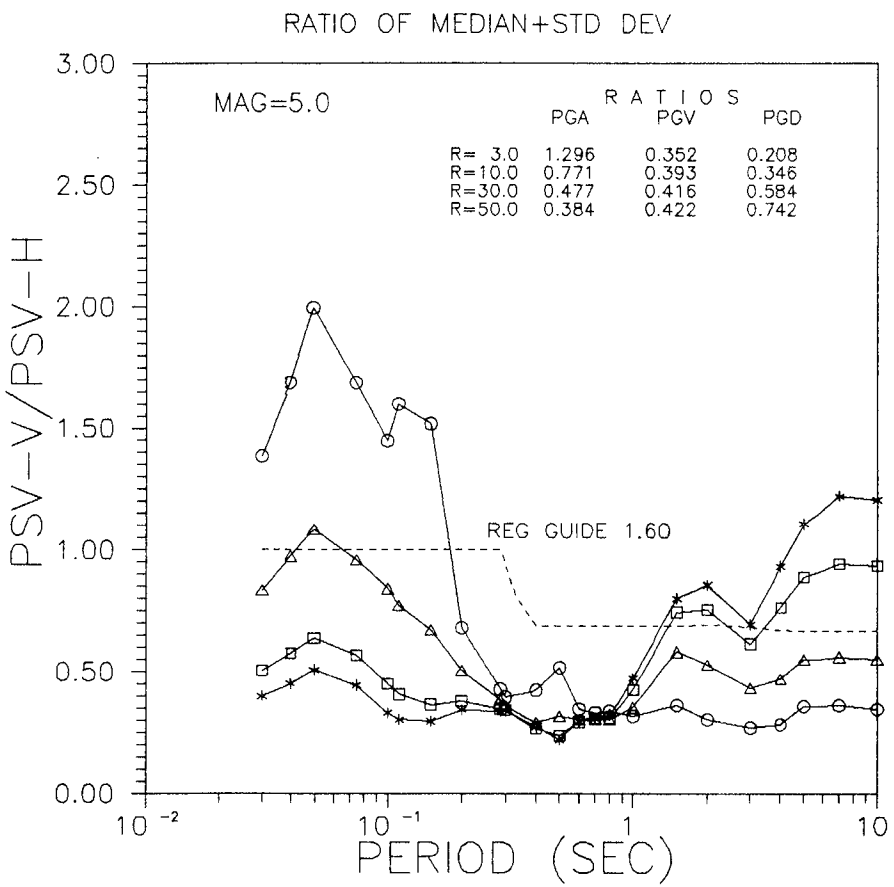

Figure 3.52 - Comparison of predicted vertical to horizontal spectral ratio (84.1% probability) for M5 at 3, 10, 30 and 50 km distances with Reg. Guide 1.60 prediction.

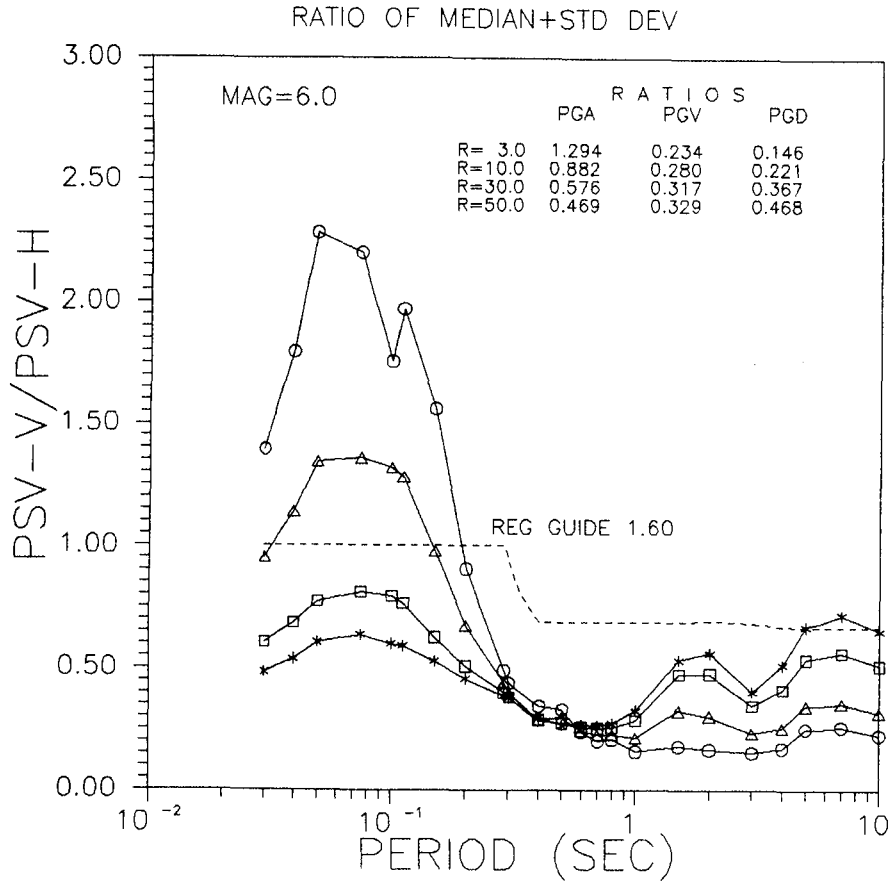

Figure 3.53 - Comparison of predicted vertical to horizontal spectral ratio (84.1% probability) for M6 at 3, 10, 30 and 50 km distances with Reg. Guide 1.60 prediction.

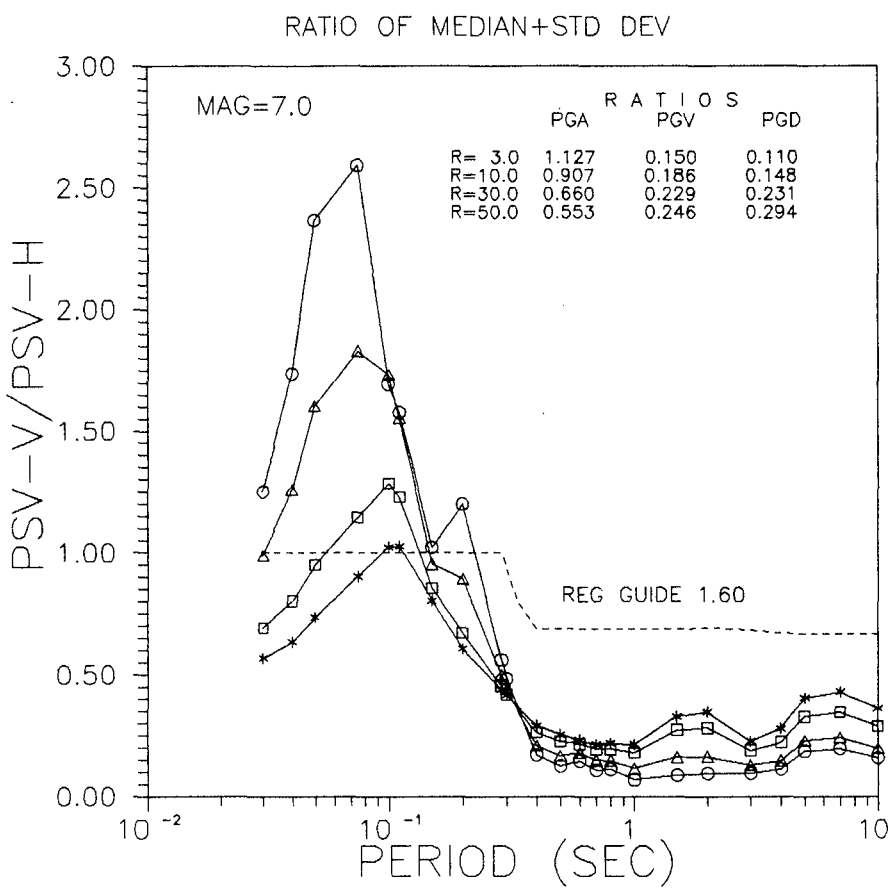

Figure 3.54 - Comparison of predicted vertical to horizontal spectral ratio (84.1% probability) for M7 at 3, 10, 30 and 50 km distances with Reg. Guide 1.60 prediction.

3.7 MAGNITUDE SATURATION

Since very little near-field strong-motion data exist above magnitude 7.0, the functional form of the ground-motion model must be relied on to extrapolate amplitudes for larger magnitude events. In particular, the c_2 parameter, which models the saturation of ground motion with increasing magnitude (Section 3.1), is important for predicting amplitudes for sites in the nearfield of large earthquakes.

3.7.1 Theoretical Considerations

The primary physical justification for the phenomenon of magnitude saturation is that high frequency energy is generated by smaller portions of the source than long-period energy which requires large segments of rupture (Hanks and Johnson, 1976). Therefore, ground-motion amplitudes controlled by high frequency energy should be less sensitive to the size of the source. Also, it is thought that soils have upper limits for transmitting high frequency shear motion (Mohammadioun and Pecker, 1984). Thus, as magnitude increases, the amplitude of high frequency energy may reach those limits, or saturate. Therefore, one would expect to find higher magnitude saturation closer to the source where high frequency motion dominates and where peak parameters see smaller portions of the source (Hanks and Johnson, 1976). Also, one would expect to find magnitude saturation in predominantly high frequency ground-motion parameters.

3.7.2 Frequency Dependence

As discussed in previous sections, the Degree of Magnitude Saturation (DMS) is found to vary by component and by ground-motion parameter. For example, this study finds a greater degree of saturation for the vertical component of PGA than for the horizontal. This is intuitively appealing, since vertical PGA is associated with higher frequency energy than horizontal. Nevertheless, a study performed on worldwide data by Campbell (1982) found only 20% saturation for vertical PGA, compared with 88% for the horizontal component (Campbell, 1981).

Consistent with the above discussion the high frequency spectral ordinates show nearly total magnitude saturation. This is displayed in Figure 3-55, where DMS is plotted over the frequency range of this study for both the vertical and horizontal components. However, this figure also displays a very interesting trend with respect to the saturation

of PSV over frequency. At frequencies between 5 and 10 Hz, saturation disappears, picking up again at about 0.4 and 1.5 seconds for the vertical and horizontal components, respectively.

The first unexpected observation is that magnitude saturation persists for the low frequency spectral ordinates, although DMS is only about 55%. One would expect to see less saturation at low frequencies than for the mid-range frequency ordinates where DMS ranges from 0-40%. Similarly, in Sections 3.2 and 3.3, we observed that vertical PGA displayed higher magnitude saturation (81%) than PGV or PGD (56%), consistent with the higher frequency content of PGA. However, the opposite trend was observed with horizontal PGA showing 39% saturation, while PGV and PGD showed 36% and 59%, respectively. These observations may be the result of low frequency noise distorting the results for low frequency energy (as frequency decreases, the signal-to-noise ratio also decreases). Also, as discussed in Section 3.3.2, physical factors such as coupling and dissimilar behavior of Q_α and Q_β may also play a role.

Another phenomenon displayed in Figure 3-55 is the erratic behavior of DMS at 3 to 5 Hz. Although PSV over-saturates at 5 Hz, DMS suddenly disappears at the next spectral ordinate, with a sudden resurgence at 2.5 Hz. The horizontal component also shows the sudden disappearance of magnitude saturation at about the same frequency, although it does not return until about 1.5 seconds.

There is no apparent limitation in the data that would cause this result. However, this phenomenon may be associated with geological peculiarities of the SMART 1 site. For instance, Abrahamson (1985) found a breakdown of wave coherence at 4 Hz for accelerograms recorded across the SMART-1 array. Not finding any simple physical explanation for the coherence gap at 4 Hz, he suggested the possibility of a 4 Hz resonance for the wave scatterers under the array.

3.7.3 Predominant Frequency of Peak Parameters

Figure 3-55 also displays DMS for the peak ground-motion parameters by shaded bands in what may be the predominant frequency band of the parameter. DMS for vertical PGA is consistent with DMS at about 33 Hz, while DMS for the spectral ordinates is erratic in the 4 to 10 Hz range. Similarly, DMS for horizontal PGA compares well at 33 Hz but is not consistent with 0% for the 4 to 10 Hz spectral range.

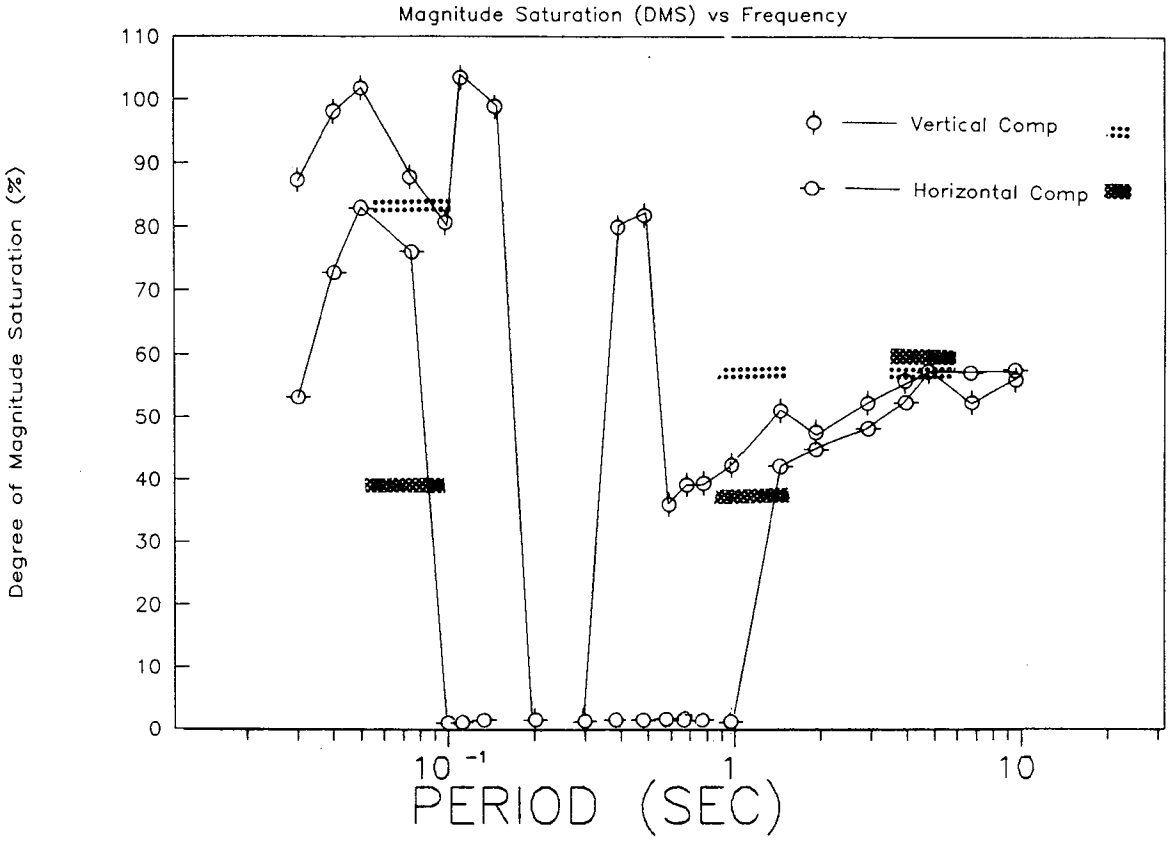

Figure 3.55 - Degree of Magnitude Saturation (DMS) as a function of frequency for vertical and horizontal spectral ordinates (see Tables 3.5 and 3.6). The estimates of DMS obtained from the regression analyses of peak ground observations are also shown by the shaded bands in the period range corresponding to PGA, PGV, and PGD.

DMS for vertical PGV is consistent with the spectral values near the 1.0 second period, but the horizontal component again shows no saturation near this period. The values for PGD are consistent for both components with the low frequency end of the spectra, although (as discussed above) results for DMS in the low frequency domain are not as well constrained as at higher frequencies.

3.7.4 Comparison with other Studies

The values predicted for peak vertical acceleration, for magnitudes 5.5, 6.5, and 7.5, are compared with those of Campbell (1982) and Donovan (1982) in Figure 3-7, Section 3.2. As noted previously, the model displays greater saturation of ground-motion amplitudes with magnitude. Also Figure 3-8 shows more saturation of PGA for the study than that of Abrahamson and Litehiser (1989).

A possible explanation for these disparities may be the non-uniformity of tectonic stresses associated with the worldwide data (used by these authors) combined with the small number of large magnitude recordings close to the source (their studies as well as this one). Thus some of those observations may be associated with high stress sources, such as those recorded in the 1976 Gazli and the 1978 Tabas earthquakes.

Results for the horizontal component are more intuitively consistent. For horizontal PGA, Campbell (1981) found more saturation than in this study: 88% vs. 39%. Also for horizontal PGV, Campbell (1984) found 100% saturation, while this study found 36%. Joyner and Boore (1981) found no magnitude saturation.

3.8 UNCERTAINTY OF PREDICTED VALUES

Independent from the regression analyses, for each event, the median and normalized standard deviation (coefficient of variation) is computed for vertical PGA, PGV, PGD, and PSV at the stations of the inner ring. This procedure assumes a log-normal distribution. This information is then used to explore the dependency of the coefficient of variation on magnitude and distance. This also allows us to study the relative contribution to the scatter of individual recordings and earthquakes.

3.8.1 Magnitude and Distance Dependency

The coefficient of variation for vertical PGA, PGV, and PGD is presented in Figures 3-56 to 3-58 as a function of magnitude. These plots display a negative trend with increasing magnitude. Expressed statistically, the correlation coefficient with respect to magnitude is calculated to be -0.617, -0.730, and -0.882 for vertical PGA, PGV, and PGD, respectively (Table 3-7). Thus, as magnitude increases, the data displays decreasing scatter.

In order to explore this trend for vertical spectral ordinates, we calculated the correlation coefficient for all periods between 0.03 and 10 seconds (Table 3-7). The correlation coefficient with respect to magnitude is found to be -0.472 (Figure 3-59), indicating a decrease in the scatter with increasing magnitude. This is the same trend as found for the peak parameters. The correlation coefficient with respect to distance is found to be -0.248 (Figure 3-60). This also indicates decreasing scatter with increasing distance, although the correlation for distance is not as robust as with magnitude.

These findings are consistent with those of Abrahamson (1988) who found the same trend with respect to magnitude for horizontal PGA. Based on his observations, Abrahamson suggested treating the standard error of PGA as magnitude dependent. Since we find the same trend with PGV and PSV, his suggestion could also be expanded to practically all ground-motion parameters.

Table 3.7 - Correlation coefficients ρ_{cov} of coefficients of variation of peak vertical ground-motion parameters and vertical spectral ordinates against magnitude

Ground-Motion Parameter	Period (sec)	ρ_{cov}
PGA		-0.637
PGV		-0.730
PGD		-0.882
PSV	0.03	-0.689
PSV	0.04	-0.724
PSV	0.05	-0.649
PSV	0.075	-0.584
PSV	0.10	-0.753
PSV	0.111	-0.657
PSV	0.15	-0.014
PSV	0.20	-0.005
PSV	0.286	-0.152
PSV	0.30	-0.169
PSV	0.40	-0.068
PSV	0.50	-0.471
PSV	0.60	-0.795
PSV	0.70	-0.886
PSV	0.80	-0.914
PSV	1.00	-0.891
PSV	1.50	-0.853
PSV	2.00	-0.835
PSV	3.00	-0.905
PSV	4.00	-0.757
PSV	5.00	-0.782
PSV	7.00	-0.713
PSV	10.00	-0.643
PSV	0.04-10	-0.472

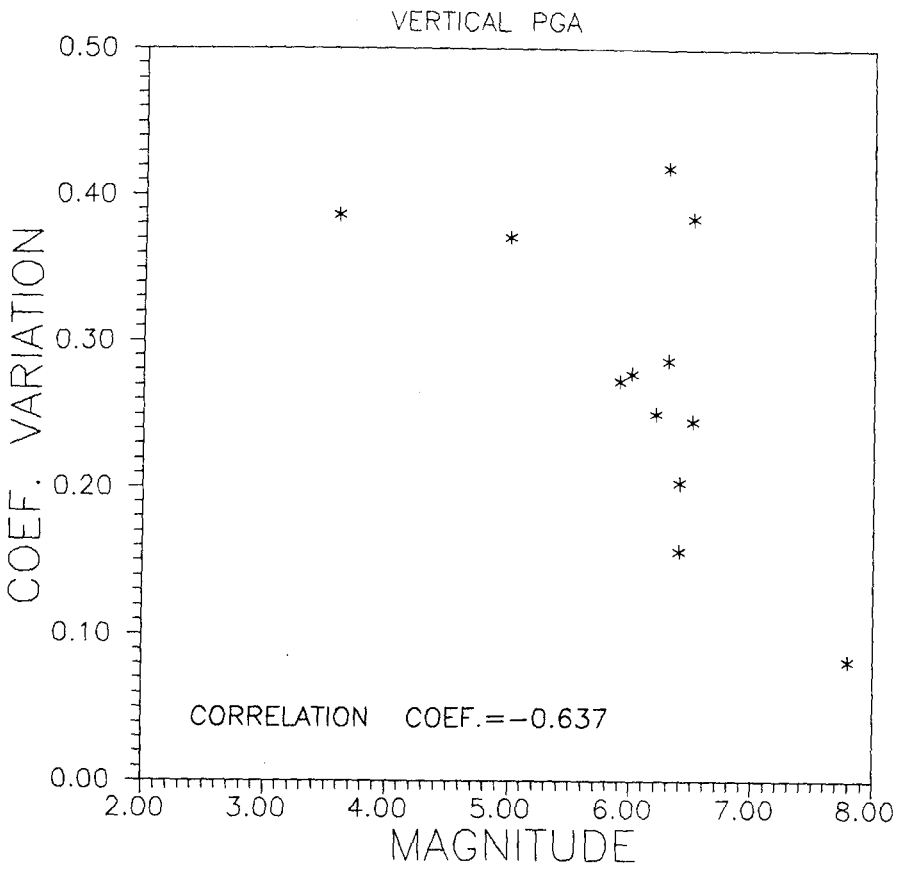

Figure 3.56 - Coefficient of variation for vertical PGA vs. event magnitude.

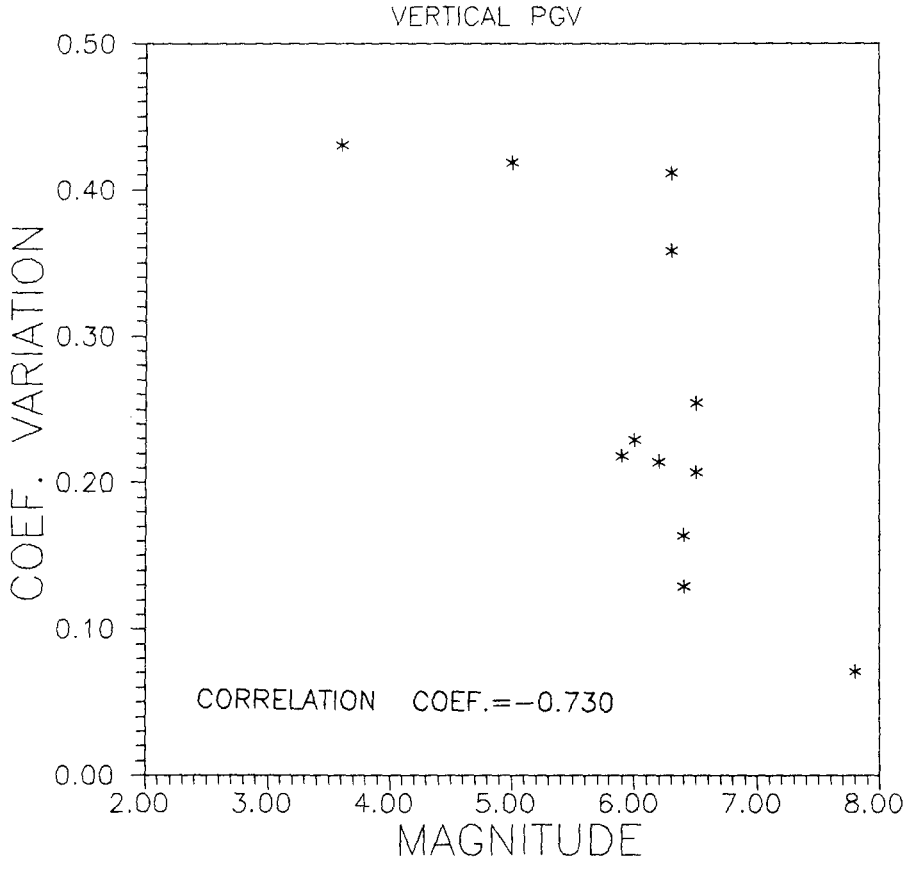

Figure 3.57 - Coefficient of variation for vertical PGV vs. event magnitude.

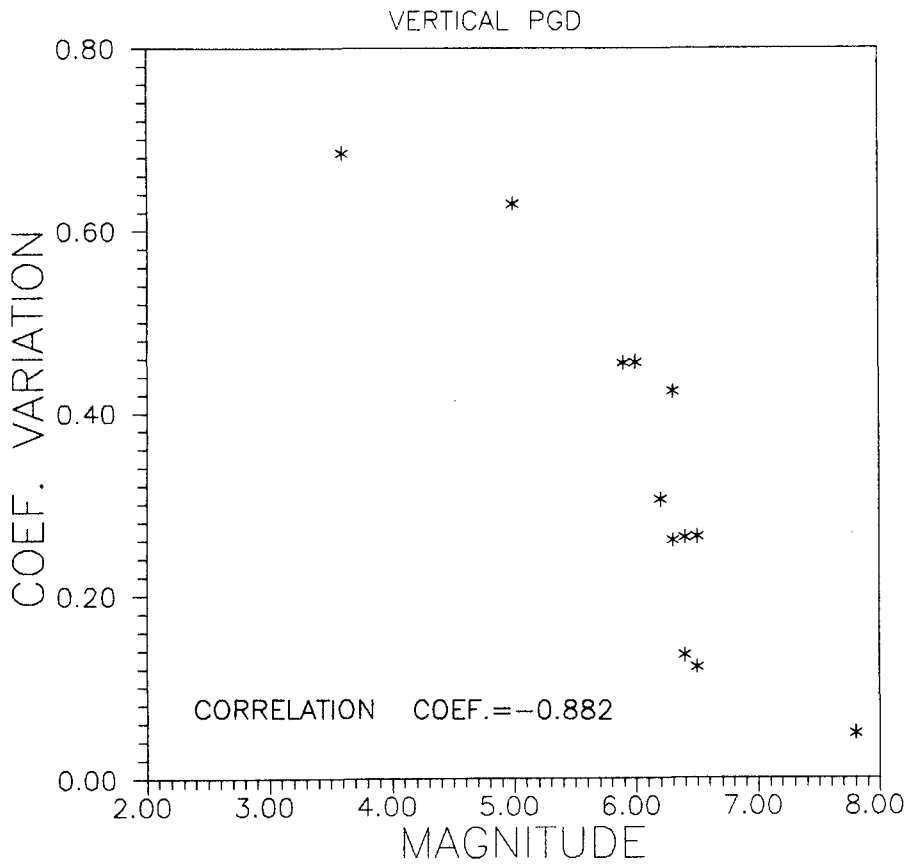

Figure 3.58 - Coefficient of variation for vertical PGD vs. event magnitude.

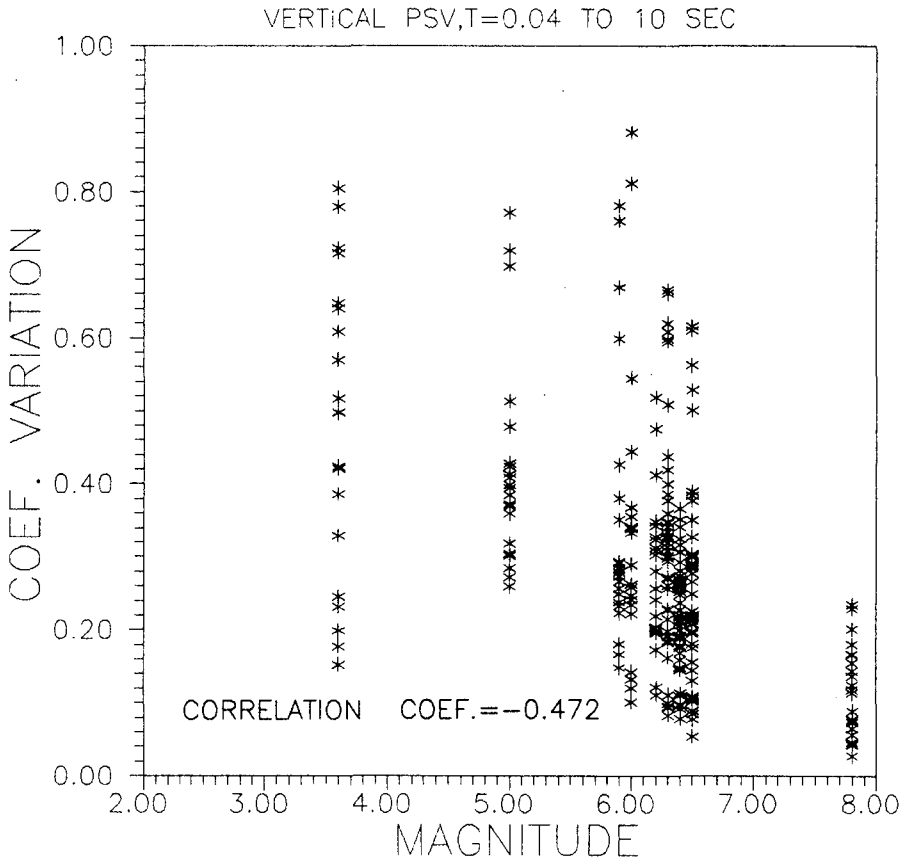

Figure 3.59 - Coefficient of variation for vertical PSV (Pseudo Spectral Velocity) in the period range 0.04-10.0 sec vs. event magnitude.

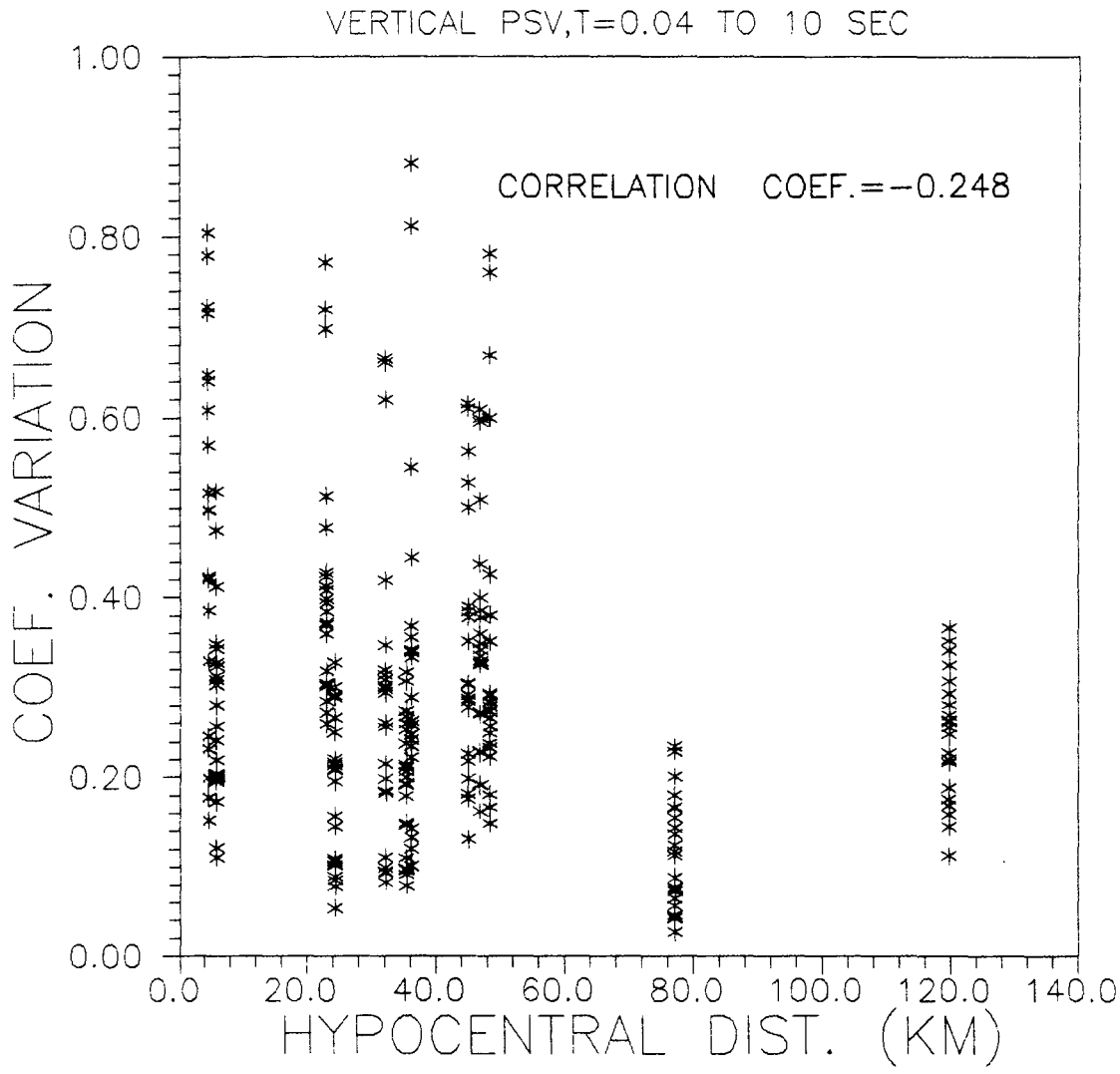

Figure 3.60 - Coefficient of variation for vertical PSV (Pseudo Spectral Velocity) in the period range 0.04-10.0 sec vs. hypocentral distance.

3.8.2 Contribution to Scatter

In order to compare the scatter of observations for an individual event with the total scatter, attention was focussed on the 200 in the inner ring. The standard deviation of the regression of the form described in Section 3.1, performed, for instance, on the vertical PGA was found to be $\sigma_{lnPGA}=0.529$. The corresponding coefficient of variation is 0.568 (after Benjamin and Cornell, 1970, pp. 265-267). In comparison, the coefficient of variation for individual events within the inner ring is found to be between 0.082 and 0.386, far less than the scatter for the whole regression. This comparison indicates that the inter-event variations are significant contributors to the overall uncertainty.

To explore this effect further, the scatter was eliminated within individual events by regressing on the mean vertical PGA value for each earthquake. The resulting standard deviation for this regression is $\sigma_{lnPGA}=0.569$, comparable to that of the regression on the individual observations and still significantly higher than that of the individual events. Therefore, the variation of the observed data (at the inner ring stations) within each earthquake, the intra-event uncertainty, does not have a significant effect on the standard error of the attenuation relationship. The major contributor to the uncertainty is the variation of ground-motion observations between earthquakes, the inter-event uncertainty. Inter-event uncertainty has been termed "modelling variability" by McGuire and Stepp (1986), as distinct from intra-event variation which they termed "probablistic variability" (randomness).

In the discussion below on Station Bias, we discuss the variation of observations from the perspective of residual analysis is discussed.

3.8.3 Analysis of Residuals

Fault Type

Recent analyses, such as Campbell (1981), have concluded that earthquakes with a reverse fault focal mechanism produce higher horizontal peak accelerations than normal or strike slip events. Among the justifications given is the possibility of higher stress drops associated with the reverse fault mechanism. This section reviews the distribution of residuals for the inner ring of the SMART 1 array to determine if the amplitudes of vertical PGA may be a function of fault mechanism.

The residuals for the nonlinear regression procedure has a mean of zero. These residuals are graphically displayed with respect to the natural log of the predicted values in Figure 3-61, for both vertical PGA and PGV. For each earthquake the mean residual of the observations within that event was computed. Table 3-8 presents the mean residual (in $\ln_{PGA}$), its standard deviation, and the focal mechanism for each event.

In Table 3-8, the three earthquakes with reverse and reverse oblique mechanisms all have positive residuals, indicating higher than predicted amplitudes. Three of the five events with normal or normal-oblique mechanisms have negative residuals, one is at the mean of the regression, and one has a very high residual of 1.149. The mean of the residuals for this latter event (number 39) is two standard deviations (1.149/0.553) from the mean of the regression. Also, the focal mechanism is not known for the remaining four events. Because of the lack of information for these four events, it is difficult to draw any conclusions with respect to the effect of fault type on the amplitude of vertical PGA.

Station Bias

As discussed in Section 2, the SMART 1 array eliminates many of the site effects which can influence the characteristics of recorded ground motion: subsurface geology is relatively uniform; the instruments are identical; they are all mounted on identical concrete mats; and variations in travel paths are reduced. Also, especially within the inner ring, the close spacing of the stations should eliminate bias with respect to focussing or radiation effects, since the stations would be uniformly placed with respect to any earthquake sources.

The mean residual for each station of the inner ring and the central station is displayed in Table 3-9 along with the standard deviation of these observations. The regression was conducted on the full vertical PGA data set, described in Section 2, with only the information on the inner ring and central station provided in the table. For this reason the residuals for the stations listed in Table 3-9 do not have a mean of zero, like the full regression.

Table 3.8 - Mean and standard deviation of regression residuals on ln(PGA) over the inner ring and central station per individual events

EVENT NO.	MEAN RESIDUAL	STAND. DEV.	SOURCE TYPE
5	0.212	0.260	Reverse
14	-0.470	0.343	
15	0.092	0.354	
20	0.751	0.177	Obliq.R
22	-0.335	0.196	Normal
29	-0.370	0.274	
31	0.225	0.265	
33	-0.224	0.362	Obliq.N
36	0.050	0.386	Normal
39	1.149	0.234	Normal
43	-0.118	0.250	Normal
45	0.168	0.090	Reverse

Table 3.9 - Mean and standard deviations of regression residuals on ln(PGA) over all 12 events per central and the inner ring stations

STATION	MEAN RESIDUAL	STAND. DEV.
C00	0.056	0.460
I01	0.111	0.545
I02	0.033	0.441
I03	0.046	0.490
I04	0.038	0.600
I05	0.183	0.498
I06	0.098	0.458
I07	-0.227	0.498
I08	0.131	0.532
I09	0.459	0.472
I10	-0.048	0.496
I11	0.213	0.607
I12	0.151	0.606

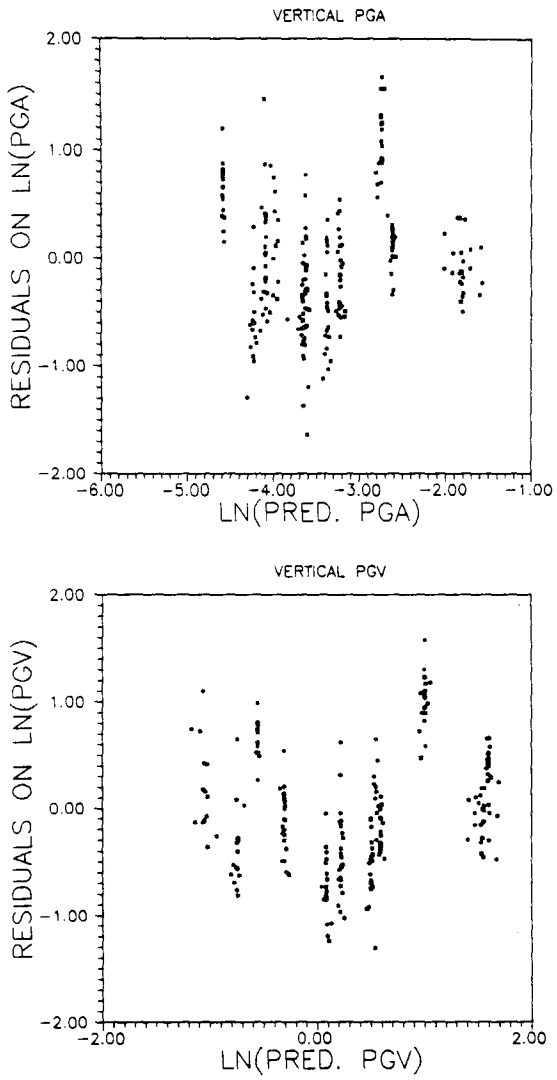

Figure 3.61 - Scattergram of regression residuals for vertical PGA and PGV vs. predicted values. Note, in both regressions, residuals have zero mean.

As expected for stations with such uniform site characteristics, the mean residuals are relatively small compared with the standard deviation. This indicates that the variation between stations is significantly less than the variation among earthquakes for each station. Another way of looking at this is that the inter-event uncertainty contributes more to the scatter than the variation in observations due to station bias.

Nevertheless, there are stations with mean residuals higher than others. Particularly, the mean for station I09 is about one standard deviation higher than the mean of the regression. Thus, almost 84% of the observations for this station fall above the predicted values based on all the stations. It is interesting that, in Section 2.5, it was pointed out that this station appeared to have a high energy content for event 22, in Figure 2-5. Apparently this station also records higher amplitudes for other earthquakes. It was not in the scope of this study to conduct site specific investigations to determine a possible cause for this trend.

3.9 SOIL AMPLIFICATION

As described in Section 2.1, the SMART-1 array is located near the southern boundary of the Lan-Yang Plain, underlain by recent alluvium. The central station is about 5 km from the southern edge of the valley where basement rock, slate of Miocene age, emerges to the surface. Here two stations, parts of an extended array, provide a unique opportunity to study the amplification of the peak parameters and spectral amplitudes by sedimentary overburden.

Station E2 is located on rock, whereas E1 is located nearly two kilometers to the north of E2 on about 150 meters of sedimentary materials. Their locations with respect to the rest of the array is shown in Figure 2-1. Because these stations were not operational until 1984, recordings are available for only six of the earthquakes in the data base.

For each of the three components of the triaxial accelerograms, the ratio of peak and spectral amplitudes recorded at the soil site to those at the rock site were computed. This was done for each of the recordings from the six earthquakes, for each peak parameter, and the 23 spectral ordinates considered in this study.

Figures 3-62 to 3-64 present these ratios for the three corresponding components. Ratios from the six events are indicated for each period studied. The solid line represents the mean of the ratios through each period, while the dashed lines indicate the mean plus and minus one standard deviation values. The horizontal solid line refers to a ratio of unity.

The first noticeable feature of these plots is that the mean ratio is almost always above unity, indicating that the soil site has higher spectral amplitudes than the rock site. Furthermore, the minus one standard deviation line generally remains above one.

For the vertical component, the soil site has about 1.5 times the amplitude of the rock site in the high frequency range, below 0.5 second. The ratio increases to nearly three in the mid frequency range (0.5 to 2 seconds) and falls off to about unity for the long-period ordinates. A study by Wen (1989) of nearby, down-hole rock and soil stations also found the dominant amplification centered in this frequency range.

The shape of the spectral ratios with respect to frequency are similar for the two horizontal components. They are relatively flat in the high frequency range, increase in the mid-period range and then decrease at longer periods. However, the horizontal ratios peak at about two seconds, while the maximum vertical ratio is at 0.8 second. The north-south component has ratios of about 1.35 at high frequencies, increasing to about three between 1 and 2 seconds, and decreasing to around 2.4 at longer periods. The east-west component shows higher ratios, starting at about 2 at the high frequency end of the spectrum, increasing to as high as 7 near two seconds, and falling off to 2 again at longer periods.

The mean ratios of soil to rock are given below for the peak parameters:

Soil/Rock (E1/E2)			
Component	PGA	PGV	PGD
E-W	2.1	3.0	2.4
N-S	1.3	1.7	2.4
Vertical	1.5	1.3	1.2

These results are, in most instances, consistent with those of the spectra at the comparable frequency range. Thus the peak parameters display the same general trends with frequency as described in the discussion above.

For the east-west component, PGA at a ratio of 2.1 is similar to the ratio of 2.0 for the high frequency range of PSV. The mid-frequency PGV increases to a ratio of three, though not as high as the one second spectral ordinate at about 5.0. Finally, low frequency PGD compares well at 2.4 with the low period spectral ordinates varying between 2 and 3.

For the north-south component, PGA matches the high frequency spectral ordinates with a ratio of 1.3. The ratio for PGV also increases in the mid-frequency range but not as much as for PSV. The ratio for PGD increases to 2.4 which is comparable to the low frequency ordinates.

The vertical component matches the high and low frequency spectral ordinates with the ratios for PGA and PGD, respectively. However, the ratio for PGV is smaller than that of PGA, whereas the ratio for the mid frequency ordinates are significantly higher than for PGA.

The ratio for the vertical component showed remarkably little variation between the six earthquakes, especially with respect to PGA. While the mean ratio for PGA is 1.5, the standard variation is only 0.07.

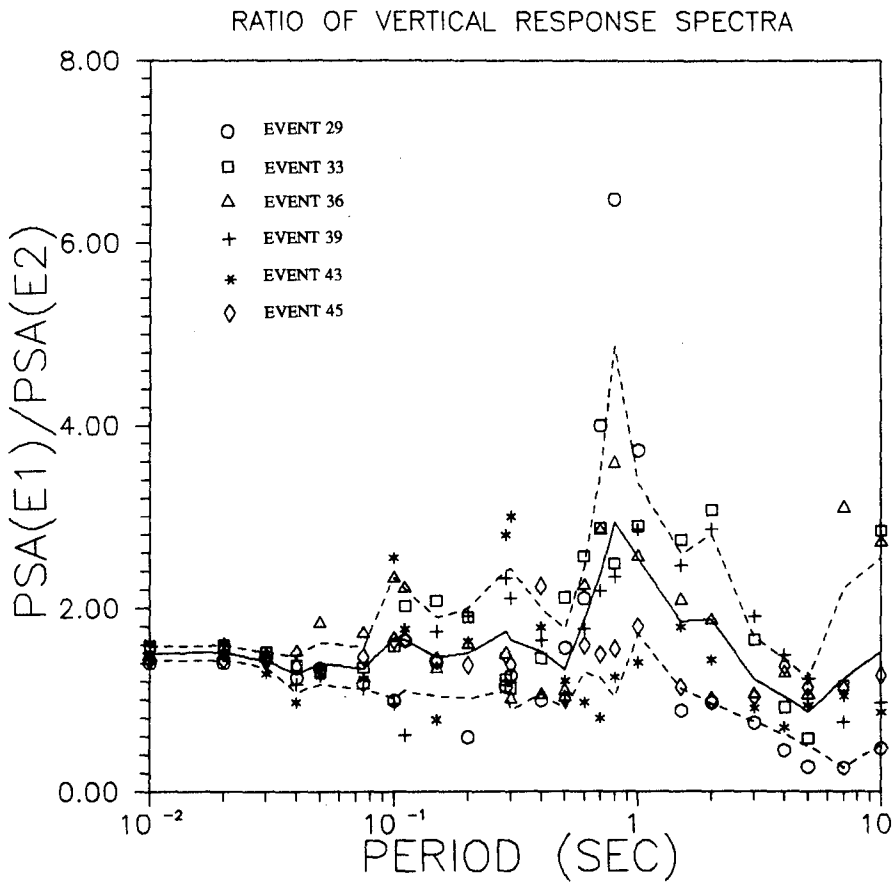

Figure 3.62 - Observed soil amplification at site E1 (Figure 1.1) relative to the neighboring rock site E2 for vertical spectral ordinates. Solid curve shows pointwise computed mean and dashed lines show one standard deviation band.

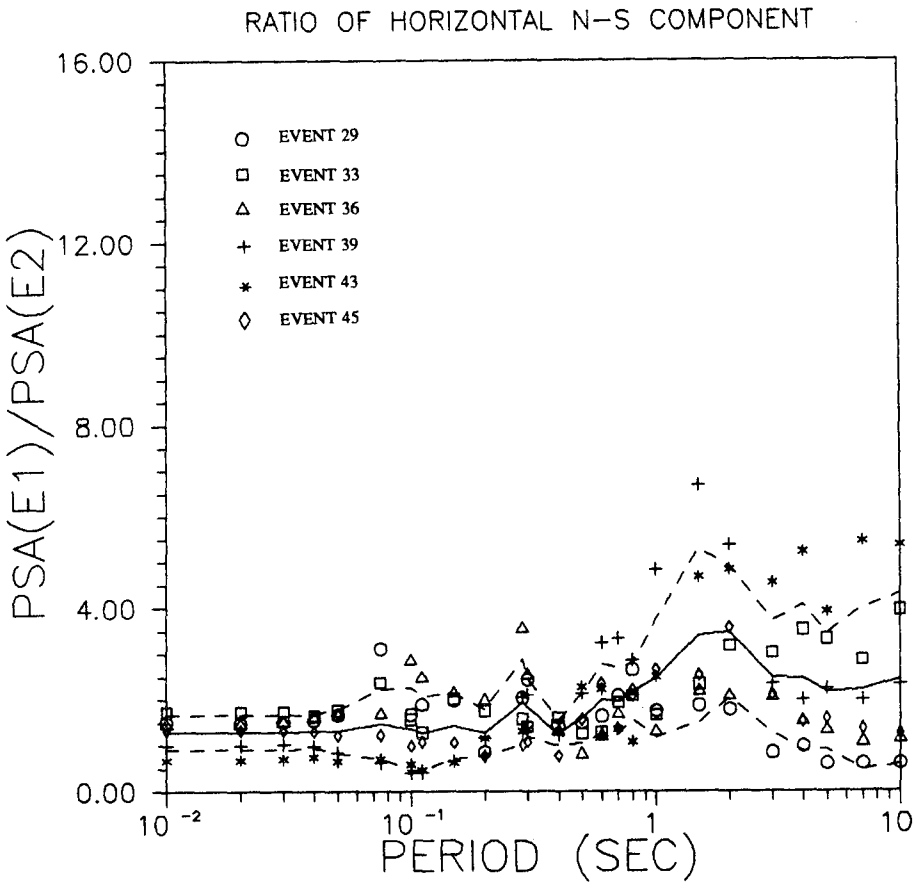

Figure 3.63 - Observed soil amplification at site E1 (Figure 1.1) relative to the neighboring rock site E2 for horizontal(N-S) spectral ordinates. Solid curve shows pointwise computed mean and dashed lines show one standard deviation band.

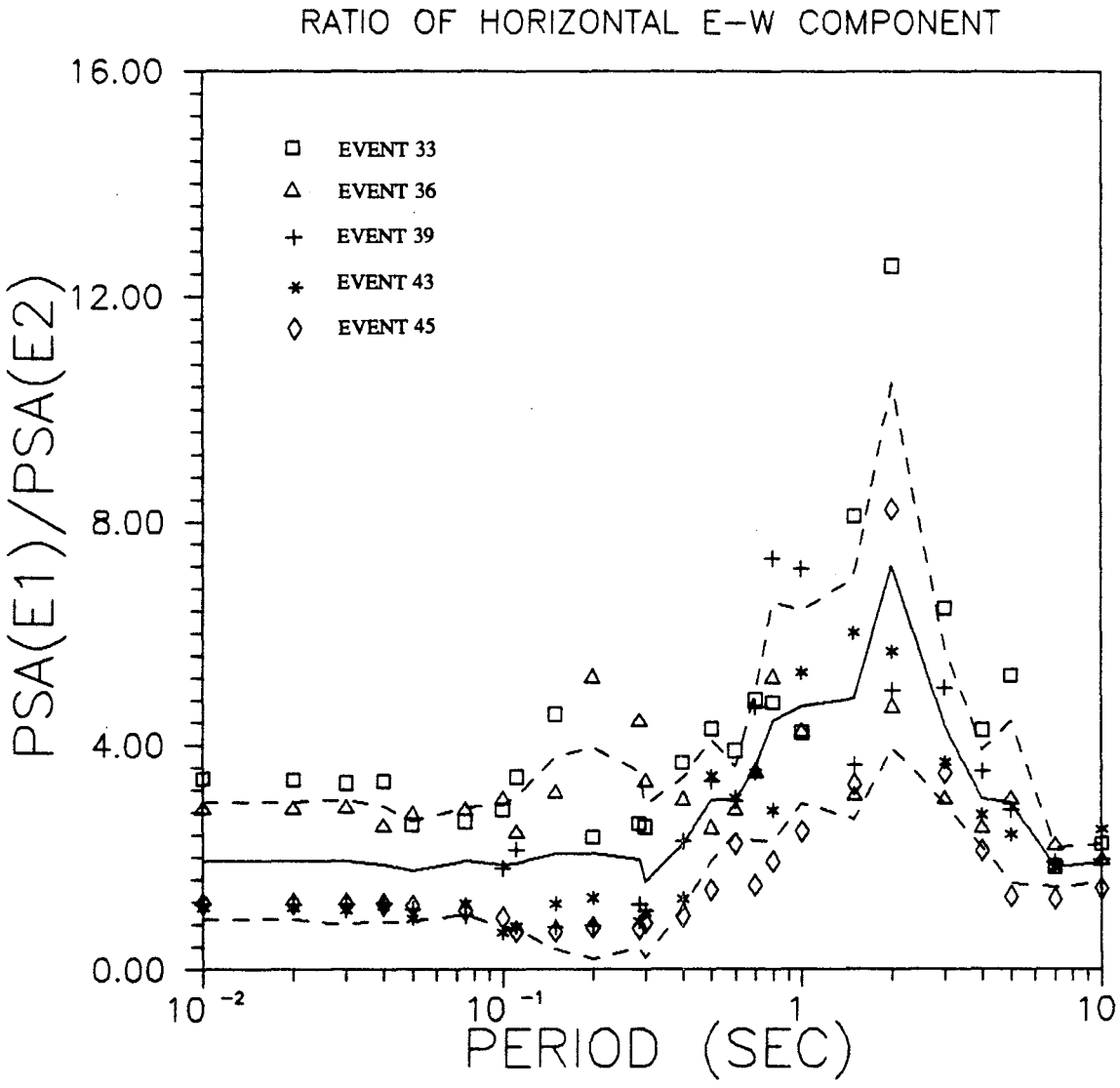

Figure 3.64 - Observed soil amplification at site E1 (Figure 1.1) relative to the neighboring rock site E2 for horizontal(E-W) spectral ordinates. Solid curve shows pointwise computed mean and dashed lines show one standard deviation band.

3.10 OBSERVED RATIOS PGV/PGA AND PGD/PGA

This study examined the ratios PGV/PGA and PGD/PGA for magnitude 5.0 to 6.5 earthquakes. The results of this analysis are discussed separately in Niazi and Bozorgnia (1990) and are summarized below.

The data used in this analysis are presented in Tables 3-10 and 3-11. These tables list the observed values of PGA, PGV, and PGD, for the inner ring stations which recorded each earthquake analyzed. The observed ratios with respect to PGA for each station and each event are also provided. The tables then present the mean and standard deviation of these parameters computed for each earthquake.

In terms of in./sec./g and in./g the mean and standard deviation values for all events for vertical PGV/PGA (V/A), PGD/PGA (D/A), and PGA*PGD/PGV^2 (AD/V^2) are 16.00 ± 3.08, 5.05 ± 2.18, and 7.53 ± 2.07, respectively. The corresponding estimates for the horizontal component are 31.88 ± 13.96, 7.74 ± 4.66, and 3.07 ± 0.91, which demonstrate much larger variability than the vertical. We find that the ratios for the vertical component are more stable than those for the horizontal.

The significance of these ratios is in their application to the design basis of critical facilities. In a statistical study of earthquake response spectra, Hall et al. (1976) studied the range of variation of V/A and AD/V^2 for a data base of 56 accelerograms produced by 22 moderate to strong earthquakes located mainly in the western U.S. A previously suggested design spectra (Newmark et al., 1973) implied a fairly constant value for these ratios, depending on site geology. Based on these studies Newmark and Hall (1982) recommended ratios for V/A of 48 in./sec/g and AD/V^2 of 6 for competent soil conditions for construction design spectra.

Assuming a normal distribution, the 84th percentile horizontal estimate for V/A approaches the predictions of Hall et al. (1976). However, the recommended ratio for the vertical component exceeds the 84th percentile estimate by nearly a factor of 2. This observation implicitly leads to different shapes for the horizontal and vertical response spectra. Such differences in the behavior of vertical and horizontal ground motion are not reported by Hall et al. (1976). Concerning the values of AD/V^2, the findings of this study are slightly above 6 for the vertical and substantially below 6 for the horizontal components.

Hall et al. (1976) divided their observations into three ranges of recorded PGA (0.05-0.10, 0.10-0.20, and >0.20), implying that the ratios may be dependent on the amplitude of PGA. However, this study did not reveal a clear dependence on PGA, for any of the ratios, except AD/V^2 which shows a weak inverse correlation with magnitude.

Table 3-10

Ratio of Observed Vertical Peak Values at each Station for each Event and Mean and Standard Deviation for each Event

Event	Sta.	Comp.	PGA (cm/sec^2)	PGV (cm/sec)	PGD (cm)	D/A (in/g)	V/A (in/s/g)	A*D/V/V
5	C00	v	43.4800	2.0100	.6600	5.8626	17.8543	7.1030
5	I06	v	31.9600	1.6700	.4700	5.6797	20.1811	5.3861
5	I09	v	66.7000	3.3200	.8800	5.0956	19.2242	5.3252
5	I12	v	59.6700	2.1000	.6500	4.2072	13.5925	8.7949
	M E A N		50.4525	2.2750	.6650	5.2113	17.7130	6.6523
	STD DEV		13.5972	.6243	.1453	.6452	2.5186	1.4282
14	I02	v	7.9000	.3400	.2400	11.7333	16.6221	16.4014
14	I04	v	5.4800	.2100	.0700	4.9335	14.8004	8.6984
14	I05	v	13.0000	.3600	.1000	2.9709	10.6953	10.0309
14	I07	v	7.8700	.3600	.2900	14.2318	17.6670	17.6103
14	I08	v	10.4200	.3500	.2000	7.4131	12.9729	17.0122
14	I09	v	18.9400	.9100	.4000	8.1567	18.5565	9.1487
14	I11	v	5.6900	.2200	.1100	7.4665	14.9330	12.9318
14	I12	v	7.2500	.5100	.2900	15.4488	27.1686	8.0834
	M E A N		9.5688	.4075	.2125	9.0443	16.6770	12.4896
	STD DEV		4.2298	.2090	.1070	4.1061	4.6186	3.7611
15	C00	v	20.5700	.4100	.2100	3.9429	7.6981	25.6972
15	I01	v	37.8400	1.0300	.6800	6.9405	10.5129	24.2541
15	I03	v	17.8200	.4100	.1600	3.4677	8.8861	16.9613
15	I07	v	15.1400	.5400	.5000	12.7550	13.7754	25.9602
15	I08	v	26.8300	.4000	.1200	1.7274	5.7580	20.1225
15	I10	v	12.8200	.3300	.1900	5.7240	9.9417	22.3673
15	I12	v	27.8800	.5300	.3100	4.2944	7.3421	30.7682
	M E A N		22.7000	.5214	.3100	5.5503	9.1306	23.7330
	STD DEV		8.0731	.2189	.1912	3.3162	2.4150	4.1290
20	C00	v	15.5100	1.0200	.5800	14.4428	25.3994	8.6465
20	I04	v	20.6600	1.0600	.2800	5.2344	19.8158	5.1485
20	I07	v	17.1500	1.1600	.4700	10.5845	26.1234	5.9903
20	I08	v	21.6100	1.2500	.3100	5.5404	22.3404	4.2874
20	I09	v	32.6600	1.5300	.3900	4.6119	18.0930	5.4412
20	I10	v	23.9300	1.2000	.3300	5.3261	19.3675	5.4840
20	I11	v	21.2200	1.1800	.5000	9.1004	21.4769	7.6199
	M E A N		21.8200	1.2000	.4086	7.8343	21.8023	6.0883
	STD DEV		5.1455	.1537	.1030	3.4129	2.8193	1.4046

Table 3-10 (Continued)

22	I01	v	33.2300	1.2800	.4200	4.8815	14.8770	8.5184
22	I03	v	24.5100	1.2000	.4700	7.4061	18.9092	7.9998
22	I04	v	24.7600	1.2300	.6000	9.3591	19.1862	9.8196
22	I06	v	33.3000	1.7900	.6300	7.3069	20.7608	6.5475
22	I07	v	30.0200	1.4500	.6000	7.7193	18.6549	8.5669
22	I09	v	38.3800	2.0200	.4700	4.7296	20.3274	4.4208
22	I10	v	22.5700	1.3000	.5100	8.7272	22.2458	6.8111
22	I11	v	18.8900	1.2700	.4800	9.8140	25.9661	5.6217
22	I12	v	25.1600	1.2900	.4300	6.6007	19.8022	6.5013
	M E A N		27.8689	1.4256	.5122	7.3938	20.0811	7.2008
	STD DEV		5.8721	.2699	.0739	1.6882	2.8129	1.5772
29	I02	v	20.5400	.6800	.3500	6.5812	12.7863	15.5471
29	I03	v	14.1500	.5600	.0800	2.1836	15.2851	3.6097
29	I05	v	22.3000	.7100	.1500	2.5979	12.2967	6.6356
29	I06	v	23.8300	.7200	.2700	4.3760	11.6693	12.4115
29	I07	v	11.2300	.4600	.1600	5.5027	15.8203	8.4915
29	I11	v	28.7500	1.0300	.1600	2.1494	13.8368	4.3359
29	I12	v	17.2700	.5200	.1700	3.8018	11.6291	10.8576
	M E A N		19.7243	.6686	.1914	3.8846	13.3319	8.8413
	STD DEV		5.5404	.1742	.0827	1.5901	1.5718	4.0433
31	C00	v	16.9200	.6000	.1700	3.8805	13.6958	7.9900
31	I01	v	23.5600	.9000	.2500	4.0983	14.7538	7.2716
31	I02	v	19.9400	.6600	.2600	5.0360	12.7836	11.9017
31	I05	v	24.3100	.7800	.2900	4.6073	12.3921	11.5876
31	I06	v	18.1200	.5700	.0900	1.9183	12.1493	5.0194
31	I07	v	15.1300	.6600	.3100	7.9133	16.8477	10.7674
31	I08	v	24.5900	.8000	.2500	3.9266	12.5651	9.6055
31	I09	v	38.7800	1.2500	.1900	1.8923	12.4491	4.7156
31	I10	v	22.5800	.8400	.1000	1.7105	14.3678	3.2001
31	I11	v	24.3000	.8300	.1400	2.2251	13.1919	4.9383
31	I12	v	16.7900	.5400	.2900	6.6709	12.4216	16.6979
	M E A N		22.2745	.7664	.2127	3.9890	13.4198	8.5177
	STD DEV		6.1813	.1913	.0750	1.9326	1.3585	3.8571
33	C00	v	21.2500	.8200	.3400	6.1795	14.9036	10.7451
33	I02	v	47.5000	1.3800	.1800	1.4636	11.2207	4.4896
33	I03	v	21.0600	1.0500	.2500	4.5848	19.2560	4.7755
33	I06	v	22.1200	.8200	.3400	5.9365	14.3174	11.1850
	M E A N		27.9825	1.0175	.2775	4.5411	14.9244	7.7988
	STD DEV		11.2755	.2294	.0672	1.8778	2.8657	3.1717

Table 3-10 (Continued)

36	C00	v	23.0600	.8500	.2100	3.5172	14.2362	6.7026
36	I01	v	18.6400	.6000	.1900	3.9368	12.4320	9.8378
36	I02	v	34.3400	1.1900	.2200	2.4743	13.3839	5.3349
36	I04	v	31.2100	1.1100	.4400	5.4450	13.7361	11.1455
36	I05	v	56.4000	2.3100	.2400	1.6435	15.8186	2.5367
36	I07	v	13.7400	.6500	.1400	3.9353	18.2710	4.5529
36	I08	v	24.1500	1.0900	.4600	7.3566	17.4319	9.3502
36	I11	v	46.2200	1.6900	.2100	1.7548	14.1219	3.3984
	M E A N		30.9700	1.1862	.2637	3.7579	14.9289	6.6074
	STD DEV		13.4566	.5334	.1110	1.8045	1.9171	2.9848
39	C00	v	216.3800	8.0200	1.2400	2.2133	14.3150	4.1715
39	I01	v	219.5600	9.3300	1.3000	2.2868	16.4121	3.2789
39	I02	v	159.8900	8.8300	1.4800	3.5750	21.3292	3.0350
39	I03	v	179.1300	8.2900	1.2000	2.5873	17.8740	3.1278
39	I04	v	206.5700	6.6800	1.4700	2.7484	12.4895	6.8051
39	I05	v	157.6200	7.0800	1.4800	3.6265	17.3483	4.6538
39	I06	v	184.7500	7.7300	1.2800	2.6758	16.1596	3.9576
39	I07	v	125.7100	6.1700	1.1200	3.4410	18.9562	3.6984
39	I08	v	233.0300	6.9500	1.2900	2.1380	11.5188	6.2235
39	I09	v	227.6000	8.0400	1.3000	2.2060	13.6433	4.5772
39	I11	v	215.2400	10.0000	1.3900	2.4942	17.9437	2.9918
39	I12	v	329.7700	13.1700	1.8000	2.1081	15.4245	3.4223
	M E A N		204.6042	8.3575	1.3625	2.6750	16.1178	4.1619
	STD DEV		49.1230	1.7994	.1711	.5432	2.6988	1.1882
43	C00	v	166.8800	4.6100	.8100	1.8746	10.6692	6.3604
43	I01	v	136.1300	3.0100	.7100	2.0144	8.5398	10.6679
43	I02	v	105.7400	3.0300	.5500	2.0089	11.0672	6.3346
43	I03	v	125.6400	3.5400	.7000	2.1518	10.8820	7.0181
43	I04	v	113.4000	4.1500	1.4700	5.0066	14.1342	9.6791
43	I05	v	136.2500	4.6300	.6000	1.7008	13.1244	3.8135
43	I06	v	157.6100	4.8200	.6300	1.5438	11.8113	4.2740
43	I07	v	98.5600	2.9800	.6600	2.5863	11.6775	7.3251
43	I08	v	140.5100	3.5300	.8500	2.3364	9.7029	9.5847
43	I09	v	139.7600	5.5900	.9500	2.6253	15.4477	4.2490
43	I10	v	126.0300	3.3400	.5300	1.6242	10.2355	5.9877
43	I11	v	224.7100	3.9300	.5000	.8594	6.7547	7.2746
43	I12	v	225.2400	5.1900	.9800	1.6804	8.8993	8.1948
	M E A N		145.8815	4.0269	.7646	2.1548	10.9958	6.9818
	STD DEV		38.2843	.8428	.2515	.9388	2.2552	2.0745

Table 3-10 (Continued)

45	C00	v	72.8800	7.2700	2.9800	15.7922	38.5267	4.1092
45	I01	v	76.4100	7.5800	3.0600	15.4670	38.3137	4.0694
45	I02	v	78.0700	6.3800	3.0900	15.2866	31.5625	5.9265
45	I03	v	96.8800	6.7400	3.0900	12.3186	26.8696	6.5898
45	I04	v	83.2100	7.6800	3.5000	16.2453	35.6468	4.9377
45	I05	v	78.8100	8.1700	3.2700	16.0251	40.0383	3.8609
45	I06	v	92.4700	8.2400	3.4500	14.4097	34.4161	4.6986
45	I07	v	87.4500	7.5500	3.2900	14.5302	33.3444	5.0473
45	I08	v	86.6000	7.5200	3.1500	14.0484	33.5379	4.8238
45	I09	v	93.7200	7.6600	3.0700	12.6515	31.5669	4.9036
45	I11	v	80.3300	7.2800	3.0000	14.4238	35.0017	4.5471
45	I12	v	94.7500	7.5100	3.0800	12.5547	30.6123	5.1743
	M E A N		85.1317	7.4650	3.1692	14.4794	34.1197	4.8907
	STD DEV		7.6834	.4985	.1633	1.3156	3.5835	.7401

Table 3-11

Ratios of Observed Horizontal Peak Values at each Station for each Event and Mean and Standard Deviation for each Event

Event	Sta.	Comp	PGA (cm/sec^2)	PGV (cm/sec)	PGD (cm)	D/A (in/g)	V/A (in/sec/g)	$A*D/V^2$
5	C00	H	107.2450	10.2350	1.6000	5.7621	36.8592	1.6380
5	I03	H	84.1200	9.6250	1.7050	7.8282	44.1913	1.5482
5	I06	H	85.2000	8.1100	1.4400	6.5277	36.7635	1.8654
5	I09	H	88.2600	9.1600	1.5400	6.7389	40.0836	1.6199
5	I12	H	127.4400	9.0250	1.6950	5.1369	27.3512	2.6520
	M E A N		98.4530	9.2310	1.5960	6.3987	37.0498	1.8647
	STD DEV		16.7482	.7025	.0992	.9136	5.5567	.4078
14	C00	H	23.0300	1.0100	.1100	1.8447	16.9380	2.4834
14	I02	H	27.9650	1.1700	.2550	3.5218	16.1587	5.2093
14	I05	H	21.2250	1.0700	.1150	2.0926	19.4702	2.1320
14	I07	H	12.6350	.8550	.2750	8.4061	26.1352	4.7531
14	I08	H	20.5700	1.0250	.1850	3.4735	19.2453	3.6221
14	I09	H	19.1300	1.3400	.4350	8.7823	27.0536	4.6344
14	I11	H	14.0300	.7600	.2450	6.7444	20.9214	5.9511
14	I12	H	17.8000	1.1000	.2950	6.4008	23.8676	4.3397
	M E A N		19.5481	1.0412	.2394	5.1583	21.2238	4.1406
	STD DEV		4.5866	.1678	.0988	2.5893	3.8112	1.2313
15	C00	H	11.2800	.2650	.1000	3.4239	9.0734	16.0627
15	I01	H	26.4900	.5950	.3800	5.5403	8.6750	28.4336
15	I02	H	14.7250	.3000	.1200	3.1475	7.8687	19.6333
15	I03	H	11.7300	.5850	.5350	17.6153	19.2616	18.3375
15	I08	H	9.2850	.1600	.1050	4.3676	6.6554	38.0830
15	I12	H	18.0050	.4850	.3600	7.7223	10.4036	27.5557
	M E A N		15.2525	.3983	.2667	6.9695	10.3230	24.6843
	STD DEV		5.7436	.1660	.1678	4.9982	4.1565	7.5493
20	C00	H	36.3850	2.4350	1.0800	11.4640	25.8471	6.6275
20	I01	H	44.4950	3.5600	.8250	7.1611	30.9011	2.8964
20	I06	H	27.7050	2.9350	.6450	8.9916	40.9153	2.0744
20	I10	H	37.1350	2.9200	.6600	6.8643	30.3693	2.8745
20	I11	H	37.3950	3.0500	.9350	9.6568	31.5008	3.7586
20	I12	H	42.2000	3.2950	.6800	6.2235	30.1563	2.6431
	M E A N		37.5525	3.0325	.8042	8.3935	31.6150	3.4791
	STD DEV		5.2967	.3480	.1608	1.8234	4.5454	1.4926

Table 3-11 (Continued)

22	C00	H	42.2450	3.5000	1.2300	11.2451	31.9984	4.2417
22	I01	H	51.5200	3.8650	1.4400	10.7950	28.9740	4.9664
22	I02	H	60.6000	3.9350	1.3900	8.8589	25.0788	5.4400
22	I03	H	44.8050	3.5550	1.3600	11.7232	30.6442	4.8215
22	I06	H	33.4950	4.0300	1.4750	17.0078	46.4687	3.0420
22	I07	H	25.6050	3.2500	1.2650	19.0810	49.0223	3.0665
22	I11	H	32.4800	3.3700	1.2400	14.7449	40.0728	3.5463
22	I12	H	38.8000	3.5850	1.3250	13.1892	35.6856	4.0001
	M E A N		41.1937	3.6362	1.3406	13.3306	35.9931	4.1406
	STD DEV		10.4959	.2609	.0859	3.2009	7.9780	.8350
29	I01	H	38.0050	2.0500	.2600	2.6422	20.8328	2.3513
29	I03	H	33.8900	1.9800	.2550	2.9061	22.5647	2.2044
29	I05	H	33.1900	1.6100	.3250	3.7819	18.7350	4.1614
29	I06	H	30.2000	1.4900	.3450	4.4121	19.0552	4.6930
29	I07	H	23.5750	1.2800	.2050	3.3584	20.9698	2.9498
29	I08	H	29.7700	1.8850	.7550	9.7950	24.4550	6.3256
29	I11	H	46.2500	2.0450	.2050	1.7119	17.0772	2.2671
29	I12	H	43.3500	3.5950	1.2850	11.4485	32.0291	4.3102
	M E A N		34.7788	1.9919	.4544	5.0070	21.9649	3.6578
	STD DEV		6.9853	.6607	.3555	3.3514	4.3719	1.3749
31	I01	H	46.2000	3.1950	.4300	3.5947	26.7094	1.9461
31	I02	H	53.7150	2.5050	.2850	2.0492	18.0114	2.4396
31	I03	H	45.1900	2.5800	.3300	2.8204	22.0502	2.2404
31	I04	H	75.0650	2.9850	.6500	3.3443	15.3583	5.4760
31	I05	H	53.7050	2.7050	.3900	2.8047	19.4531	2.8625
31	I06	H	46.6750	2.6300	.2500	2.0687	21.7624	1.6870
31	I07	H	31.2900	2.4100	.2750	3.3944	29.7472	1.4815
31	I08	H	47.7600	2.5550	.3850	3.1134	20.6615	2.8167
31	I09	H	54.9900	2.8250	.3000	2.1070	19.8413	2.0671
31	I10	H	75.6150	3.1400	.2750	1.4046	16.0382	2.1090
31	I11	H	52.2650	2.5200	.2200	1.6257	18.6219	1.8106
31	I12	H	39.9250	2.5550	.3600	3.4825	24.7162	2.2017
	M E A N		51.8663	2.7171	.3458	2.6508	21.0809	2.4282
	STD DEV		12.2657	.2496	.1097	.7350	4.0765	1.0003
33	I02	H	98.1100	4.0550	1.0900	4.2909	15.9629	6.5037
33	I03	H	65.7350	4.0000	.6450	3.7896	23.5017	2.6499
33	I04	H	108.5600	4.5900	.6800	2.4192	16.3297	3.5039
33	I05	H	71.6950	3.3800	.6150	3.3130	18.2080	3.8595
33	I06	H	52.5200	3.3050	.5850	4.3020	24.3042	2.8128
33	I12	H	75.3600	3.3200	.5050	2.5881	17.0150	3.4527
	M E A N		78.6633	3.7750	.6867	3.4505	19.2203	3.7971
	STD DEV		19.0704	.4791	.1884	.7497	3.3919	1.2792

Table 3-11 (Continued)

36	C00	H	56.0650	2.4750	.3450	2.3766	17.0498	3.1576
36	I01	H	74.6000	2.9650	.3950	2.0450	15.3505	3.3519
36	I04	H	92.9150	3.8100	.5200	2.1615	15.8371	3.3284
36	I06	H	48.1150	2.0550	.3550	2.8496	16.4955	4.0447
36	I07	H	23.9800	1.6300	.2700	4.3486	26.2527	2.4369
36	I08	H	34.2150	2.3100	.5950	6.7164	26.0754	3.8151
36	I11	H	77.1150	2.9100	.4950	2.4791	14.5744	4.5077
36	I12	H	60.2800	2.7550	.3650	2.3386	17.6516	2.8988
	M E A N		58.4106	2.6137	.4175	3.1644	18.6609	3.4427
	STD DEV		21.4721	.6178	.1014	1.5062	4.4236	.6170
39	C00	H	246.3050	39.0400	8.8750	13.9165	61.2170	1.4342
39	I01	H	230.0850	32.2600	7.7900	13.0763	54.1516	1.7223
39	I02	H	235.0200	35.4650	7.7800	12.7853	58.2815	1.4537
39	I03	H	193.2700	32.4600	8.0950	16.1766	64.8663	1.4849
39	I04	H	214.3950	34.8600	9.0650	16.3301	62.7983	1.5993
39	I05	H	173.2750	31.1250	8.2050	18.2885	69.3759	1.4676
39	I06	H	161.3350	30.3450	7.9500	19.0315	72.6430	1.3929
39	I07	H	167.0550	27.5200	8.0450	18.5995	63.6245	1.7746
39	I08	H	176.7750	30.5250	8.5750	18.7348	66.6914	1.6268
39	I09	H	191.8600	30.3350	7.8100	15.7218	61.0653	1.6283
39	I11	H	218.3600	31.8650	7.5000	13.2655	56.3607	1.6129
39	I12	H	236.4100	33.5900	8.0650	13.1757	54.8756	1.6899
	M E A N		203.6788	32.4492	8.1463	15.7585	62.1626	1.5739
	STD DEV		28.7645	2.8676	.4483	2.3604	5.4798	.1189
43	C00	H	179.5850	19.7300	4.8300	10.3875	42.4319	2.2282
43	I01	H	163.4000	19.7150	5.4100	12.7873	46.5994	2.2743
43	I02	H	142.5600	17.9950	6.3250	17.1356	48.7517	2.7845
43	I04	H	144.7000	19.4000	5.3100	14.1730	51.7808	2.0415
43	I05	H	126.8150	17.3050	4.7550	14.4816	52.7031	2.0136
43	I06	H	124.8350	17.3000	4.8000	14.8505	53.5236	2.0021
43	I07	H	130.5300	18.4300	5.0150	14.8387	54.5319	1.9272
43	I08	H	151.8800	19.9550	5.7850	14.7109	50.7442	2.2065
43	I09	H	147.6050	19.0750	5.5950	14.6398	49.9113	2.2697
43	I10	H	136.1400	17.2150	4.7300	13.4187	48.8379	2.1729
43	I11	H	146.4800	17.6850	4.9200	12.9725	46.6296	2.3043
43	I12	H	142.4200	19.3150	5.5050	14.9287	52.3792	2.1015
	M E A N		144.7458	18.5933	5.2483	14.1104	49.9020	2.1939
	STD DEV		14.7989	1.0104	.4755	1.5563	3.3248	.2135

Table 3-11 (Continued)

45	C00	H	138.7150	28.6350	9.0650	25.2394	79.7277	1.5335
45	I01	H	137.1150	30.0950	9.0800	25.5762	84.7705	1.3746
45	I02	H	153.7050	31.5000	9.8500	24.7505	79.1513	1.5258
45	I03	H	146.4950	30.4050	9.5750	25.2436	80.1600	1.5173
45	I04	H	150.0750	28.8950	8.9900	23.1359	74.3618	1.6159
45	I05	H	125.3900	26.8350	8.6150	26.5355	82.6559	1.5001
45	I06	H	114.4600	24.4850	8.5750	28.9345	82.6193	1.6371
45	I07	H	121.1150	24.7350	8.9050	28.3969	78.8768	1.7628
45	I08	H	120.3150	26.9850	9.0500	29.0512	86.6239	1.4953
45	I09	H	113.7850	27.1300	9.1550	31.0748	92.0874	1.4153
45	I11	H	112.4650	27.2250	8.8850	30.5123	93.4944	1.3482
45	I12	H	126.9300	29.4650	8.8950	27.0656	89.6556	1.3005
	M E A N		130.0471	28.0325	9.0533	27.1264	83.6820	1.5022
	STD DEV		14.0797	2.0921	.3438	2.3642	5.5766	.1255

3.11 GROUND-MOTION COHERENCE

The variation of ground-motion coherence with respect to frequency was studied for the vertical component over the stations of the 200 m radius inner-ring sub-array. As a measure of coherence, the following ratio, suggested by Smith et al. (1982) was used: the ratio of the response spectra computed for the mean of the individual time histories across the array to the mean of the individual response spectra for recordings over the array. However, since the central station (C00) is located at the geometric center of the sub-array, the acceleration time-history of this station served as the empirical mean of the inner-ring time histories.

For each event, Figures 3-65 and 3-66 plot the ratio of the C00 spectral ordinates to the mean of all spectral ordinates recorded for the eleven corresponding events (for clarity they are reproduced on two figures). Event 31 is not included, since it did not produce a usable record at C00. All response spectra are at 5% critical damping.

The mean and standard deviation of these ratios are presented in Figure 3-67 as the coherence parameter. The dashed portions of the curves (in Figures 3-65 and 3-66) for events 14, 15, and 20 are erratic and are not used in computing the coherence parameter; events 14 and 15 are small with no significant long-period energy, and event 20 is in the farfield, over 100 km from the array.

The coherence parameter in Figure 3-67 indicates that vertical ground motion is relatively coherent across the entire spectral band of engineering interest. As expected a decreasing trend towards higher frequencies is evident but is not very strong, indicating that the vertical ground motion response of a single degree of freedom oscillator behaves coherently across the frequency spectrum at distance spacing relevant to the inner ring. This observation is in general agreement with the results obtained for the vertical accelerograms of the 1979 Imperial Valley, California earthquake across the El Centro Differential Array (Niazi, 1985 and 1986).

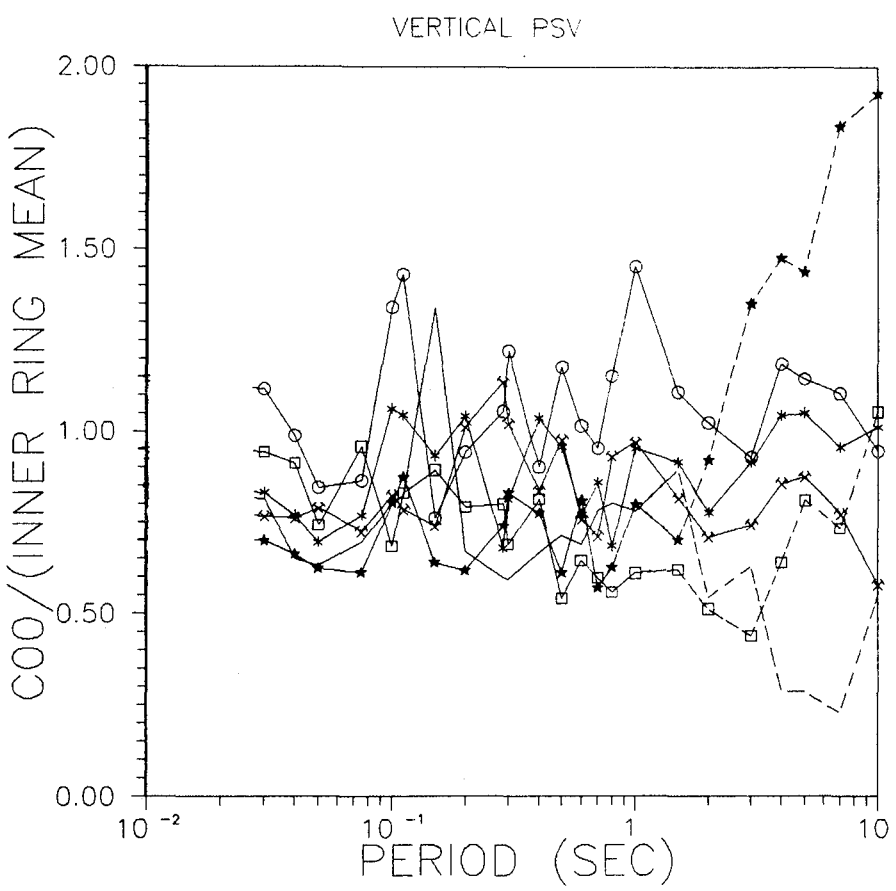

Figure 3.65 - Ratio of response spectra at central station C00 to the mean spectra for the recorded sites of the inner ring, for events 5, 14, 15, 20, 22, and 29.

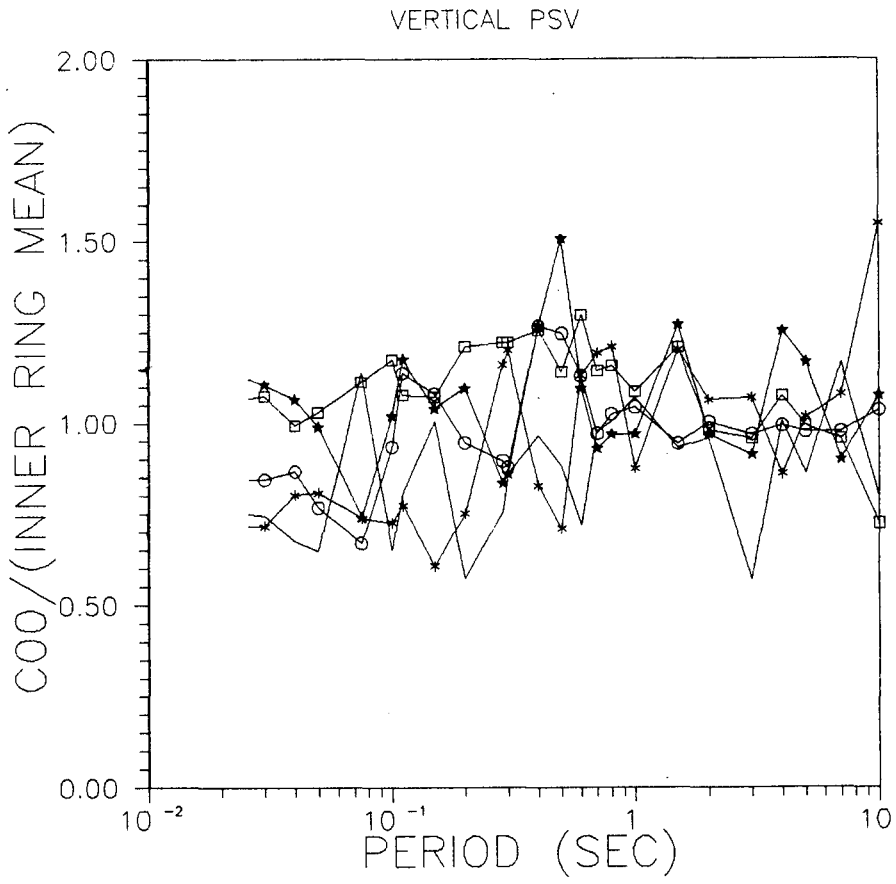

Figure 3.66 - Ratio of response spectra at central station C00 to the mean spectra for the recorded sites of the inner ring, for events 29, 33, 39, 43 and 45.

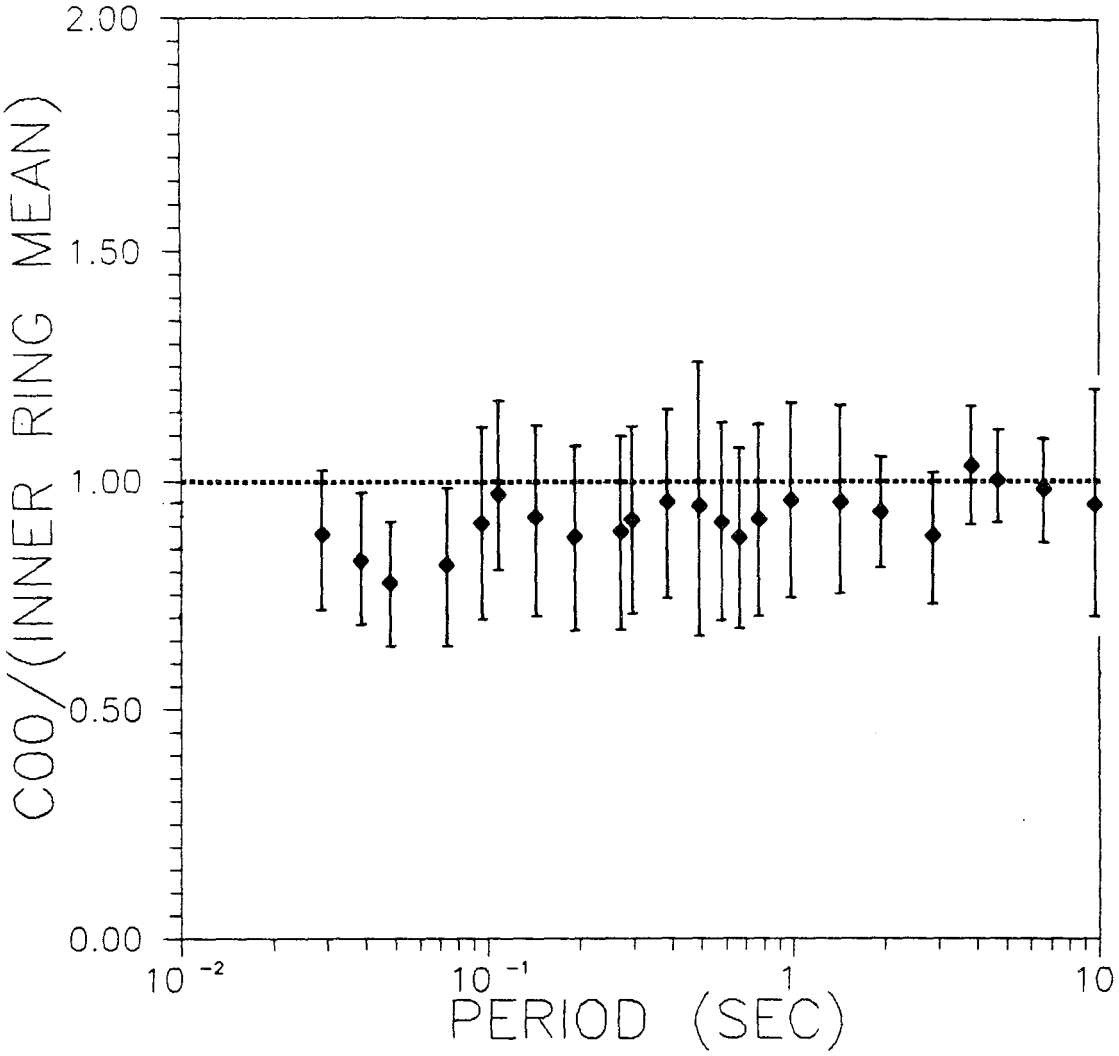

Figure 3.67 - Mean and standard deviation of the observed ratios displayed in Figures 3.65 and 3.66 and interpreted here as a measure of coherence of ground motion.

4.0 CONCLUSIONS

This study analyzed over 700 accelerograms from 12 earthquakes recorded at the SMART 1 array in northeast Taiwan. The digital time-histories and processed data represent approximately 4 million data points. From this data base, relationships were developed for the following vertical and horizontal ground motion parameters:

- PGA
- PGV
- PGD
- response spectral ordinates at 5% critical damping and at 23 discrete frequencies in the range of engineering interest

This study is unique, since previous discussions of peak vertical ground motion have seldom gone beyond PGA, and none have considered digital high quality data from a dense array with similar subsurface conditions.

The analysis of ground motion parameters utilized the nonlinear attenuation equation of the form suggested by Campbell (1981):

$$\ln(Y) = a + bM + d \ln[R + c_1 e^{C_2 M}]$$

Attenuation relationships for the ground motion parameters studied are provided in Tables 3-2 to 3-6.

COMPARISON WITH R.G. 1.60

This study confirms the conservatism of the R.G. 1.60 horizontal spectra, except at high magnitudes between about 0.15 and 2.0 seconds. In this range, the near-field spectra significantly exceed those recommended by the regulatory guide.

For the vertical component, the spectra calculated in this study exceed those of the regulatory guide in the high frequency range, in the very nearfield. However, the regulatory guide appears very conservative with respect to the present results beyond about 0.25 second. It is also conservative at all frequencies for distances greater than about 50 kilometers.

RATIO OF VERTICAL TO HORIZONTAL GROUND MOTION

This study found that the ratio of the vertical to horizontal component is sensitive to frequency content, distance, and magnitude. The ratios are larger for both high frequency energy at short distances and low frequency energy at long distances. Also, as magnitude increases, the ratio in the nearfield increases. These results indicate that, at distances less than ten kilometers, vertical ground motion controls the high frequency excitation and that low frequency excitation is controlled by the horizontal motion. The cross-over frequency lies between 5 and 10 Hz.

The results of this study tend to indicate that the value of 2/3 for the ratio of vertical to horizontal ground motion, commonly used in engineering applications, is unconservative in the very nearfield for high frequency ground motion. For PGA and for spectral ordinates less than 0.20 second, the ratio exceeds 2/3 at distances less than 25 km and exceeds unity within 5 km of the hypocenter.

One major conclusion is that the spectral ratios are less than 2/3 for

- periods longer than about 0.20 second
- for all frequencies at distances greater than 30-50 km
- for PGA at distances greater than 30 km

This is especially pronounced for the larger magnitude earthquakes, which are of primary engineering significance. These results support the design basis of many structures in the eastern United States, since their seismic hazard is largely from large distant earthquakes and the associated long-period motion.

In order to reduce some of the uncertainties associated with this analysis and to extend the validity of the results to other regions, this methodology should be applied to an enhanced, worldwide data base . It is especially important to constrain the results concerning magnitude saturation, since this significantly affected the predicted amplitudes for large magnitude events on the upper boundary of the data.

FREQUENCY DEPENDENCE

Inconsistent and unexpected trends were observed with respect to the response of ground motion with changing frequency.

As expected, horizontal PGA exhibits lower attenuation (d=-0.81) than does the vertical component (d=-1.22), which has a higher frequency content than the horizontal. Similarly, the coefficient d for the vertical component decreases from PGA to PGV to PGD, indicating decreasing attenuation with decreasing frequency. Also, the far-field coefficient d for vertical spectral ordinates tends to diminish as frequency increases. These observations are expected, since it is thought that higher frequency energy is absorbed faster than the lower frequencies. Thus, scaling with distance should decrease with decreasing frequency.

Contrary to the above, the longer period PGD attenuates more rapidly than the higher frequency PGA, for the horizontal component. Also, the far-field coefficient d tends to increase with decreasing frequency, indicating a larger scaling with distance as frequency decreases.

This counter-intuitive trend is also seen in the values of DMS. While vertical DMS decreases from PGA to PGD, the horizontal values of DMS increase. These are also opposing trends with respect to frequency, since magnitude saturation is thought to be associated with high frequency energy content.

At this time, we do not have a definite explanation for these phenomena. However, these effects could be due to either

- different behavior of Q_α and Q_β with respect to frequency, or
- coupling between high frequency Lg and other forms of seismic energy. Since the propagation of Lg is geologically controlled, this effect would then be region specific.

MAGNITUDE SCALING

For the horizontal component, the values of b increase almost monotonically as period increases from 0.1 to 3 seconds. This trend is also observed by Joyner and Boore (1982) from 0.1 to 2 seconds. To a lesser extent, the vertical component displays the same trend.

This increase of magnitude scaling with increasing wavelength is expected since longer period energy is produced by larger portions of the source. However, the reverse trend is seen as b decreases beyond the three second ordinate.

MAGNITUDE SATURATION

The Degree of Magnitude Saturation (DMS) is found to vary by component and by ground-motion parameter. For example, this study finds a greater degree of saturation for the vertical component of PGA than for the horizontal. This is intuitively appealing, since vertical PGA is associated with higher frequency energy than horizontal PGA.

For both the vertical and horizontal components, the high frequency spectral ordinates show nearly total magnitude saturation. However, DMS suddenly disappears at about 4 to 6 Hz with a sudden resurgence at 2.5 and 0.67 Hz, for the vertical and horizontal components, respectively. DMS is around 50% for the long period spectral ordinates, even though magnitude saturation is thought to be associated with high-frequency energy.

The apparent persistence of magnitude saturation into the long periods may be caused by a decreasing signal-to-noise ratio as period increases. Also, the sudden disappearance of DMS at about 4 Hz may be associated with geological peculiarities of the SMART 1 site.

UNCERTAINTY OF PREDICTED VALUES

Magnitude Dependence of Uncertainty

For all peak values and response spectral ordinates studied, the observed dispersion of the data decreases as magnitude increases. Therefore, the standard error of the regression can be modelled as magnitude dependent for these parameters, reducing the uncertainty associated with predicted amplitudes of large magnitude events.

Contribution to Scatter

The SMART 1 array eliminates many of the site effects which can influence the characteristics of recorded ground motion: subsurface geology is relatively uniform; the instruments are identical; they are all mounted on identical concrete mats; and variations in travel-paths are reduced. Also, especially within the inner ring, the close spacing of the stations should eliminate bias with respect to focussing or radiation effects, since the stations would be uniformly placed with respect to any earthquake sources. These array characteristics allow the following conclusions for recorded ground motion when factors such as geology, structure type, and azimuth do not vary:

- The scatter of observations at adjacent locations is as large as for stations placed further apart.
- The major contributor to the uncertainty is the variation of ground-motion observations between earthquakes (inter-event uncertainty).
- The inter-event uncertainty contributes more to the scatter than the variation in observations due to station bias.

The addition of the outer stations enhances the control of the far-field attenuation by increasing the spread of data with respect to distance for the individual earthquakes.

SOIL AMPLIFICATION

For all peak parameters and over all frequencies, a recording station located on soil shows significant amplification of ground motion with respect to an adjacent station located on rock. However, this amplification varied significantly by component and frequency content of the parameter studied.

The ratio of spectral amplitudes for soil to rock is between 1.3 to 2.0 for high frequency ordinates. It peaks between 3 and 7 at 0.8 to 2.0 seconds and decreases for the long period ordinates. The peak parameters display the same general trends with frequency as displayed by the spectral ordinates.

FREQUENCY DEPENDENCE OF ATTENUATION

At distances less than twenty kilometers the slope of the attenuation curve for the higher frequency spectral ordinate is greater than that of the lower frequencies. This indicates more rapid attenuation of high frequency motion at short distances. Also, beyond about twenty kilometers, the slope of the attenuation curves for the three periods are roughly the same, indicating more or less uniform attenuation with frequency.

SPECTRAL SHAPE

Assuming a normal distribution, the 84th percentile horizontal estimate for V/A approaches the predictions of Hall et al. (1976). However, Hall's ratio for the vertical component exceeds the 84th percentile estimate by nearly a factor of 2. This observation implicitly leads to different shapes for the horizontal and vertical response spectra.

Concerning the values of AD/V^2, the present findings for the vertical component are slightly above the recommended value of 6 (Hall et al., 1976) and substantially below 6 for the horizontal.

This study did not observe a clear dependence on PGA, for any of the ratios.

COMPARISON WITH OTHER STUDIES

The values predicted by this model for peak vertical acceleration, for magnitudes 5.5, 6.5, and 7.5, are compared with those of Campbell (1982) and Donovan (1982) in Figure 3-7, and with Abrahamson and Litehiser (1989) in Figure 3-8. Results for horizontal PGA (Table 3-4) are compared with those of Campbell (1981) and Joyner and Boore (1981) in Figure 3-16. These are discussed at length in the body of the report.

The most general features of the present predictions with respect to the other studies are

- lower far-field attenuation for PGA and PGV
- lower near-source amplitudes of PGA
- higher magnitude saturation for vertical PGA
- lower magnitude saturation than Campbell for horizontal PGA
- higher magnitude scaling for PGA.

FUTURE WORK

The novelty of the data used in this study, relates to the fact that the earthquake sources as well as recording stations are concentrated within a small region of less than 100 km radius. Moreover, instrumentation across the array is uniform. In this context, our results may be termed site specific. These circumstances served to reduce the scatter of observations and consequently helped to reveal a number of interesting trends.

However, these are reasonable grounds for believing that some of the observed trends are generic in nature, and it is recommended that their validity be examed for other regions of the world where a sufficient quantity of high quality data exists; i.e. in Japan and California.

Also, the inclusion of small and intermediate magnitude events in this data set, and an insufficiency of information regarding source geometries prevented the use of more meaningful distance scaling in terms of source distances. Instead, distance scaling was expressed in terms of hypocentral distance which represents the point of rupture initiation on the fault surface. Since this study was begun, several large earthquakes with sufficient coverage by the SMART1 array have occurred. In addition, new studies

concerning source geometry of larger events, (5, 43, and 45) have been published. With these new data at hand, a sensitivity study should be conducted by applying the regression analyses of this study to a new integrated data file, in which distances to the rupture surface are included.

5.0 REFERENCES

Abrahamson, N.A., (1985), Estimation of Seismic Wave Coherency and Rupture Velocity Using the SMART-1 Strong Motion Array Recordings, Ph.D. Thesis, University of California, Berkeley.

Abrahamson, N.A., (1988), Statistical properties of peak ground accelerations recorded by the SMART-1 array, Bull. Seis. Soc. of Am., Vol. 78, No. 1, 26-41,

Abrahamson, N.A. and J.J. Litehiser, (1989), Attenuation of vertical peak acceleration, Bull. Seis. Soc. of Am., 79, 549-580.

Benjamin, J. and C.A. Cornell (1970), Probability, Statistics and Decision for Civil Engineers, McGraw-Hill Co.

Bolt, B.A., C.H. Loh, J. Penzien, Y.B. Tsai and Y.T. Yeh, (1982), Preliminary Report on the SMART-1 Strong Motion Array in Taiwan, Earthquake Engineering Research Center, UC/EERC-82/13, University of California, Berkeley.

Boore, D.M., Wm. B. Joyner, A.A. Oliver, III and R.A. Page, (1980), Peak acceleration, velocity and displacement from strong-motion records, Bull. Seis. Soc. of Am., 70, 305-321.

Campbell, K.W. (1981), Near-source attenuation of peak horizontal acceleration, Bull. Seis. Soc. of Am., Vol. 71, No. 6, pp. 2039-2070.

Campbell, K.W. (1982), A Study of the near-source behavior of peak vertical Acceleration, (Abstract), E0S, Trans. Am. Geophys. Un., 45, 1037.

Campbell, K.W. (1984), Near-source attenuation of strong ground motion for moderate to large earthquakes -- an update and suggested application to the Wasatch fault zone of north-central Utah, in Proc. of Workshop on..., U.S. Geol. Surv. Open-File Report 84-763, 483-499.

Campbell, K.W. (1989), The dependence of peak horizontal acceleration on magnitude, distance, and site effect for small-magnitude earthquakes in California and eastern North America, Bull. Seism. Soc. of Am., 79, 1311-1346.

Chang, L-S., and Y-T. Yeh (1983), The Q-value of strong ground motions in Taiwan, Bull. Inst. Earth Sci., Academia Sinica, 3, 127-148.

Cornell, C.A., H. Banon, and A.F. Shakal (1979), Seismic motion and response prediction alternatives, J. Earthquake Eng. Struct. Dyn., 7, 295-315.

Donovan, N.C. (1981), Attenuation of Vertical Acceleration and a Review of Attenuation Processes, Proceedings of Workshop XVI -- The Dynamic Characteristics of Faulting Inferred from Recordings of Strong Ground Motion, Incline Village, California, U.S.G.S. Open-File Report 82-591, pp. 185-202.

Hall, W.J., B. Moharz, and N.M. Newmark (1976), Statistical studies of vertical and horizontal earthquake spectra, Nathan M. Newmark Consulting Engineering Services, Report prepared for NRC under contract No. AT(49-5)-2667, 128 pp.

Hanks, T.C. and D.A. Johnson (1976), Geophysical assessment of peak accelerations, Bull. Seism. Soc. of Am., 66, 959-968.

Hasegawa, H.S., P.W. Basham, and M.J. Berry (1981), Attenuation relations for strong seismic ground motion, Bull. Seism. Soc. of Am., 71, 2071-2095.

Housner, G.W. (1970), Strong Ground Motion, Chapter 4 of Earthquake Engineering, ed. R.L. Wiegel, Prentice Hall.

Joyner, W.B., and Boore, D.M., (1981), Peak horizontal acceleration and velocity from strong-motion records including records from the 1979 Imperial Valley, California earthquake, Bull. Seis. Soc. of Am., 71, 6, 2011-2038.

Joyner, W.B. and Boore, D.M., (1982), Estimation of response spectral values as functions of magnitude, distance, and site conditions, USGS Open File Report 82-881.

Loh, C-H, (1984), Seismic hazard analysis on attenuation equation model, Bulletin of the Institute of Earth Sciences, Academia Sinica, 4, 73-99.

McGuire, R.K. and J.C. Stepp (1986), Sensitivity of Earthquake Hazard in the Central and Eastern U.S. to Alternative Input Interpretations, Proc. 3rd Nat'l Conf. on Earthquake Engineering, Charleston, S.C.

McGuire, R.K. (1977), Seismic design spectra and mapping procedures using hazard analysis based directly on oscillator response, J. Earthquake Eng. Struct. Dyn. 5, 211-234.

Mohamamadioun, B. and A. Pecker, (1984), Low-frequency transfer of seismic energy by superficial soil deposits and soft rocks, Earthquake Eng. and Struct. Dyn., 12, 537-564.

Newmark, N.M., Blume, J.A., and Kapur, K.K. (1973), Seismic design spectra for nuclear power plants, Journal of the Power Division, 99, P02, 287-303.

Newmark, N.M. and W.J. Hall (1982), Earthquake Spectra and Design, EERI Monograph.

Niazi, M. (1985), Spatial coherence of the ground motion produced by the 1979 Imperial Valley earthquake across El Centro Differential Array, Phys. Earth Planet. Int. 38, 162-173.

Niazi, M. (1986), Inferred displacements, velocities, and rotations of a long rigid foundation located at El Centro Differential Array Site during the 1979 Imperial Valley, California earthquake. Earthquake Eng. Struc. Dyn., 14, 531-542.

Niazi, M. and Y. Bozorgnia (1990), Observed ratios of PGV/PGA and PGD/PGA for deep soil sites across SMART1 2D array, Taiwan, Proc. 4th Natl. Conf. Earthquake Eng., Vol. 1, pp. 367-374, Palm Springs, CA, May 20-24, 1990.

Nuttli, O.W. and R.B. Hermann (1984), Ground motion of Mississippi valley earthquakes, J. Tech. Topics in Civil Engineering, ASCE, 110, 54-69.

SAS User's Guide: Statistics Version 5 Edition (1985), SAS Institute Inc., Cray, N.C.

Singh, S. (1981), Regionalization of Crustal Q in the Continental United States, Ph.D. Thesis, Saint Louis University.

Smith, S.W., J.E. Ehrenberg, and E.N. Hernandez (1982), Analysis of the El Centro Differential Array for the 1979 Imperial Valley Earthquake, Bull. Seis. Soc. Am., 72, 237-258.

Sunder, S.S. (1981), Some Contributions to Strong-Motion Earthquake signal processing, Ph.D. Thesis, MIT.

Tsai, Y-B, and B.A. Bolt (1983), An analysis of horizontal peak ground acceleration and velocity from SMART-1 array data, Bull. Inst. Earth Sci., Academia Sinica, 3, 105-126.

Wen, K-L, and Y-T Yeh (1988), Characteristics of the strong ground motions in Lotung, Proceedings of the CNNAA-AIT Joint Seminar on Research and Application of Multiple Hazards Mitigation, Taipei, April 1988.

Wen, K-L (1984), Seismic velocity structure beneath the SMART1 array, Bull. Inst. Earth Sci., Academia Sinica, 4, 51-72.

EARTHQUAKE ENGINEERING RESEARCH CENTER REPORT SERIES

EERC reports are available from the National Information Service for Earthquake Engineering(NISEE) and from the National Technical Information Service(NTIS). Numbers in parentheses are Accession Numbers assigned by the National Technical Information Service; these are followed by a price code. Contact NTIS, 5285 Port Royal Road, Springfield Virginia, 22161 for more information. Reports without Accession Numbers were not available from NTIS at the time of printing. For a current complete list of EERC reports (from EERC 67-1) and availablity information, please contact University of California, EERC, NISEE, 1301 South 46th Street, Richmond, California 94804.

UCB/EERC-81/01 "Control of Seismic Response of Piping Systems and Other Structures by Base Isolation," by Kelly, J.M., January 1981, (PB81 200 735)A05.

UCB/EERC-81/02 "OPTNSR- An Interactive Software System for Optimal Design of Statically and Dynamically Loaded Structures with Nonlinear Response," by Bhatti, M.A., Ciampi, V. and Pister, K.S., January 1981, (PB81 218 851)A09.

UCB/EERC-81/03 "Analysis of Local Variations in Free Field Seismic Ground Motions," by Chen, J.-C., Lysmer, J. and Seed, H.B., January 1981, (AD-A099508)A13.

UCB/EERC-81/04 "Inelastic Structural Modeling of Braced Offshore Platforms for Seismic Loading," by Zayas, V.A., Shing, P.-S.B., Mahin, S.A. and Popov, E.P., January 1981, INEL4, (PB82 138 777)A07.

UCB/EERC-81/05 "Dynamic Response of Light Equipment in Structures," by Der Kiureghian, A., Sackman, J.L. and Nour-Omid, B., April 1981, (PB81 218 497)A04.

UCB/EERC-81/06 "Preliminary Experimental Investigation of a Broad Base Liquid Storage Tank," by Bouwkamp, J.G., Kollegger, J.P. and Stephen, R.M., May 1981, (PB82 140 385)A03.

UCB/EERC-81/07 "The Seismic Resistant Design of Reinforced Concrete Coupled Structural Walls," by Aktan, A.E. and Bertero, V.V., June 1981, (PB82 113 358)A11.

UCB/EERC-81/08 "Unassigned," by Unassigned, 1981.

UCB/EERC-81/09 "Experimental Behavior of a Spatial Piping System with Steel Energy Absorbers Subjected to a Simulated Differential Seismic Input," by Stiemer, S.F., Godden, W.G. and Kelly, J.M., July 1981, (PB82 201 898)A04.

UCB/EERC-81/10 "Evaluation of Seismic Design Provisions for Masonry in the United States," by Sveinsson, B.I., Mayes, R.L. and McNiven, H.D., August 1981, (PB82 166 075)A08.

UCB/EERC-81/11 "Two-Dimensional Hybrid Modelling of Soil-Structure Interaction," by Tzong, T.-J., Gupta, S. and Penzien, J., August 1981, (PB82 142 118)A04.

UCB/EERC-81/12 "Studies on Effects of Infills in Seismic Resistant R/C Construction," by Brokken, S. and Bertero, V.V., October 1981, (PB82 166 190)A09.

UCB/EERC-81/13 "Linear Models to Predict the Nonlinear Seismic Behavior of a One-Story Steel Frame," by Valdimarsson, H., Shah, A.H. and McNiven, H.D., September 1981, (PB82 138 793)A07.

UCB/EERC-81/14 "TLUSH: A Computer Program for the Three-Dimensional Dynamic Analysis of Earth Dams," by Kagawa, T., Mejia, L.H., Seed, H.B. and Lysmer, J., September 1981, (PB82 139 940)A06.

UCB/EERC-81/15 "Three Dimensional Dynamic Response Analysis of Earth Dams," by Mejia, L.H. and Seed, H.B., September 1981, (PB82 137 274)A12.

UCB/EERC-81/16 "Experimental Study of Lead and Elastomeric Dampers for Base Isolation Systems," by Kelly, J.M. and Hodder, S.B., October 1981, (PB82 166 182)A05.

UCB/EERC-81/17 "The Influence of Base Isolation on the Seismic Response of Light Secondary Equipment," by Kelly, J.M., April 1981, (PB82 255 266)A04.

UCB/EERC-81/18 "Studies on Evaluation of Shaking Table Response Analysis Procedures," by Blondet, J. M., November 1981, (PB82 197 278)A10.

UCB/EERC-81/19 "DELIGHT.STRUCT: A Computer-Aided Design Environment for Structural Engineering," by Balling, R.J., Pister, K.S. and Polak, E., December 1981, (PB82 218 496)A07.

UCB/EERC-81/20 "Optimal Design of Seismic-Resistant Planar Steel Frames," by Balling, R.J., Ciampi, V. and Pister, K.S., December 1981, (PB82 220 179)A07.

UCB/EERC-82/01 "Dynamic Behavior of Ground for Seismic Analysis of Lifeline Systems," by Sato, T. and Der Kiureghian, A., January 1982, (PB82 218 926)A05.

UCB/EERC-82/02 "Shaking Table Tests of a Tubular Steel Frame Model," by Ghanaat, Y. and Clough, R.W., January 1982, (PB82 220 161)A07.

UCB/EERC-82/03 "Behavior of a Piping System under Seismic Excitation: Experimental Investigations of a Spatial Piping System supported by Mechanical Shock Arrestors," by Schneider, S., Lee, H.-M. and Godden, W. G., May 1982, (PB83 172 544)A09.

UCB/EERC-82/04 "New Approaches for the Dynamic Analysis of Large Structural Systems," by Wilson, E.L., June 1982, (PB83 148 080)A05.

UCB/EERC-82/05 "Model Study of Effects of Damage on the Vibration Properties of Steel Offshore Platforms," by Shahrivar, F. and Bouwkamp, J.G., June 1982, (PB83 148 742)A10.

UCB/EERC-82/06 "States of the Art and Pratice in the Optimum Seismic Design and Analytical Response Prediction of R/C Frame Wall Structures," by Aktan, A.E. and Bertero, V.V., July 1982, (PB83 147 736)A05.

UCB/EERC-82/07 "Further Study of the Earthquake Response of a Broad Cylindrical Liquid-Storage Tank Model," by Manos, G.C. and Clough, R.W., July 1982, (PB83 147 744)A11.

UCB/EERC-82/08 "An Evaluation of the Design and Analytical Seismic Response of a Seven Story Reinforced Concrete Frame," by Charney, F.A. and Bertero, V.V., July 1982, (PB83 157 628)A09.

UCB/EERC-82/09 "Fluid-Structure Interactions: Added Mass Computations for Incompressible Fluid," by Kuo, J.S.-H., August 1982, (PB83 156 281)A07.

UCB/EERC-82/10 "Joint-Opening Nonlinear Mechanism: Interface Smeared Crack Model," by Kuo, J.S.-H., August 1982, (PB83 149 195)A05.

UCB/EERC-82/11 "Dynamic Response Analysis of Techi Dam," by Clough, R.W., Stephen, R.M. and Kuo, J.S.-H., August 1982, (PB83 147 496)A06.

UCB/EERC-82/12 "Prediction of the Seismic Response of R/C Frame-Coupled Wall Structures," by Aktan, A.E., Bertero, V.V. and Piazzo, M., August 1982, (PB83 149 203)A09.

UCB/EERC-82/13 "Preliminary Report on the Smart 1 Strong Motion Array in Taiwan," by Bolt, B.A., Loh, C.H., Penzien, J. and Tsai, Y.B., August 1982, (PB83 159 400)A10.

UCB/EERC-82/14 "Seismic Behavior of an Eccentrically X-Braced Steel Structure," by Yang, M.S., September 1982, (PB83 260 778)A12.

UCB/EERC-82/15 "The Performance of Stairways in Earthquakes," by Roha, C., Axley, J.W. and Bertero, V.V., September 1982, (PB83 157 693)A07.

UCB/EERC-82/16 "The Behavior of Submerged Multiple Bodies in Earthquakes," by Liao, W.-G., September 1982, (PB83 158 709)A07.

UCB/EERC-82/17 "Effects of Concrete Types and Loading Conditions on Local Bond-Slip Relationships," by Cowell, A.D., Popov, E.P. and Bertero, V.V., September 1982, (PB83 153 577)A04.

UCB/EERC-82/18 "Mechanical Behavior of Shear Wall Vertical Boundary Members: An Experimental Investigation," by Wagner, M.T. and Bertero, V.V., October 1982, (PB83 159 764)A05.

UCB/EERC-82/19 "Experimental Studies of Multi-support Seismic Loading on Piping Systems," by Kelly, J.M. and Cowell, A.D., November 1982, (PB90 262 684)A07.

UCB/EERC-82/20 "Generalized Plastic Hinge Concepts for 3D Beam-Column Elements," by Chen, P. F.-S. and Powell, G.H., November 1982, (PB83 247 981)A13.

UCB/EERC-82/21 "ANSR-II: General Computer Program for Nonlinear Structural Analysis," by Oughourlian, C.V. and Powell, G.H., November 1982, (PB83 251 330)A12.

UCB/EERC-82/22 "Solution Strategies for Statically Loaded Nonlinear Structures," by Simons, J.W. and Powell, G.H., November 1982, (PB83 197 970)A06.

UCB/EERC-82/23 "Analytical Model of Deformed Bar Anchorages under Generalized Excitations," by Ciampi, V., Eligehausen, R., Bertero, V.V. and Popov, E.P., November 1982, (PB83 169 532)A06.

UCB/EERC-82/24 "A Mathematical Model for the Response of Masonry Walls to Dynamic Excitations," by Sucuoglu, H., Mengi, Y. and McNiven, H.D., November 1982, (PB83 169 011)A07.

UCB/EERC-82/25 "Earthquake Response Considerations of Broad Liquid Storage Tanks," by Cambra, F.J., November 1982, (PB83 251 215)A09.

UCB/EERC-82/26 "Computational Models for Cyclic Plasticity, Rate Dependence and Creep," by Mosaddad, B. and Powell, G.H., November 1982, (PB83 245 829)A08.

UCB/EERC-82/27 "Inelastic Analysis of Piping and Tubular Structures," by Mahasuverachai, M. and Powell, G.H., November 1982, (PB83 249 987)A07.

UCB/EERC-83/01 "The Economic Feasibility of Seismic Rehabilitation of Buildings by Base Isolation," by Kelly, J.M., January 1983, (PB83 197 988)A05.

UCB/EERC-83/02 "Seismic Moment Connections for Moment-Resisting Steel Frames.," by Popov, E.P., January 1983, (PB83 195 412)A04.

UCB/EERC-83/03 "Design of Links and Beam-to-Column Connections for Eccentrically Braced Steel Frames," by Popov, E.P. and Malley, J.O., January 1983, (PB83 194 811)A04.

UCB/EERC-83/04 "Numerical Techniques for the Evaluation of Soil-Structure Interaction Effects in the Time Domain," by Bayo, E. and Wilson, E.L., February 1983, (PB83 245 605)A09.

UCB/EERC-83/05 "A Transducer for Measuring the Internal Forces in the Columns of a Frame-Wall Reinforced Concrete Structure," by Sause, R. and Bertero, V.V., May 1983, (PB84 119 494)A06.

UCB/EERC-83/06 "Dynamic Interactions Between Floating Ice and Offshore Structures," by Croteau, P., May 1983, (PB84 119 486)A16.

UCB/EERC-83/07 "Dynamic Analysis of Multiply Tuned and Arbitrarily Supported Secondary Systems," by Igusa, T. and Der Kiureghian, A., July 1983, (PB84 118 272)A11.

UCB/EERC-83/08 "A Laboratory Study of Submerged Multi-body Systems in Earthquakes," by Ansari, G.R., June 1983, (PB83 261 842)A17.

UCB/EERC-83/09 "Effects of Transient Foundation Uplift on Earthquake Response of Structures," by Yim, C.-S. and Chopra, A.K., June 1983, (PB83 261 396)A07.

UCB/EERC-83/10 "Optimal Design of Friction-Braced Frames under Seismic Loading," by Austin, M.A. and Pister, K.S., June 1983, (PB84 119 288)A06.

UCB/EERC-83/11 "Shaking Table Study of Single-Story Masonry Houses: Dynamic Performance under Three Component Seismic Input and Recommendations," by Manos, G.C., Clough, R.W. and Mayes, R.L., July 1983, (UCB/EERC-83/11)A08.

UCB/EERC-83/12 "Experimental Error Propagation in Pseudodynamic Testing," by Shiing, P.B. and Mahin, S.A., June 1983, (PB84 119 270)A09.

UCB/EERC-83/13 "Experimental and Analytical Predictions of the Mechanical Characteristics of a 1/5-scale Model of a 7-story R/C Frame-Wall Building Structure," by Aktan, A.E., Bertero, V.V., Chowdhury, A.A. and Nagashima, T., June 1983, (PB84 119 213)A07.

UCB/EERC-83/14 "Shaking Table Tests of Large-Panel Precast Concrete Building System Assemblages," by Oliva, M.G. and Clough, R.W., June 1983, (PB86 110 210/AS)A11.

UCB/EERC-83/15 "Seismic Behavior of Active Beam Links in Eccentrically Braced Frames," by Hjelmstad, K.D. and Popov, E.P., July 1983, (PB84 119 676)A09.

UCB/EERC-83/16 "System Identification of Structures with Joint Rotation," by Dimsdale, J.S., July 1983, (PB84 192 210)A06.

UCB/EERC-83/17 "Construction of Inelastic Response Spectra for Single-Degree-of-Freedom Systems," by Mahin, S. and Lin, J., June 1983, (PB84 208 834)A05.

UCB/EERC-83/18 "Interactive Computer Analysis Methods for Predicting the Inelastic Cyclic Behaviour of Structural Sections," by Kaba, S. and Mahin, S., July 1983, (PB84 192 012)A06.

UCB/EERC-83/19 "Effects of Bond Deterioration on Hysteretic Behavior of Reinforced Concrete Joints," by Filippou, F.C., Popov, E.P. and Bertero, V.V., August 1983, (PB84 192 020)A10.

UCB/EERC-83/20 "Correlation of Analytical and Experimental Responses of Large-Panel Precast Building Systems," by Oliva, M.G., Clough, R.W., Velkov, M. and Gavrilovic, P., May 1988, (PB90 262 692)A06.

UCB/EERC-83/21 "Mechanical Characteristics of Materials Used in a 1/5 Scale Model of a 7-Story Reinforced Concrete Test Structure," by Bertero, V.V., Aktan, A.E., Harris, H.G. and Chowdhury, A.A., October 1983, (PB84 193 697)A05.

UCB/EERC-83/22 "Hybrid Modelling of Soil-Structure Interaction in Layered Media," by Tzong, T.-J. and Penzien, J., October 1983, (PB84 192 178)A08.

UCB/EERC-83/23 "Local Bond Stress-Slip Relationships of Deformed Bars under Generalized Excitations," by Eligehausen, R., Popov, E.P. and Bertero, V.V., October 1983, (PB84 192 848)A09.

UCB/EERC-83/24 "Design Considerations for Shear Links in Eccentrically Braced Frames," by Malley, J.O. and Popov, E.P., November 1983, (PB84 192 186)A07.

UCB/EERC-84/01 "Pseudodynamic Test Method for Seismic Performance Evaluation: Theory and Implementation," by Shing, P.-S.B. and Mahin, S.A., January 1984, (PB84 190 644)A08.

UCB/EERC-84/02 "Dynamic Response Behavior of Kiang Hong Dian Dam," by Clough, R.W., Chang, K.-T., Chen, H.-Q. and Stephen, R.M., April 1984, (PB84 209 402)A08.

UCB/EERC-84/03 "Refined Modelling of Reinforced Concrete Columns for Seismic Analysis," by Kaba, S.A. and Mahin, S.A., April 1984, (PB84 234 384)A06.

UCB/EERC-84/04 "A New Floor Response Spectrum Method for Seismic Analysis of Multiply Supported Secondary Systems," by Asfura, A. and Der Kiureghian, A., June 1984, (PB84 239 417)A06.

UCB/EERC-84/05 "Earthquake Simulation Tests and Associated Studies of a 1/5th-scale Model of a 7-Story R/C Frame-Wall Test Structure," by Bertero, V.V., Aktan, A.E., Charney, F.A. and Sause, R., June 1984, (PB84 239 409)A09.

UCB/EERC-84/06 "R/C Structural Walls: Seismic Design for Shear," by Aktan, A.E. and Bertero, V.V., 1984.

UCB/EERC-84/07 "Behavior of Interior and Exterior Flat-Plate Connections subjected to Inelastic Load Reversals," by Zee, H.L. and Moehle, J.P., August 1984, (PB86 117 629/AS)A07.

UCB/EERC-84/08 "Experimental Study of the Seismic Behavior of a Two-Story Flat-Plate Structure," by Moehle, J.P. and Diebold, J.W., August 1984, (PB86 122 553/AS)A12.

UCB/EERC-84/09 "Phenomenological Modeling of Steel Braces under Cyclic Loading," by Ikeda, K., Mahin, S.A. and Dermitzakis, S.N., May 1984, (PB86 132 198/AS)A08.

UCB/EERC-84/10 "Earthquake Analysis and Response of Concrete Gravity Dams," by Fenves, G. and Chopra, A.K., August 1984, (PB85 193 902/AS)A11.

UCB/EERC-84/11 "EAGD-84: A Computer Program for Earthquake Analysis of Concrete Gravity Dams," by Fenves, G. and Chopra, A.K., August 1984, (PB85 193 613/AS)A05.

UCB/EERC-84/12 "A Refined Physical Theory Model for Predicting the Seismic Behavior of Braced Steel Frames," by Ikeda, K. and Mahin, S.A., July 1984, (PB85 191 450/AS)A09.

UCB/EERC-84/13 "Earthquake Engineering Research at Berkeley - 1984," by , August 1984, (PB85 197 341/AS)A10.

UCB/EERC-84/14 "Moduli and Damping Factors for Dynamic Analyses of Cohesionless Soils," by Seed, H.B., Wong, R.T., Idriss, I.M. and Tokimatsu, K., September 1984, (PB85 191 468/AS)A04.

UCB/EERC-84/15 "The Influence of SPT Procedures in Soil Liquefaction Resistance Evaluations," by Seed, H.B., Tokimatsu, K., Harder, L.F. and Chung, R.M., October 1984, (PB85 191 732/AS)A04.

UCB/EERC-84/16 "Simplified Procedures for the Evaluation of Settlements in Sands Due to Earthquake Shaking," by Tokimatsu, K. and Seed, H.B., October 1984, (PB85 197 887/AS)A03.

UCB/EERC-84/17 "Evaluation of Energy Absorption Characteristics of Highway Bridges Under Seismic Conditions - Volume I (PB90 262 627)A16 and Volume II (Appendices) (PB90 262 635)A13," by Imbsen, R.A. and Penzien, J., September 1986.

UCB/EERC-84/18 "Structure-Foundation Interactions under Dynamic Loads," by Liu, W.D. and Penzien, J., November 1984, (PB87 124 889/AS)A11.

UCB/EERC-84/19 "Seismic Modelling of Deep Foundations," by Chen, C.-H. and Penzien, J., November 1984, (PB87 124 798/AS)A07.

UCB/EERC-84/20 "Dynamic Response Behavior of Quan Shui Dam," by Clough, R.W., Chang, K.-T., Chen, H.-Q., Stephen, R.M., Ghanaat, Y. and Qi, J.-H., November 1984, (PB86 115177/AS)A07.

UCB/EERC-85/01 "Simplified Methods of Analysis for Earthquake Resistant Design of Buildings," by Cruz, E.F. and Chopra, A.K., February 1985, (PB86 112299/AS)A12.

UCB/EERC-85/02 "Estimation of Seismic Wave Coherency and Rupture Velocity using the SMART 1 Strong-Motion Array Recordings," by Abrahamson, N.A., March 1985, (PB86 214 343)A07.

UCB/EERC-85/03 "Dynamic Properties of a Thirty Story Condominium Tower Building," by Stephen, R.M., Wilson, E.L. and Stander, N., April 1985, (PB86 118965/AS)A06.

UCB/EERC-85/04 "Development of Substructuring Techniques for On-Line Computer Controlled Seismic Performance Testing," by Dermitzakis, S. and Mahin, S., February 1985, (PB86 132941/AS)A08.

UCB/EERC-85/05 "A Simple Model for Reinforcing Bar Anchorages under Cyclic Excitations," by Filippou, F.C., March 1985, (PB86 112 919/AS)A05.

UCB/EERC-85/06 "Racking Behavior of Wood-framed Gypsum Panels under Dynamic Load," by Oliva, M.G., June 1985, (PB90 262 643)A04.

UCB/EERC-85/07 "Earthquake Analysis and Response of Concrete Arch Dams," by Fok, K.-L. and Chopra, A.K., June 1985, (PB86 139672/AS)A10.

UCB/EERC-85/08 "Effect of Inelastic Behavior on the Analysis and Design of Earthquake Resistant Structures," by Lin, J.P. and Mahin, S.A., June 1985, (PB86 135340/AS)A08.

UCB/EERC-85/09 "Earthquake Simulator Testing of a Base-Isolated Bridge Deck," by Kelly, J.M., Buckle, I.G. and Tsai, H.-C., January 1986, (PB87 124 152/AS)A06.

UCB/EERC-85/10 "Simplified Analysis for Earthquake Resistant Design of Concrete Gravity Dams," by Fenves, G. and Chopra, A.K., June 1986, (PB87 124 160/AS)A08.

UCB/EERC-85/11 "Dynamic Interaction Effects in Arch Dams," by Clough, R.W., Chang, K.-T., Chen, H.-Q. and Ghanaat, Y., October 1985, (PB86 135027/AS)A05.

UCB/EERC-85/12 "Dynamic Response of Long Valley Dam in the Mammoth Lake Earthquake Series of May 25-27, 1980," by Lai, S. and Seed, H.B., November 1985, (PB86 142304/AS)A05.

UCB/EERC-85/13 "A Methodology for Computer-Aided Design of Earthquake-Resistant Steel Structures," by Austin, M.A., Pister, K.S. and Mahin, S.A., December 1985, (PB86 159480/AS)A10 .

UCB/EERC-85/14 "Response of Tension-Leg Platforms to Vertical Seismic Excitations," by Liou, G.-S., Penzien, J. and Yeung, R.W., December 1985, (PB87 124 871/AS)A08.

UCB/EERC-85/15 "Cyclic Loading Tests of Masonry Single Piers: Volume 4 - Additional Tests with Height to Width Ratio of 1," by Sveinsson, B., McNiven, H.D. and Sucuoglu, H., December 1985.

UCB/EERC-85/16 "An Experimental Program for Studying the Dynamic Response of a Steel Frame with a Variety of Infill Partitions," by Yanev, B. and McNiven, H.D., December 1985, (PB90 262 676)A05.

UCB/EERC-86/01 "A Study of Seismically Resistant Eccentrically Braced Steel Frame Systems," by Kasai, K. and Popov, E.P., January 1986, (PB87 124 178/AS)A14.

UCB/EERC-86/02 "Design Problems in Soil Liquefaction," by Seed, H.B., February 1986, (PB87 124 186/AS)A03.

UCB/EERC-86/03 "Implications of Recent Earthquakes and Research on Earthquake-Resistant Design and Construction of Buildings," by Bertero, V.V., March 1986, (PB87 124 194/AS)A05.

UCB/EERC-86/04 "The Use of Load Dependent Vectors for Dynamic and Earthquake Analyses," by Leger, P., Wilson, E.L. and Clough, R.W., March 1986, (PB87 124 202/AS)A12.

UCB/EERC-86/05 "Two Beam-To-Column Web Connections," by Tsai, K.-C. and Popov, E.P., April 1986, (PB87 124 301/AS)A04.

UCB/EERC-86/06 "Determination of Penetration Resistance for Coarse-Grained Soils using the Becker Hammer Drill," by Harder, L.F. and Seed, H.B., May 1986, (PB87 124 210/AS)A07.

UCB/EERC-86/07 "A Mathematical Model for Predicting the Nonlinear Response of Unreinforced Masonry Walls to In-Plane Earthquake Excitations," by Mengi, Y. and McNiven, H.D., May 1986, (PB87 124 780/AS)A06.

UCB/EERC-86/08 "The 19 September 1985 Mexico Earthquake: Building Behavior," by Bertero, V.V., July 1986.

UCB/EERC-86/09 "EACD-3D: A Computer Program for Three-Dimensional Earthquake Analysis of Concrete Dams," by Fok, K.-L., Hall, J.F. and Chopra, A.K., July 1986, (PB87 124 228/AS)A08.

UCB/EERC-86/10 "Earthquake Simulation Tests and Associated Studies of a 0.3-Scale Model of a Six-Story Concentrically Braced Steel Structure," by Uang, C.-M. and Bertero, V.V., December 1986, (PB87 163 564/AS)A17.

UCB/EERC-86/11 "Mechanical Characteristics of Base Isolation Bearings for a Bridge Deck Model Test," by Kelly, J.M., Buckle, I.G. and Koh, C.-G., November 1987, (PB90 262 668)A04.

UCB/EERC-86/12 "Effects of Axial Load on Elastomeric Isolation Bearings," by Koh, C.-G. and Kelly, J.M., November 1987.

UCB/EERC-87/01 "The FPS Earthquake Resisting System: Experimental Report," by Zayas, V.A., Low, S.S. and Mahin, S.A., June 1987.

UCB/EERC-87/02 "Earthquake Simulator Tests and Associated Studies of a 0.3-Scale Model of a Six-Story Eccentrically Braced Steel Structure," by Whittaker, A., Uang, C.-M. and Bertero, V.V., July 1987.

UCB/EERC-87/03 "A Displacement Control and Uplift Restraint Device for Base-Isolated Structures," by Kelly, J.M., Griffith, M.C. and Aiken, I.D., April 1987.

UCB/EERC-87/04 "Earthquake Simulator Testing of a Combined Sliding Bearing and Rubber Bearing Isolation System," by Kelly, J.M. and Chalhoub, M.S., 1987.

UCB/EERC-87/05 "Three-Dimensional Inelastic Analysis of Reinforced Concrete Frame-Wall Structures," by Moazzami, S. and Bertero, V.V., May 1987.

UCB/EERC-87/06 "Experiments on Eccentrically Braced Frames with Composite Floors," by Ricles, J. and Popov, E., June 1987.

UCB/EERC-87/07 "Dynamic Analysis of Seismically Resistant Eccentrically Braced Frames," by Ricles, J. and Popov, E., June 1987.

UCB/EERC-87/08 "Undrained Cyclic Triaxial Testing of Gravels-The Effect of Membrane Compliance," by Evans, M.D. and Seed, H.B., July 1987.

UCB/EERC-87/09 "Hybrid Solution Techniques for Generalized Pseudo-Dynamic Testing," by Thewalt, C. and Mahin, S.A., July 1987.

UCB/EERC-87/10 "Ultimate Behavior of Butt Welded Splices in Heavy Rolled Steel Sections," by Bruneau, M., Mahin, S.A. and Popov, E.P., September 1987.

UCB/EERC-87/11 "Residual Strength of Sand from Dam Failures in the Chilean Earthquake of March 3, 1985," by De Alba, P., Seed, H.B., Retamal, E. and Seed, R.B., September 1987.

UCB/EERC-87/12 "Inelastic Seismic Response of Structures with Mass or Stiffness Eccentricities in Plan," by Bruneau, M. and Mahin, S.A., September 1987, (PB90 262 650)A14.

UCB/EERC-87/13 "CSTRUCT: An Interactive Computer Environment for the Design and Analysis of Earthquake Resistant Steel Structures," by Austin, M.A., Mahin, S.A. and Pister, K.S., September 1987.

UCB/EERC-87/14 "Experimental Study of Reinforced Concrete Columns Subjected to Multi-Axial Loading," by Low, S.S. and Moehle, J.P., September 1987.

UCB/EERC-87/15 "Relationships between Soil Conditions and Earthquake Ground Motions in Mexico City in the Earthquake of Sept. 19, 1985," by Seed, H.B., Romo, M.P., Sun, J., Jaime, A. and Lysmer, J., October 1987.

UCB/EERC-87/16 "Experimental Study of Seismic Response of R. C. Setback Buildings," by Shahrooz, B.M. and Moehle, J.P., October 1987.

UCB/EERC-87/17 "The Effect of Slabs on the Flexural Behavior of Beams," by Pantazopoulou, S.J. and Moehle, J.P., October 1987, (PB90 262 700)A07.

UCB/EERC-87/18 "Design Procedure for R-FBI Bearings," by Mostaghel, N. and Kelly, J.M., November 1987, (PB90 262 718)A04.

UCB/EERC-87/19 "Analytical Models for Predicting the Lateral Response of R C Shear Walls: Evaluation of their Reliability," by Vulcano, A. and Bertero, V.V., November 1987.

UCB/EERC-87/20 "Earthquake Response of Torsionally-Coupled Buildings," by Hejal, R. and Chopra, A.K., December 1987.

UCB/EERC-87/21 "Dynamic Reservoir Interaction with Monticello Dam," by Clough, R.W., Ghanaat, Y. and Qiu, X-F., December 1987.

UCB/EERC-87/22 "Strength Evaluation of Coarse-Grained Soils," by Siddiqi, F.H., Seed, R.B., Chan, C.K., Seed, H.B. and Pyke, R.M., December 1987.

UCB/EERC-88/01 "Seismic Behavior of Concentrically Braced Steel Frames," by Khatib, I., Mahin, S.A. and Pister, K.S., January 1988.

UCB/EERC-88/02 "Experimental Evaluation of Seismic Isolation of Medium-Rise Structures Subject to Uplift," by Griffith, M.C., Kelly, J.M., Coveney, V.A. and Koh, C.G., January 1988.

UCB/EERC-88/03 "Cyclic Behavior of Steel Double Angle Connections," by Astaneh-Asl, A. and Nader, M.N., January 1988.

UCB/EERC-88/04 "Re-evaluation of the Slide in the Lower San Fernando Dam in the Earthquake of Feb. 9, 1971," by Seed, H.B., Seed, R.B., Harder, L.F. and Jong, H.-L., April 1988.

UCB/EERC-88/05 "Experimental Evaluation of Seismic Isolation of a Nine-Story Braced Steel Frame Subject to Uplift," by Griffith, M.C., Kelly, J.M. and Aiken, I.D., May 1988.

UCB/EERC-88/06 "DRAIN-2DX User Guide.," by Allahabadi, R. and Powell, G.H., March 1988.

UCB/EERC-88/07 "Cylindrical Fluid Containers in Base-Isolated Structures," by Chalhoub, M.S. and Kelly, J.M. , April 1988.

UCB/EERC-88/08 "Analysis of Near-Source Waves: Separation of Wave Types using Strong Motion Array Recordings," by Darragh, R.B., June 1988.

UCB/EERC-88/09 "Alternatives to Standard Mode Superposition for Analysis of Non-Classically Damped Systems," by Kusainov, A.A. and Clough, R.W., June 1988.

UCB/EERC-88/10 "The Landslide at the Port of Nice on October 16, 1979," by Seed, H.B., Seed, R.B., Schlosser, F., Blondeau, F. and Juran, I., June 1988.

UCB/EERC-88/11 "Liquefaction Potential of Sand Deposits Under Low Levels of Excitation," by Carter, D.P. and Seed, H.B., August 1988.

UCB/EERC-88/12 "Nonlinear Analysis of Reinforced Concrete Frames Under Cyclic Load Reversals," by Filippou, F.C. and Issa, A., September 1988.

UCB/EERC-88/13 "Implications of Recorded Earthquake Ground Motions on Seismic Design of Building Structures," by Uang, C.-M. and Bertero, V.V., November 1988.

UCB/EERC-88/14 "An Experimental Study of the Behavior of Dual Steel Systems," by Whittaker, A.S. , Uang, C.-M. and Bertero, V.V., September 1988.

UCB/EERC-88/15 "Dynamic Moduli and Damping Ratios for Cohesive Soils," by Sun, J.I., Golesorkhi, R. and Seed, H.B., August 1988.

UCB/EERC-88/16 "Reinforced Concrete Flat Plates Under Lateral Load: An Experimental Study Including Biaxial Effects," by Pan, A. and Moehle, J., October 1988.

UCB/EERC-88/17 "Earthquake Engineering Research at Berkeley - 1988," by EERC, November 1988.

UCB/EERC-88/18 "Use of Energy as a Design Criterion in Earthquake-Resistant Design," by Uang, C.-M. and Bertero, V.V., November 1988.

UCB/EERC-88/19 "Steel Beam-Column Joints in Seismic Moment Resisting Frames," by Tsai, K.-C. and Popov, E.P., November 1988.

UCB/EERC-88/20 "Base Isolation in Japan, 1988," by Kelly, J.M., December 1988.

UCB/EERC-89/01 "Behavior of Long Links in Eccentrically Braced Frames," by Engelhardt, M.D. and Popov, E.P., January 1989.

UCB/EERC-89/02 "Earthquake Simulator Testing of Steel Plate Added Damping and Stiffness Elements," by Whittaker, A., Bertero, V.V., Alonso, J. and Thompson, C., January 1989.

UCB/EERC-89/03 "Implications of Site Effects in the Mexico City Earthquake of Sept. 19, 1985 for Earthquake-Resistant Design Criteria in the San Francisco Bay Area of California," by Seed, H.B. and Sun, J.I., March 1989.

UCB/EERC-89/04 "Earthquake Analysis and Response of Intake-Outlet Towers," by Goyal, A. and Chopra, A.K., July 1989.

UCB/EERC-89/05 "The 1985 Chile Earthquake: An Evaluation of Structural Requirements for Bearing Wall Buildings," by Wallace, J.W. and Moehle, J.P., July 1989.

UCB/EERC-89/06 "Effects of Spatial Variation of Ground Motions on Large Multiply-Supported Structures," by Hao, H., July 1989.

UCB/EERC-89/07 "EADAP - Enhanced Arch Dam Analysis Program: Users's Manual," by Ghanaat, Y. and Clough, R.W., August 1989.

UCB/EERC-89/08 "Seismic Performance of Steel Moment Frames Plastically Designed by Least Squares Stress Fields," by Ohi, K. and Mahin, S.A., August 1989.

UCB/EERC-89/09 "Feasibility and Performance Studies on Improving the Earthquake Resistance of New and Existing Buildings Using the Friction Pendulum System," by Zayas, V., Low, S., Mahin, S.A. and Bozzo, L., July 1989.

UCB/EERC-89/10 "Measurement and Elimination of Membrane Compliance Effects in Undrained Triaxial Testing," by Nicholson, P.G., Seed, R.B. and Anwar, H., September 1989.

UCB/EERC-89/11 "Static Tilt Behavior of Unanchored Cylindrical Tanks," by Lau, D.T. and Clough, R.W., September 1989.

UCB/EERC-89/12 "ADAP-88: A Computer Program for Nonlinear Earthquake Analysis of Concrete Arch Dams," by Fenves, G.L., Mojtahedi, S. and Reimer, R.B., September 1989.

UCB/EERC-89/13 "Mechanics of Low Shape Factor Elastomeric Seismic Isolation Bearings," by Aiken, I.D., Kelly, J.M. and Tajirian, F., December 1989.

UCB/EERC-89/14 "Preliminary Report on the Seismological and Engineering Aspects of the October 17, 1989 Santa Cruz (Loma Prieta) Earthquake," by EERC, October 1989.

UCB/EERC-89/15 "Experimental Studies of a Single Story Steel Structure Tested with Fixed, Semi-Rigid and Flexible Connections," by Nader, M.N. and Astaneh-Asl, A., August 1989.

UCB/EERC-89/16 "Collapse of the Cypress Street Viaduct as a Result of the Loma Prieta Earthquake," by Nims, D.K., Miranda, E., Aiken, I.D., Whittaker, A.S. and Bertero, V.V., November 1989.

UCB/EERC-90/01 "Mechanics of High-Shape Factor Elastomeric Seismic Isolation Bearings," by Kelly, J.M., Aiken, I.D. and Tajirian, F.F., March 1990.

UCB/EERC-90/02 "Javid's Paradox: The Influence of Preform on the Modes of Vibrating Beams," by Kelly, J.M., Sackman, J.L. and Javid, A., May 1990.

UCB/EERC-90/03 "Earthquake Simulator Tests of Viscoelastic Dampers for Medium Rise Structures," by Kelly, J.M. and Aiken, I.D., May 1990.

UCB/EERC-90/04 "Damage to the San Francisco-Oakland Bay Bridge During the October 17, 1989 Earthquake," by Astaneh, A., June 1990.

UCB/EERC-90/05 "Preliminary Report on the Principal Geotechnical Aspects of the October 17, 1989 Loma Prieta Earthquake," by Seed, R.B., Dickenson, S.E., Riemer, M.F., Bray, J.D., Sitar, N., Mitchell, J.K., Idriss, I.M., Kayen, R.E., Kropp, A., Harder, L.F., Jr. and Power, M.S., April 1990.

UCB/EERC-90/06 "Models of Critical Regions in Reinforced Concrete Frames Under Seismic Excitations," by Zulfiqar, N. and Filippou, F., May 1990.

UCB/EERC-90/07 "A Unified Earthquake-Resistant Design Method for Steel Frames Using ARMA Models," by Takewaki, I., Conte, J.P., Mahin, S.A. and Pister, K.S., June 1990.

UCB/EERC-90/08 "Soil Conditions and Earthquake Hazard Mitigation in the Marina District of San Francisco," by Mitchell, J.K., Masood, T., Kayen, R.E. and Seed, R.B., May 1990.

UCB/EERC-90/09 "Influence of the Earthquake Ground Motion Process and Structural Properties on Response Characteristics of Simple Structures," by Conte, J.P., Pister, K.S. and Mahin, S.A., July 1990.

UCB/EERC-90/10 "Experimental Testing of the Resilient-Friction Base Isolation Sytsem," by Clark, P.W. and Kelly, J.M., July 1990.

UCB/EERC-90/11 "Seismic Hazard Analysis: Improved Models, Uncertainties and Sensitivities," by Araya, R. and Der Kiureghian, A., March 1988.

UCB/EERC-90/12 "Effects of Torsion on the Linear and Nonlinear Seismic Response of Structures," by Sedarat, H. and Bertero, V.V., September 1989.

UCB/EERC-90/13 "The Effects of Tectonic Movements on Stresses and Deformations in Earth Embankments," by Bray, J. D., Seed, R. B. and Seed, H. B., September 1989.

UCB/EERC-90/14 "Inelastic Seismic Response of One-Story, Asymmetric - Plan Systems," by Goel, R.K. and Chopra, A.K., October 1990.

UCB/EERC-90/15 "Dynamic Crack Propagation: A Model for Near-Field Ground Motion.," by Seyyedian, H. and Kelly, J.M., 1990.

UCB/EERC-90/16 "Sensitivity of Long-Period Response Spectra to System Initial Conditions," by Blasquez, R., Ventura, C. and Kelly, J.M., 1990.

UCB/EERC-90/17 "Behavior of Peak Values and Spectral Ordinates of Near-Source Strong Ground-Motion over a Dense Array," by Niazi, M., June 1990.